NASA CR-137483

STUDY OF THE SINGLE-BODY YAWED-WING
AIRCRAFT CONCEPT

By Robert M. Kulfan, James W. Nisbet, Frank D. Neumann,
Edward J. Hamilton, James K. Murakami,
John P. McBarron, Kazuo Kumasaka

May 1974

CONTENTS (Concluded)

STUDY OF THE SINGLE-BODY YAWED-WING AIRCRAFT CONCEPT

By Robert M. Kulfan, James W. Nisbet, Frank D. Neumann,
Edward J. Hamilton, James K. Murakami, John P. McBarron,
Kazuo Kumasaka

SUMMARY

During the NASA-sponsored "High Transonic Speed Transport Aircraft Study" (refs. 1 and 2), five aircraft concepts were studied for flight in the high transonic speed regime. The results of that study indicated potential for one of the concepts—the single-fuselage yawed-wing airplane—to achieve good performance at low noise levels. The study reported herein was subsequently undertaken to investigate three areas relating to the development and improvement of this concept.

The threefold objectives of this follow-on study were to:

Task 1: Develop an alternate single-fuselage, yawed-wing-configuration arrangement with a simplified engine arrangement

Task 2: Determine the structural design speed placard that would allow the engine-airframe match for optimum airplane performance

Task 3: Conduct an aeroelastic stability and control analysis of the flexible yawed-wing configuration

The methods and results of the initial design study of the yawed-wing aircraft concept (NASA Ames Research Center sponsored contract "High Transonic Speed Transport Aircraft Study") were used as important inputs (ref. 1). The results of the current study were as follows.

Task 1:

The design criteria for the alternate configuration included:

Cruise Mach number: M = 1.2

Range: 5560 km (3000 nmi)

Passenger payload: 195 passengers (18 140 kg [40 000 lb])

Aircraft noise goal: 15 EPNdB below FAR Part 36

Technology level: Projected for 1985 subject to the completion of
                            required technology development programs

The alternate yawed-wing configuration (model 5-4-1a) developed in this study has two strut-mounted engines on the aft fuselage. This is a less complex engine arrangement than the configuration that evolved in the initial yawed-wing design study, which had four engines buried in the aft fuselage (model 5-3-2). The gross weight of the alternate (two-engine) configuration is approximately 2-1/2% higher than that of the buried-engine arrangement for equal design range and community noise levels. The "boomless" supersonic mission requirements can be met at FAR Part 36 noise levels by the alternate configuration at 217 700 kg (480 000 lb). A gross weight of 226 800 kg (500 000 lb) would be required to achieve the noise goal of FAR Part 36 minus 15 EPNdB considering only the propulsion noise. However, airframe noise may prohibit this lower noise level from being achieved. The detailed characteristics of this configuration are described on page 36.

Task 2:

A modified structural design speed placard was developed. This placard allowed the Mach 1.2 cruise altitudes to be lowered to 10 360 m (34 000 ft). This reduced the required engine size. Cruising at the lower altitudes decreased the required takeoff gross weight for the buried-engine yawed-wing configuration and the alternate two-engine configuration by 8% and 6%, respectively.

Task 3:

The dynamic stability characteristics of the single-fuselage yawed-wing configuration were found to be very dependent on the magnitude of the roll/pitch coupling term, C_{ℓ_α}, and the static longitudinal stability. The contribution of wing flexibility to this roll/pitch coupling is beneficial. The single-fuselage yawed-wing configuration as defined initially was determined to have divergent aircraft response to control surface deflections; however, configuration changes in terms of wing pivot location, center-of-gravity location, tail size, and stability augmentation that produce convergent responses were identified.

The three-phase development that had been recommended in the initial study period to develop the potential of the yawed-wing concept has been modified to reflect the results of the study reported herein.

INTRODUCTION

This document is the final report of the work accomplished by the Boeing Commercial Airplane Company under a 5-month extension of contract NAS2-7031, "High Transonic Speed Transport Aircraft Study," for the NASA Ames Research Center. The contract extension work began on July 1, 1973, and was completed on December 1, 1973.

There has been an increased interest in aircraft designed for transonic cruise speeds that would avoid the generation of sonic boom over populated land masses. The NASA "High Transonic Speed Transport Aircraft Study" conducted by Boeing explored the high transonic regime (up to Mach 1.2 and beyond). During that study five aircraft concepts were studied for flight in the high transonic speed regime. These included:

- Aircraft with fixed swept wing

- Aircraft with variable sweep wing

- Delta-like planform aircraft

- Twin-fuselage yawed-wing aircraft

- Single-fuselage yawed-wing aircraft

The results indicated potential for the single-fuselage yawed-wing concept to achieve good performance at low noise levels. A three-phase follow-on effort consisting of analyses, wind tunnel tests, and a full-scale hardware demonstration was recommended to establish the full potential of the yawed-wing concept and to study critical research areas pertaining to its development.

The purpose of the study reported herein was to investigate three of these recommended research areas related to the development and improvement of the single-body yawed-wing concept. These three tasks included:

- Developing an alternate configuration with a less complex engine installation than that developed for the single-body yawed-wing configuration during the initial contract study period

- Determining the structural design speed placard that would allow the engine-airframe match for optimum airplane performance

3

- Analyzing the aeroelastic stability and control characteristics of the flexible yawed-wing airplane and defining the control system requirements

This document presents the results of these three study tasks.

SYMBOLS AND ABBREVIATIONS

alt	altitude
app	approach
AR	aspect ratio
ATT	advanced technology transport
A_{wet}	wetted area
a.c.	aerodynamic center
$(B \cdot N)_{interf}$	body and nacelle mutual wave drag interference
BPR	bypass ratio of engine
b	wing span
C_D	drag coefficient
C_{D_F}	friction drag coefficient
C_{D_W}	volume wave drag coefficient
C_L	lift coefficient
CLR	ratio of initial cruise lift coefficient to the lift coefficient for $(L/D)_{max}$
C_ℓ	rolling moment coefficient, section lift coefficient
C_{ℓ_n}	rolling moment stability derivative due to vertical acceleration
$C_{\ell_{\hat{p}}}$	rolling moment stability derivative due to roll rate
$C_{\ell_{\hat{q}}}$	rolling moment stability derivative due to pitch rate
$C_{\ell_{\hat{r}}}$	rolling moment stability derivative due to yaw rate

5

C_{ℓ_α}	rolling moment stability derivative due to angle of attack
C_{ℓ_β}	rolling moment stability derivative due to sideslip
$C_{\ell_{\delta_a}}$	rolling moment stability derivative due to aileron deflection
$C_{\ell_{\delta_r}}$	rolling moment stability derivative due to rudder deflection
C_m	pitching moment coefficient
C_{m_n}	pitching moment stability derivative due to vertical acceleration
$C_{m_{\hat{p}}}$	pitching moment stability derivative due to roll rate
$C_{m_{\hat{q}}}$	pitching moment stability derivative due to pitch rate
$C_{m_{\hat{r}}}$	pitching moment stability derivative due to yaw rate
C_{m_α}	pitching moment stability derivative due to angle of attack
$C_{m_{\hat{\alpha}}}$	pitching moment stability derivative due to angle of attack rate
C_{m_β}	pitching moment stability derivative due to sideslip
$C_{m_{\delta_a}}$	pitching moment stability derivative due to aileron deflection
$C_{m_{\delta_e}}$	pitching moment stability derivative due to elevator deflection
C_{n_n}	yawing moment stability derivative due to vertical acceleration
$C_{n_{\hat{p}}}$	yawing moment stability derivative due to roll rate
$C_{n_{\hat{q}}}$	yawing moment stability derivative due to pitch rate
$C_{n_{\hat{r}}}$	yawing moment stability derivative due to yaw rate
C_{n_α}	yawing moment stability derivative due to angle of attack
C_{n_β}	yawing moment stability derivative due to sideslip

$C_{n_{\delta_a}}$ yawing moment stability derivative due to aileron deflection

$C_{n_{\delta_r}}$ yawing moment stability derivative due to rudder deflection

C_x horizontal force coefficient

$C_{y_{\hat{p}}}$ side force stability derivative due to roll rate

$C_{y_{\hat{r}}}$ side force stability derivative due to yaw rate

C_{y_β} side force stability derivative due to sideslip

$C_{y_{\delta_r}}$ side force stability derivative due to rudder deflection

C_z vertical force coefficient

C_{z_n} vertical force stability derivative due to vertical acceleration

$C_{z_{\hat{p}}}$ vertical force stability derivative due to roll rate

$C_{z_{\hat{q}}}$ vertical force stability derivative due to pitch rate

$C_{z_{\hat{r}}}$ vertical force stability derivative due to yaw rate

C_{z_α} vertical force stability derivative due to angle of attack

$C_{z_{\hat{\alpha}}}$ vertical force stability derivative due to angle of attack rate

C_{z_β} vertical force stability derivative due to sideslip

$C_{z_{\delta_a}}$ vertical force due to stability derivative aileron deflection

$C_{z_{\delta_e}}$ vertical force stability derivative due to elevator deflection

c   local wing chord

$\bar{c}, \bar{c}_w$ mean aerodynamic chord for unyawed wing

c_{ave} average wing chord

7

cg	center of gravity
c_R	wing root chord
DOF	degree of freedom
deg	degrees
EAS	equivalent airspeed
EPNdB	effective perceived noise level
FAR	Federal Aviation Regulations
ft	feet
g	acceleration due to gravity
h	altitude
I_{xx}	roll moment of inertia
I_{yy}	pitch moment of inertia
I_{zz}	yaw moment of inertia
I_{xy}	roll-pitch product of inertia
I_{xz}	roll-yaw product of inertia
in.	inches
KEAS	knots equivalent airspeed
kg	kilograms
km	kilometers
kn	knots

L/D	lift-to-drag ratio	
L.E.	leading edge	
lb	pounds	
l/d	body fineness ratio, length/diameter	
M	Mach number	
MAC	mean aerodynamic chord	
M_D	design dive Mach number	
M_{MO}	maximum operating Mach number	
m	meters	
N	newtons	
nmi	nautical miles	
n	vertical acceleration, g, positive down	
OEW	operational empty weight	
p	roll rate	
$\hat{p}$	nondimensional roll rate (pb/2V)	
q	pitch rate	
$\hat{q}$	nondimensional pitch rate, $(q\bar{c}/2V)$	
R	range	
R_E/R_R	ratio of rolling moment on elastic wing to rolling moment on rigid wing	
r	yaw rate	

$\hat{r}$	nondimensional yaw rate (rb/2V)
rad	radians
SAS	stability augmentation system
SFC	specific fuel consumption
S_H	horizontal tail area
SLS	sea level static
S_{ref}	wing reference area
S_V	vertical tail area
S_w	wing area
s	seconds
T.O.	takeoff
TOFL	takeoff field length
TOGW	takeoff gross weight
T/W	thrust loading, total rated engine thrust divided by airplane takeoff gross weight
t/c	thickness-to-chord ratio
u	x-axis velocity component (stability axis)
V	true airspeed
$(V_c)_{des}$	maximum design cruise speed for altitudes below 6096 m (20 000 ft)
V_D	design dive speed
$\bar{V}_H$	horizontal tail volume coefficient

V_{MO}	maximum operating speed
$\bar{V}_V$	vertical tail volume coefficient
v	y-axis velocity component (stability axis)
W	gross weight of airplane
W_F	fuel weight
W/S	wing loading, airplane gross weight divided by wing area
$(W \cdot B)_{interf}$	wing and body mutual wave drag interference
$(W \cdot N)_{interf}$	wing and nacelle mutual wave drag interference
w	z-axis velocity component (stability axis)
α	angle of attack
$\hat{\dot{\alpha}}$	nondimensional angle of attack rate ($\dot{\alpha}\bar{c}/2V$)
β	angle of sideslip
Δ	increment
δ_a	aileron deflection about hinge line positive for trailing edge down on right wing and trailing edge up on left wing
δ_e	elevator deflection, positive trailing edge down
δ_r	rudder deflection, positive trailing edge left
Λ	yaw angle of wing
θ	pitch attitude angle
ϕ	roll angle

ω_n natural frequency of airplane response mode

ψ heading angle

TASK 1: ALTERNATE CONFIGURATION DEVELOPMENT STUDY

The lowest gross weight high transonic speed transport configuration developed during the initial study period for contract NAS2-7031 was the single-fuselage yawed-wing configuration (model 5-3-2) shown in figure 1. This configuration derived its good performance from it low aerodynamic drag. The integrated engine arrangement of this configuration was a complex design that had significant propulsion losses and weight penalties associated with long inlet ducts and exit nozzles.

The objective of this study task was to develop an alternate single-fuselage yawed-wing arrangement with a simpler engine arrangement without compromising the configuration's performance.

STUDY APPROACH

The three-engine arrangement of a previously developed configuration, model 5-2-6 (fig. 2), was used as the design starting point with emphasis placed on improving the aerodynamic efficiency of that arrangement. Three configuration derivatives of the aft-mounted engine arrangement 5-2-6 were developed. These included a two-engine arrangement and two different three-engine arrangements.

Preliminary evaluations of the structural weight, cruise drag, and engine installation losses were made for each of these configurations. Based on these calculations, the two-engine arrangement was selected with NASA Ames' concurrence for more detailed design and evaluation. This configuration was then "sized" to determine the gross weight, wing area, and engine size necessary to achieve the design mission objectives. Additional studies were made to determine the impact of the community noise objective on the airplane takeoff gross weight and to determine its Mach = 1.2 range capability.

The flight profile, mission rules, and mission design objectives shown in figure 3 were identical to those used in developing model 5-3-2. These mission rules and objectives and the design synthesis process are discussed in detail in reference 1.

The development of the alternate configuration and the results of the performance evaluations are presented in this section.
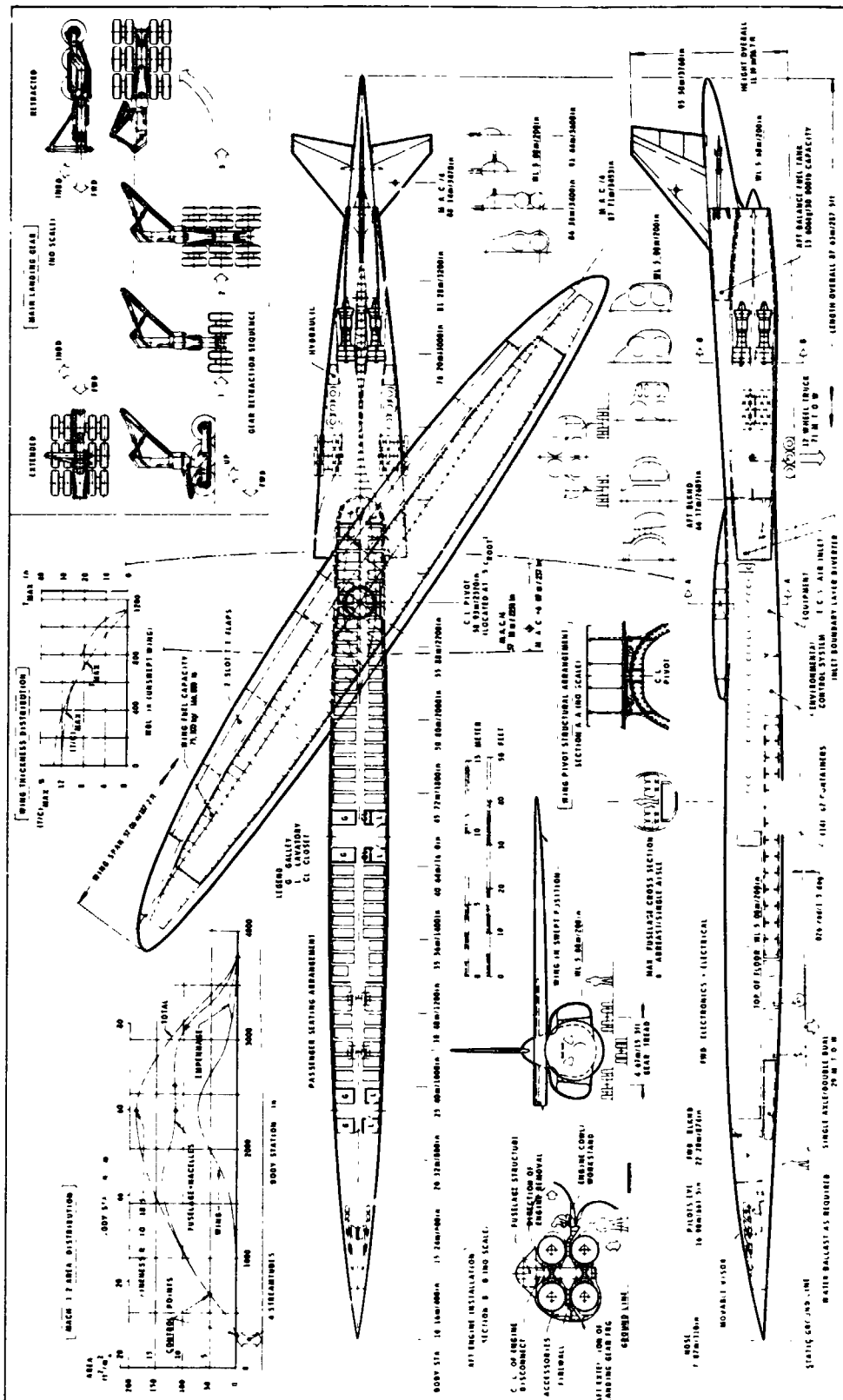
FIGURE 1.—MODEL 5-3-2 (5-3a)

14

FIGURE 2.—MODEL 5-2-6

15

Flight profile and mission rules

Basic mission ⟷ Reserves

Departure   Destination

Mission range
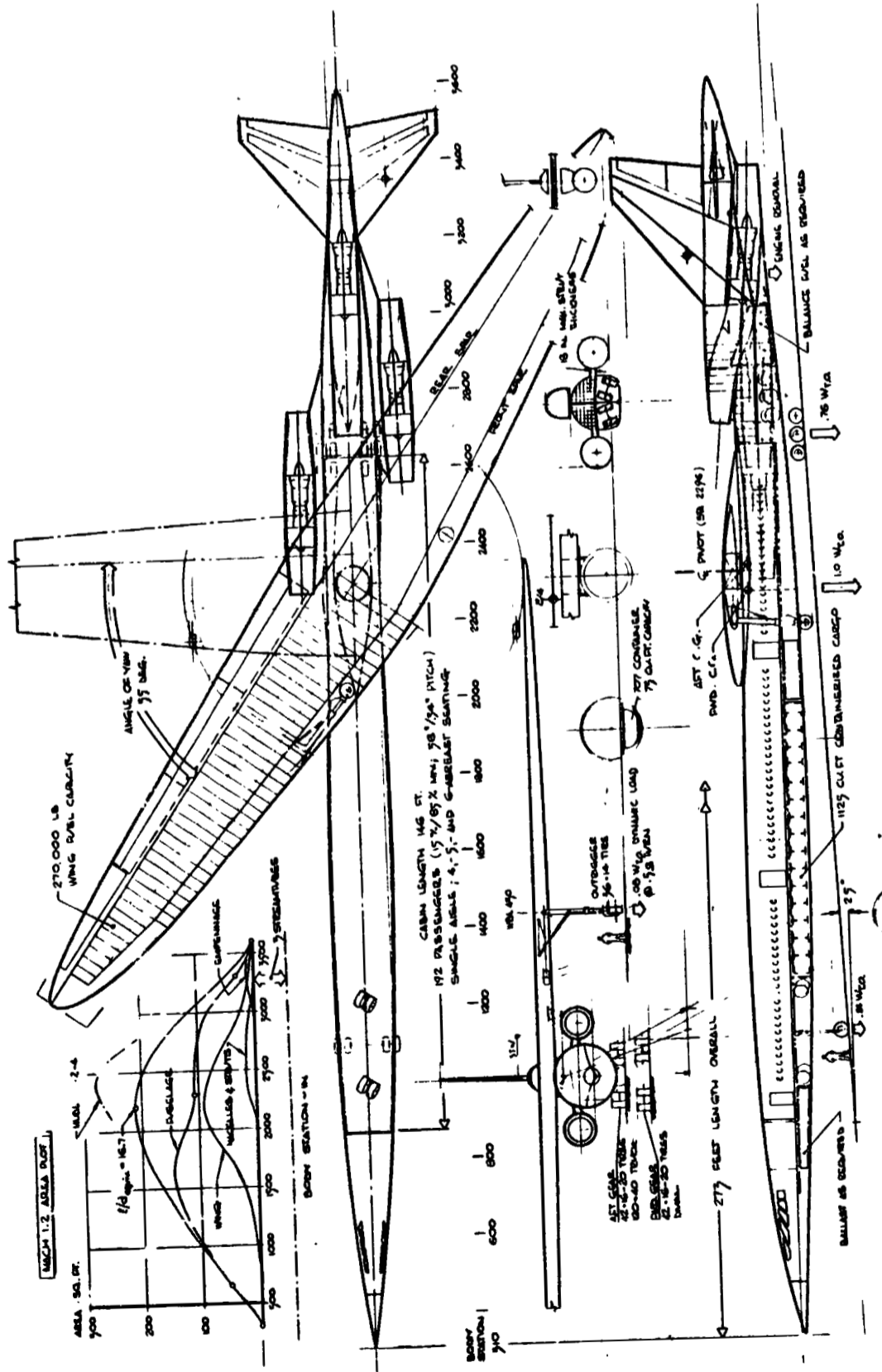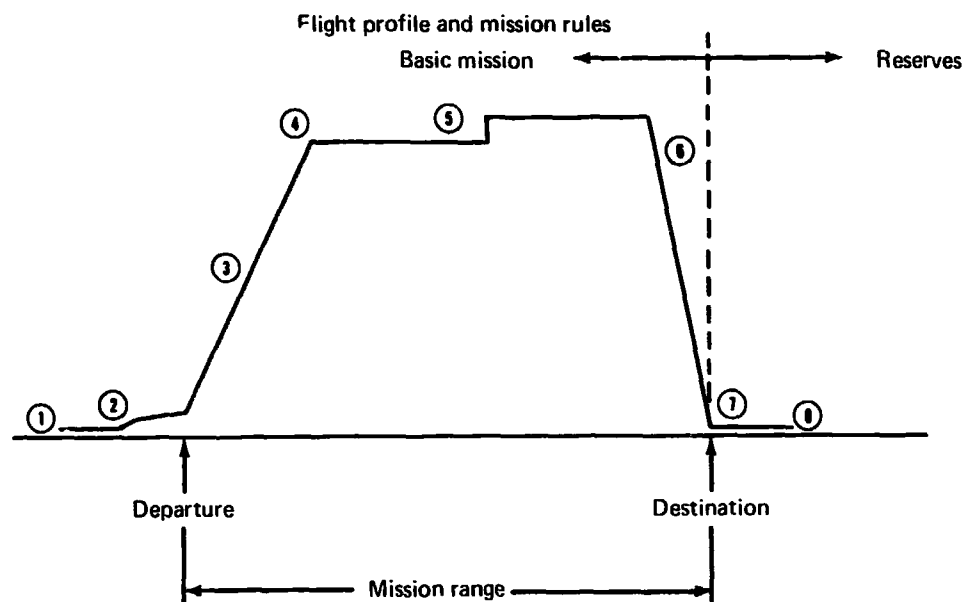
①	Taxi out	● Nine minutes taxi thrust
②	Takeoff	● Field length performance per FAR PART 25 305 m/32° C (1000 ft/90° F)
		● One minute takeoff thrust
		● Takeoff and sideline noise calc. per FAR PART 36 conditions
③	En route climb	● Δrange = 272 km (147 nmi) ΔW_F = .034 TOGW
④	Initial cruise alt	● Determined by level flight max cruise thrust, cruise Mach
⑤	Cruise	● 1219 m (4000 ft) step alt cruise
⑥	Descent	● Δrange = 306 km (165 nmi) ΔW_F = 726 kg (1600 lb)
⑦	Landing	● Field length performance per FAR PART 25 305 m (1000 ft)
		● Approach noise calc. per FAR PART 36 conditions
⑧	Taxi in	● Five minutes taxi thrust
⑨	Reserves	● .075 TOGW

Design Mission Objectives

Objectives

Payload:	18 143 kg (40 000 lb)
Range:	5560 km (3000 nmi)
Cruise Mach:	1.2

Constraints

Minimum cruise altitude:	$\geqslant$ 11 890 m (39 000 ft)
Field length:	$\leqslant$ 3 505 m (11 500 ft) maximum
Landing approach speed:	$\leqslant$ 92.7 m/s (180 kn) maximum

Noise goal   15 EPNdB below FAR PART 36

FIGURE 3.—FLIGHT PROFILE, MISSION RULES AND DESIGN OBJECTIVES

ALTERNATE CONFIGURATIONS

The three preliminary candidate configurations that were developed included:

● Model 5-4-1 – two-engine airplane with the engines strut-mounted on the aft fuselage;

● Models 5-4-2 and 5-4-3 – three-engine airplanes. Two engines are strut-mounted on the aft fuselage. The third engine is integrated into the aft fuselage, using two different design approaches.

Model 5-4-1, shown in figure 4, was derived from the design guidelines of model 5-3-2, the best configuration that had been developed during the initial system study (fig. 1). A two-engine arrangement was considered as an alternate because of the benefits expected from the design simplicity. The body length of model 5-3-2, wing size and and location as well as empennage size and location, were largely maintained on model 5-4-1. The two engines were mounted on the ends of a structural box that carried across the fuselage aft of the passenger cabin rear pressure bulkhead. The engine location was defined by the requirement to have passenger seats located outside of the burst path of rotating engine discs. Because of the large engines, a pronounced area ruling of the fuselage was necessary. A number of critical required minimum fuselage cross sections were identified. These included:

● Pilot station 4.6 m^2 (50 ft^2)

● Five-abreast, single-aisle seating plus
   wing/body fairing at a station 1.3 m
   (50 in.) ahead of the wing pivot 10.7 m^2 (115 ft^2)

● Four-abreast, single-aisle seating near
   the aft end of the passenger cabin 6.5 m^2 (70 ft^2)

● Stabilizer pivot 1.7 m^2 (18 ft^2)

● Landing gear stowage 7.8 m^2 (84 ft^2)

The fuselage was area ruled in the presence of wing, engines, struts, and empennage. A number of optimized body design iterations were necessary to develop the final body area distribution.

The section of the aft fuselage between the landing gear wheel well and the balance fuel tank can be used for optional cargo. This compartment was created by changing from integrated to
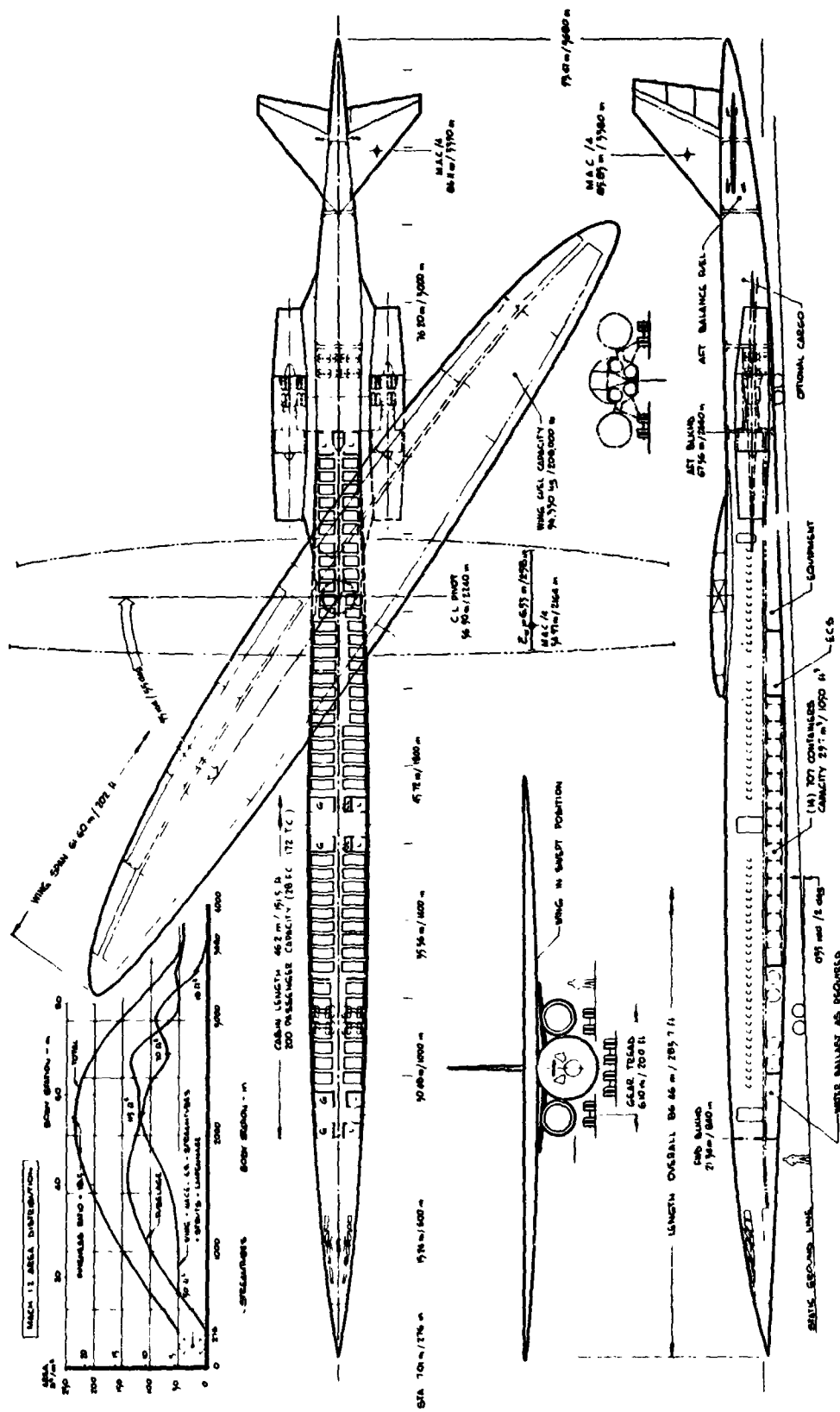
FIGURE 4.—MODEL 5-4-1

pod-mounted engines while maintaining the length of the integrated-engine configuration, model 5-3-2. The long aft fuselage resulted in small empennage size, large configuration fineness ratio, and an area distribution similar to that of model 5-3-2. The three-view drawing and the area distribution of the alternate configuration, model 5-4-1, are shown in figure 4.

Model 5-4-2, shown in figure 5, is a three-engine arrangement. Two engines are strut-mounted on the aft fuselage. The third engine is integrated into the lower aft fuselage with an S-shaped inlet duct. A similar arrangement, designated model 5-2-6 and shown in figure 2, was investigated during the initial system study. On the present configuration a higher fineness ratio was chosen along with a more desirable engine and landing gear arrangement. Except for the third engine installation and engine sizes, the definition of model 5-4-2 is nearly identical to that of model 5-4-1. Because of the space required for the third engine and inlet duct, the optional cargo bay in the aft fuselage was eliminated. The third engine is structurally supported below the fuselage primary structure. The fuselage continues aft and above the center engine for the support of the empennage. The all-movable outboard stabilizers are mounted to a carry-through structural box or spindle.

Model 5-4-3, shown in figure 6, represents a derivative of model 5-4-2. A different design approach was used for the integration of the center engine and the stabilizer. The aft fuselage closure was eliminated by fairing the fuselage into the center engine nozzle. The center engine is located aft of the vertical tail rear spar and is suspended from a cantilevered structure (similar to the Boeing 727 installation). The stabilizers are spindle-mounted at the maximum width of the inlet duct fairing. The spindles are cantilevered from the banjo-shaped rear spar fitting of the vertical tail. The aft body length and the tail arms were reduced considerably as compared to model 5-4-2.

The configuration characteristics for these three arrangements are summarized in table 1.

An additional objective of the alternate configuration development study was to improve the ground maneuver stability of the yawed-wing, single-fuselage configuration by increasing the landing gear tread. An articulated landing gear arrangement that offered a gear tread larger than on earlier models was conceived. The details of this landing gear design are shown in figure 7. The wide gear tread was made possible by means of a body-mounted, articulated support beam in combination with a liquid spring shock absorber, which is mounted far outboard on the engine structural support box. The gear is retracted rearward into the fuselage by means of a single hydraulic actuator that moves a downlock-uplock link and a support yoke. The eight wheels are mounted in pairs on the truck. This landing gear concept was incorporated in all three alternate configurations.

These three alternate configurations are simpler designs with more efficient propulsion installations than model 5-3-2, the aft integrated-engine configuration shown in figure 1. On the
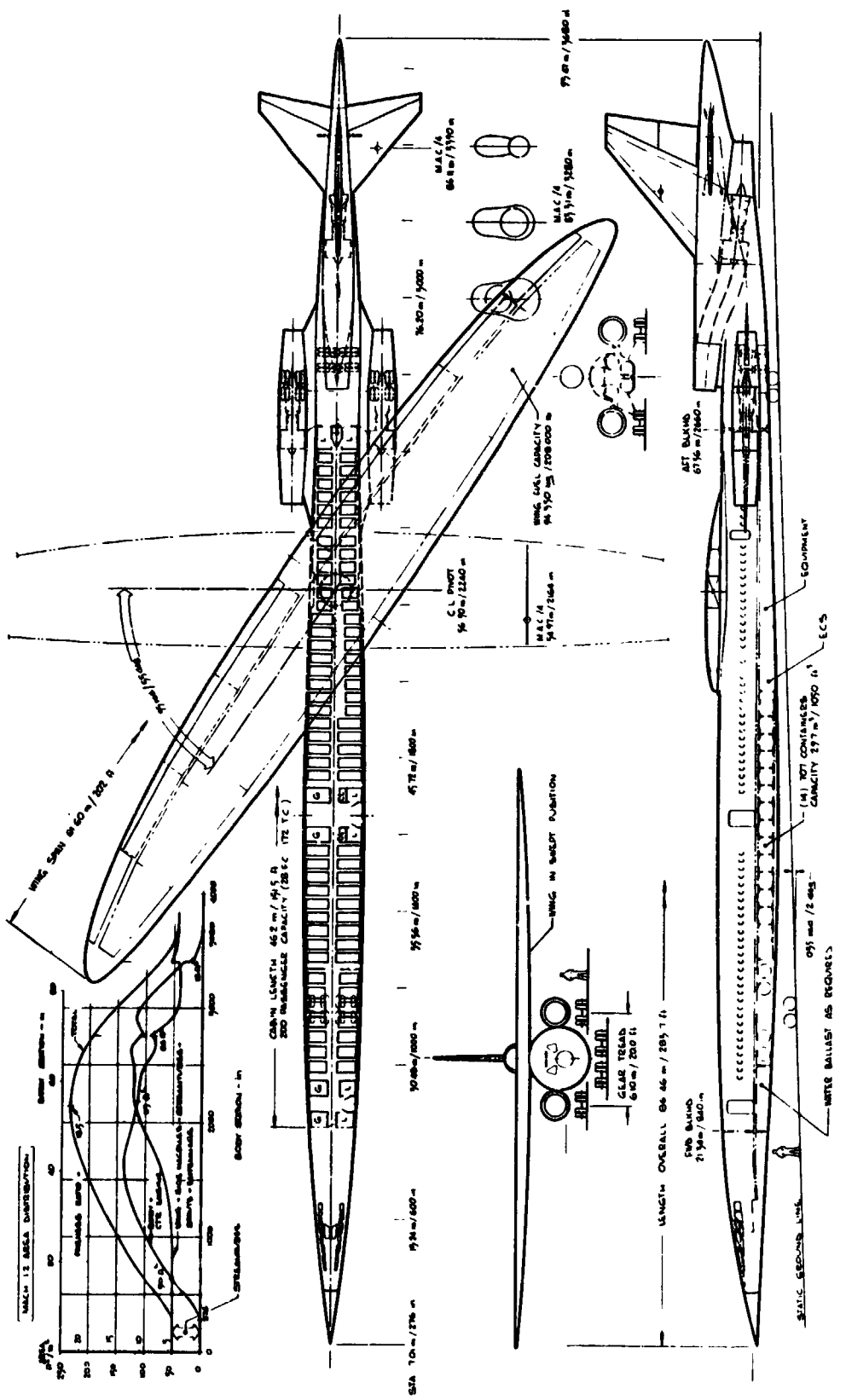
FIGURE 5.—MODEL 5-4-2

FIGURE 6.—MODEL 5-4-3

21

TABLE 1.—ALTERNATE CONFIGURATION CHARACTERISTICS

| Item			5-4-1	5-4-2	5-4-3
Model number					
Design payload		kg (lb)	18 143 (40 000)	18 143 (40 000)	18 143 (40 000)
Design range objective		km (nmi)	5 560 (3 000)	5 560 (3 000)	5 560 (3 000)
Design Mach number			1.2	1.2	1.2
TOGW		km(lb)	226 796 (500 000)	226 796 (500 000)	226 796 (500 000)
Configuration fineness ratio, l/d_{equiv}			18.5	18.5	17.6
Fuselage	Length	m (ft)	86.5 (283.7)	86.5 (283.7)	83.9 (275.2)
	Cabin length	m (ft)	46.2 (151.7)	46.2 (151.7)	46.2 (151.7)
	Min./max diameter	m/m(in./in.)	3.56/4.06 (140/160)	3.56/4.06 (140/160)	3.56/4.06 (140/160)
	Min./max abreast seating		4/6	4/6	4/6
	Passenger capacity (15%/85% mix)		190	190	190
Wing	Area	m²(ft²)	372 (4 000)	372 (4 000)	372 (4 000)
	Aspect ratio/ellipse axis ratio		10.2/8:1	10.2/8:1	10.2/8:1
	Sweep @ Mach 1.2 cruise	rad(deg)	.96 (55)	.96 (55)	.96 (55)
	Thickness ratio, root/tip (unyawed)	%/%	12/0	12/0	12/0
	$c_w/4$ location on fuselage	%	55.4	55.4	58.2
Horizontal tail	Area/$\overline{V}_H$	m²(ft²)	34.6 (372)/.44	34.6 (372)/.44	41.3 (445)/.44
	Aspect ratio		2.6	2.6	2.6
	L.E. sweep	rad (deg)	.87 (50)	.87 (50)	.87 (50)
	Thickness ratio, root/tip	%/%	4/4	4/4	4/4
	Taper ratio		.2	.2	.2
Vertical tail	Area/$\overline{V}_V$	m² (ft²)	32.2 (347)/.0432	32.2 (374)/.0432	37.6 (405)/.0432
	Aspect ratio		1.11	1.11	1.11
	L.E. sweep	rad (deg)	.87 (50)	.87 (50)	.87 (50)
	Thickness ratio, root/tip	%/%	3.5/3.5	3.5/3.5	3.5/3.5
	Taper ratio		.254	.254	.254
Propulsion	Type/BPR		ATSA 1.2-1-3000-16/1		
	Number of engines/location		2/aft fuselage	3/aft fuselage	3/aft fuselage
	Static thrust/engine SLS/90°F	N (lb)	333 630 (75 000)	222 420 (50 000)	222 420 (50 000)
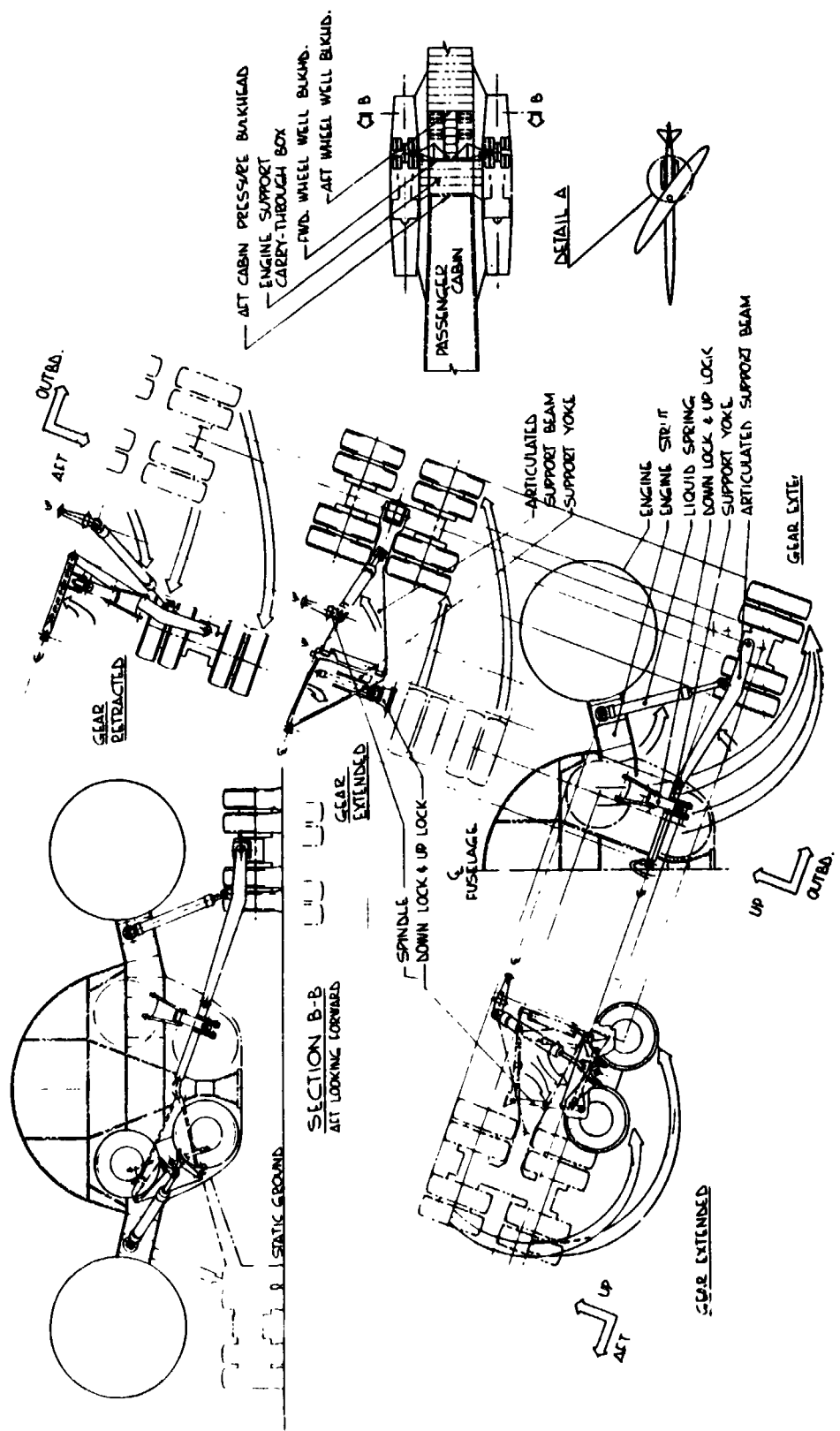
FIGURE 7.—ARTICULATED LANDING GEAR, MODELS 5-4-1, -2, -3

23

alternate configurations it was possible to eliminate some of the technical concerns that had been identified on model 5-3-2. The reduction in design technical concern is shown in figure 8.

ALTERNATE CONFIGURATIONS EVALUATIONS

The alternate configurations models 5-4-1, 5-4-2, and 5-4-3 were evaluated to determine their weight, drag, and thrust characteristics relative to the corresponding uncycled baseline configuration for model 5-3-2, which was designated model 5-3. The relative weight comparisons are summarized in table 2.

TABLE 2.—BASELINE CONFIGURATIONS WEIGHT COMPARISON

Item	Relative weight changes, kg (lb)			
	Model 5-3 4 integrated engines	Model 5-4-1 2 body engines	Model 5-4-2 2 body engines 1 center engine	Model 5-4-3 2 body engines 1 center engine
Wing	Reference	0	0	0
Body		-680 (-1500)	-230 (-500)	-2450 (-5400)
Empennage		0	90 (200)	450 (1000)
Landing gear		0	0	0
Engine installation items		-1680 (-3700)	-140 (-300)	-140 (-300)
Engine + propulsion systems		2000 (4400)	1040 (2300)	1040 (2300)
Standard and operational and miscellaneous		0	0	0
Operational empty weight	Reference	-360 (-800)	770 (1700)	-1090 (-2400)

The change from four to two engines on model 5-4-1 reduced the aft fuselage weight and eliminated the long inlet ducts that had been integrated into the aft fuselage of model 5-3. These weight reductions were nearly cancelled by the increased engine weight, because for the same total thrust two big engines weigh more than four small engines.

The body and engine support structure weights of the three-engine configuration 5-4-2 are slightly less than the corresponding weights for model 5-3. The increased engine weight for these larger engines, however, resulted in a net increase in the overall weight for this configuration.
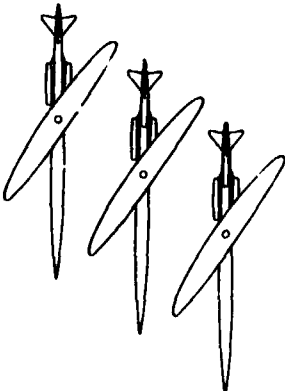
Feature	Concern
Integrated engines	—Engine failure
	—Engine accessibility
	—Structural design
	—Nozzle & thrust reverser design
Long inlet ducts	—Thrust & SFC losses
Narrow landing gear tread	—Ground maneuver stability
Long forebody	—Passenger ride quality
	—Structural design
Nonrotating takeoff and landing	—None
High wing	—Passenger safety
Aft engine location	—Balance considerations

Model 5-3-2

Alternate configurations

FIGURE 8.— TECHNICAL CONCERN FOR MODEL 5-3 VERSUS ALTERNATE CONFIGURATIONS

The other three-engine configuration, model 5-4-3, has a shorter fuselage. This resulted in a substantial savings in body weight. Larger, and therefore heavier, tails were required. The net effect, however, was a reduction in weight relative to model 5-3.

Drag evaluations of the alternate configurations were made for a cruise Mach number of 1.2. Area rule body designs were developed and analyzed "with" and "without" engines for each of the configurations. This allows the net drag effects of the various nacelle installations to be identified. The friction drag, volume wave drag, and Lft/drag ratios are shown in figure 9 for the designs with and without engines.

The drag is nearly equal for each of the "without engine" designs. The wave drag and friction drag of the alternate configuration "with engine" designs exceed the corresponding wave and friction drag of the integrated engine configuration 5-3. The friction drag increases are associated with the body nacelles and struts wetted areas. The volume wave drag increases are the refult of:

- Body shape drag associated with area ruling the body to minimize the nacelle drag

- Installed nacelle wave drag

- Strut wave drag

The estimates of the installed thrust and fuel consumption differences between the two-engine, both three-engine, and the integrated-engine installations are summarized in table 3.

TABLE 3.—INSTALLED THRUST AND SFC COMPARISON

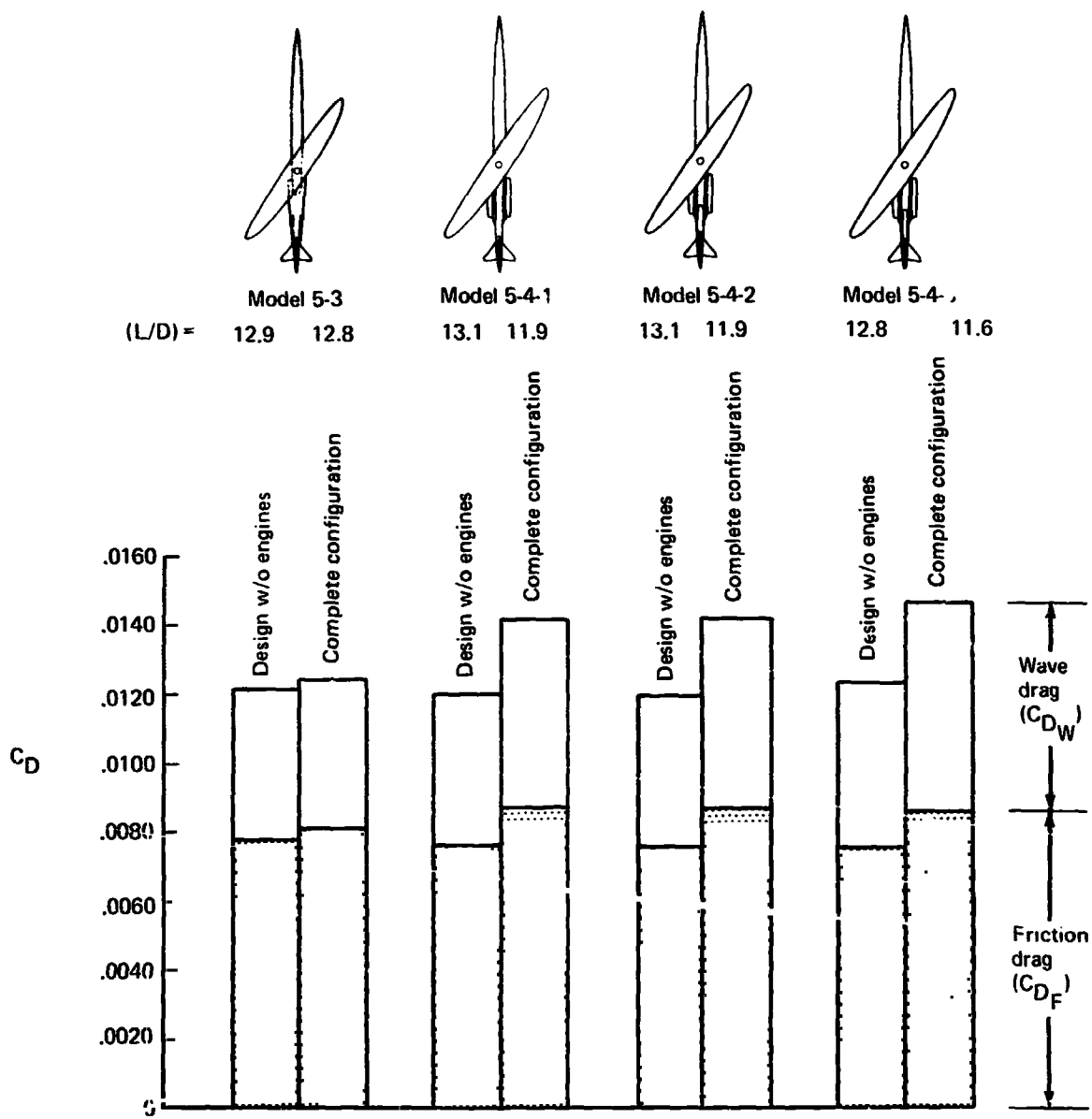| Configuration	$\dfrac{\Delta \text{ thrust}}{\text{thrust}}$	$\dfrac{\Delta \text{SFC}}{\text{SFC}}$
Model 5-3 (4 integrated engines)	Reference	Reference
Model 5-4-1 (2 body engines)	+3.6%	-1.05%
Model 5-4-2 (2 body engines, 1 center engine)	+3%	-0.9%
Model 5-4-3 (2 body engines, 1 center engine)	+3%	-0.9%

FIGURE 9.—BASELINE CONFIGURATIONS MACH 1.2 DRAG COMPARISON

The combined effects of the drag, weight, thrust, and SFC differences are related as equivalent weight changes by sensitivities in table 4. All of the alternate configurations were estimated to result in slightly heavier arrangements. The two-engine arrangement, the lightest of these alternate arrangements, was selected for further detailed performance studies.

TABLE 4 —CONFIGURATION GROSS WEIGHT CHANGES

Item	Equivalent weight changes kg (lb)			
	Model 5-3 4 integrated engines	Model 5-4-1 2 body engines	Model 5-4-2 2 body engines 1 center engine	Model 5-4-3 2 body engines 1 center engine
Weight changes $(\Delta OEW)_{wt}$		-360 (-800)	770 (1700)	-1090 (-2400)
Drag changes $(\Delta OEW)_{drag}$	Reference	7570 (16 700)	7670 (16 900)	10 340 (22 800)
SFC changes $(\Delta OEW)_{SFC}$		-950 (-2100)	-820 (-1800)	-820 (-1800)
Thrust changes $(\Delta OEW)_{thrust}$		-3900 (-8600)	-3220 (-7100)	-3220 (-7100)
$(\Delta OEW)_{net}$	Reference	2360 (5200)	4400 (9700)	5210 (11 500)

Sensitivities: $\Delta C_D = .0001 \approx \Delta OEW = 450$ kg (1000 lb)

$\dfrac{\Delta \text{thrust}}{\text{thrust}} = $ 1% $\approx \Delta OEW = 1100$ kg (2400 lb)

$\dfrac{\Delta SFC}{SFC} = $ 1% $\approx \Delta OEW = 900$ kg (2000 lb)

CONFIGURATION PERFORMANCE

The "uncycled" configuration 5-4-1 represented by figure 4 was analyzed to determine the basic weight, lift-and-drag, thrust, and noise characteristics. Additional analyses were made to determine the effects of varying engine size and wing area and to develop scaling rules that account for these changes. The results of these analyses were used as inputs to a parametric performance analysis program to "size" the airplane to achieve the mission objectives by determining the minimum gross weight, the required wing area, engine size, and tail sizes. This process is described in more detail in reference 1.

The airplane derived from the uncycled configurations by this procedure are referred to as "mission sized" configurations or as "sized" configurations. These sized configurations are distinguished from the parent uncycled configuration by the addition of a small letter after the parent configuration designator.

Example:
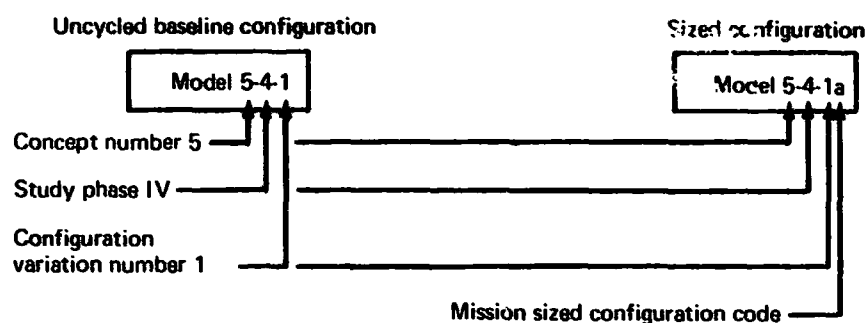
The flight profile, mission rules, and design mission objectives (fig. 3) were the same as those used to develop configuration 5-3-2.

The noise goal was a specified study objective. In order to assess the impact of the design objective on the required configuration gross weight, performance calculations were made with three different sets of propulsion data representing three levels of sound suppression. The results were then used to identify the gross weight penalty to achieve a specific noise level. The engine design characteristics for the various noise treatments are discussed in reference 1.

The design selection chart shown in figure 10 is for the two-engine configuration, model 5-4-1, with the lowest level of engine treatment, which is designated as the "peripheral treatment."

The "constrained design (5-4-1a)" indicated on the figure has the lowest gross weight for Mach 1.2 cruise above the minimum cruise altitude constraint of 11 890 m (39 000 ft). The gross weight of integrated-engine design (model 5-3a) was also set by this altitude constraint (fig. 16). The performance characteristics and design characteristics for the sized two-engine configuration 5-4-1a are compared with the corresponding data for the integrated four-engine configuration 5-3a in
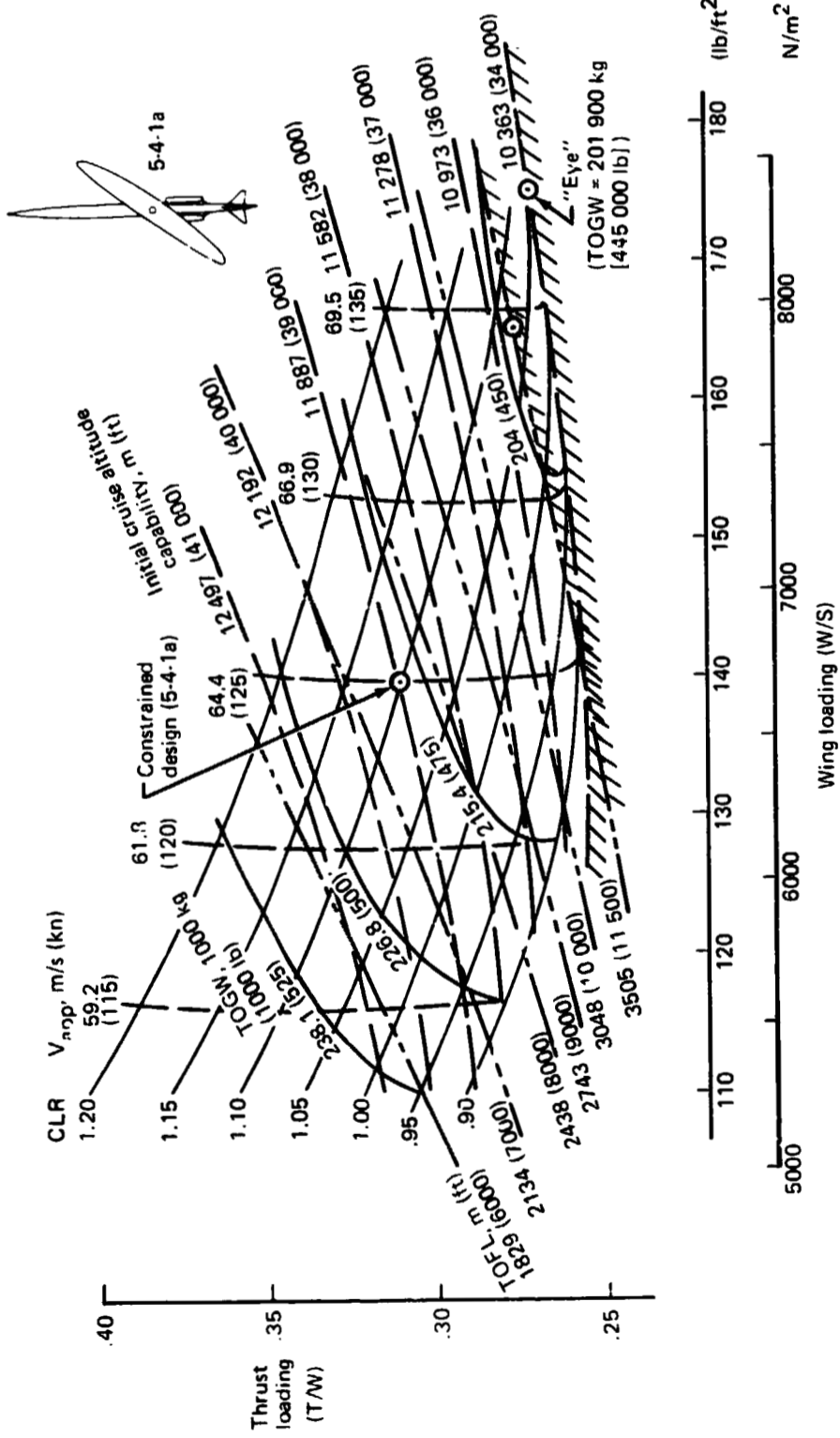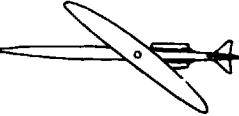
FIGURE 10.—MODEL 5-4-1a DESIGN SELECTION CHART

tables 5 and 6. A comparison of the sized airplane takeoff gross weight (TOGW) buildup is shown in figure 11 for both configurations.
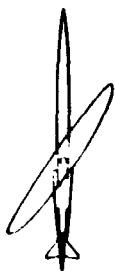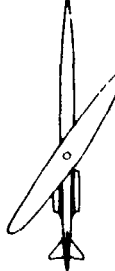
TABLE 5.—AIRCRAFT CHARACTERISTICS AND PERFORMANCE

Mach 1.2 Payload = 18 143 kg (40 000 lb) Range = 5560 km (3000 nmi) Initial cruise altitude =11 887 m (39 000 ft) Takeoff field length=3505 m (11 500 ft) Peripheral noise treatment		
Airplane configuration	5-4-1a	5-3a
Takeoff gross weight, kg (lb) Operating empty weight, kg (lb) Wing area, m^2 (ft^2) Engine thrust rating	217 000 (478 400) 114 120 (251 600) 319.6 (3440)	211 828 (467 000) 113 832 (251 000) 319.6 (3440)
Sea level static, N (lb) Number of engines/bypass ratio	330 500 (74 300) 2/1	156 113 (35 100) 4/1
Thrust loading (T/W) Wing loading (W/S), N/m^2 (lb/ft^2) L/D cruise Takeoff field length: max flaps, m (ft) reduced flaps, m (ft)	0.31 6680 (139.5) 11.5 1313 (7590) 3505 (11 500)	0.30 6512 (136) 12.3 2179 (7150) 2947 (9670)
L/D community reduced flaps Approach speed: reduced flaps, m/s (kn)	8.3 71.2 (138.3)	8.3 70.7 (137.4)
Community noise: EPNdB From FAR Part 36 Takeoff with thrust cutback at noise station Sideline Approach Traded	 -5.6 +6.2 (@ 0.25 nmi) -3.5 +4.2	 -0.4 +2.0 (@ 0.35 nm) -2.0 0

The takeoff gross weight for the two-engine configuration 5-4-1a is approximately 2% higher than that for the integrated four-engine arrangement 5-3a. The operational empty weights for both configurations are essentially equal. The slight difference in gross weight is due to increased fuel requirements associated with the higher installed nacelle drag of the two-engine arrangement.

The takeoff field length of the two-engine airplane exceeds that of the four-engine airplane because the loss of one engine is more critical for a two-engine airplane. The sideline noise of model 5-4-1a is greater than that of 5-3a since the FAR Part 36 sideline measuring station for a two-engine airplane is less than that for a four-engine airplane. The reduced takeoff and landing noise levels of

TABLE 6.—SIZED AIRCRAFT DESIGN CHARACTERISTICS

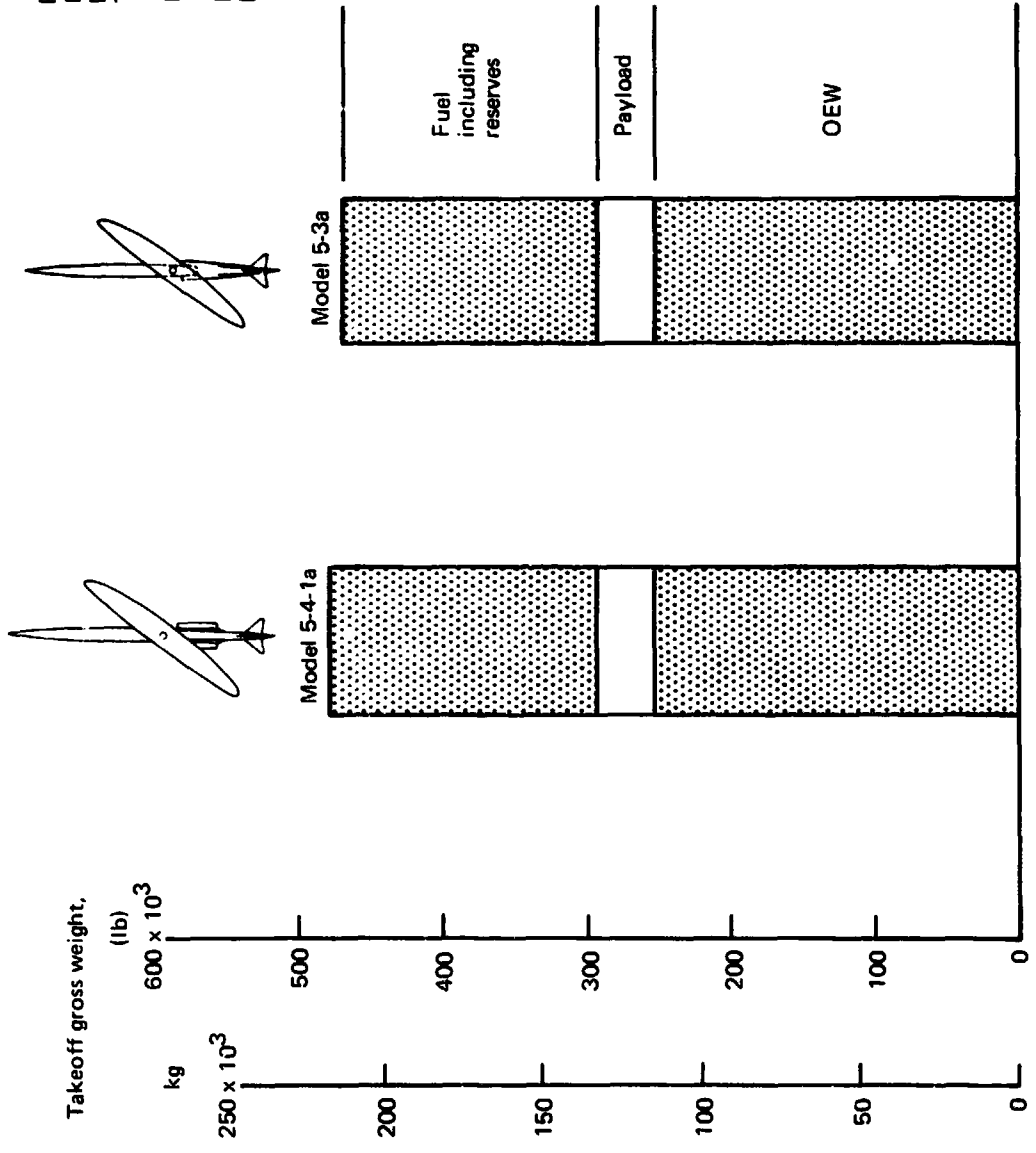|			Configuration concept	
Item				
Model number			5-3a	5-4-1a
Design payload		kg (lb)	18 143 (40 000)	
Design range objective		km (nmi)	5 560 (3 000)	
Design Mach number			1.2	
TOGW		km (lb)	211 830 (467 000)	316 820 (478 400)
Configuration fineness ratio, ℓ/d_{equiv}			18.5	18.9
Fuselage	Length	m (ft)	87.6 (287.5)	86.5 (283.7)
	Cabin length	m (ft)	44.0 (144.3)	46.2 (151.7)
	Min/max diameter	m/m (in./in.)	3.56/4.06(140/160)	3.56/4.06 (140/160)
	Min/max abreast seating		4/6	4/6
	Passenger capacity (15%/85% mix)		190	190
Wing	Area	$m^2 (ft^2)$	319.6 (3440)	
	Aspect ratio/ellipse axis ratio		10.2/8:1	
	Sweep @ Mach 1.2 cruise	rad (deg)	0.96 (55)	
	Thickness ratio, root/tip (unyawed)	%/%	12.0/0.0	
	$c_w/4$ location on fuselage	%	56.0	54.8
Horizontal tail	Area /$\bar{V}_H$	$m^2 (ft^2)$	27.4 (295)/0.44	
	Aspect ratio		2.6	
	L.E. sweep	rad (deg)	0.87 (50)	
	Thickness ratio, root/tip	%/%	4.0/4.0	
	Taper ratio		0.2	
Vertical tail	Area /$\bar{V}_V$	$m^2 (ft^2)$	25.5 (275)/0.043	
	Aspect ratio		1.11	
	L.E. sweep	rad (deg)	0.87 (50)	
	Thickness ratio, root/tip	%/%	3.5/3.5	
	Taper ratio		0.254	
Propulsion	Type/BPR		ATSA 1.2-1-3000-16/1.0	
	Number of engines/location		4/aft fuselage	2/aft fuselage
	Static thrust/engine SLS/90° F	N (lb)	156 100 (35 000)	330 500 (74 300)

FIGURE 11.—YAWED WING AIRPLANE GROSS WEIGHT COMPARISON

33

the two-engine airplane are the result of improved takeoff and landing lift-to-drag ratios obtained by deleting the leading-edge devices. This is further discussed in the section that follows.
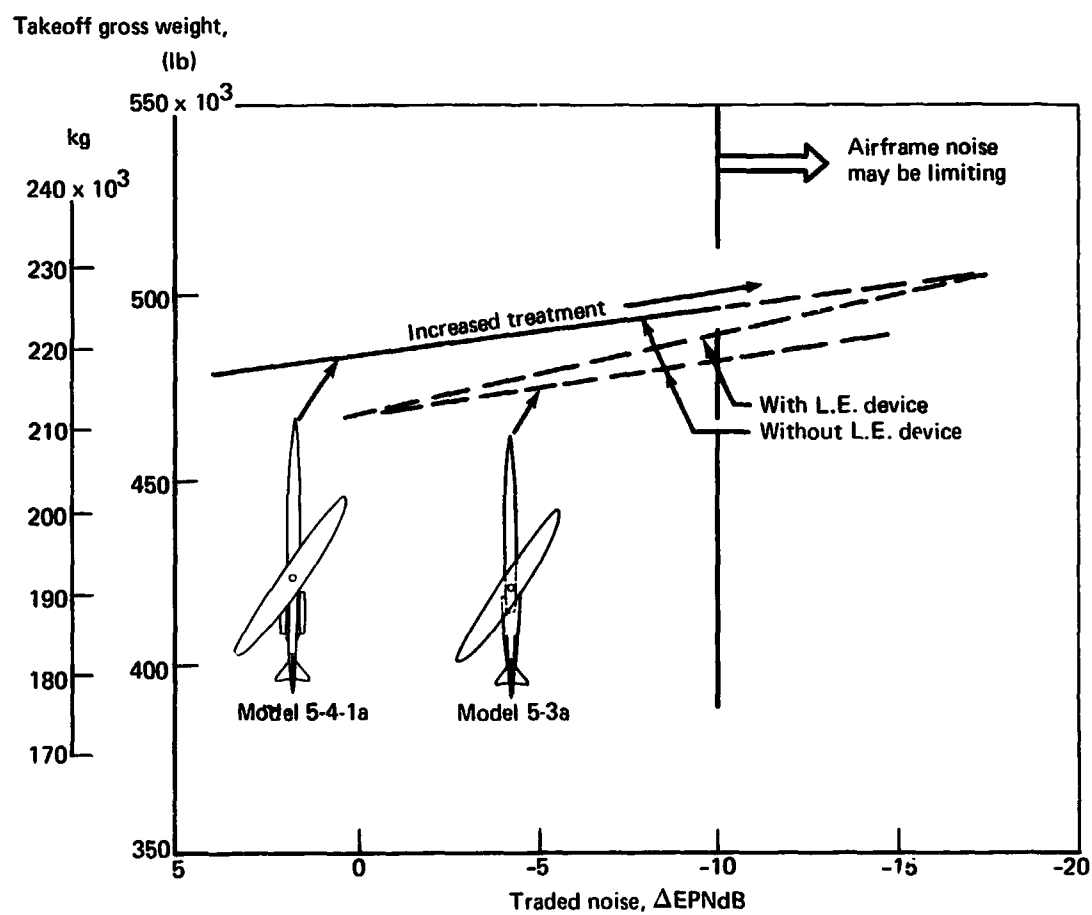
NOISE TREATMENT STUDY

The takeoff gross weight penalty to reduce community noise was determined for configuration 5-4-1 by assessing the effect of three different levels of noise treatment. The minimum noise treatment level consisted of acoustically lined walls for the engine nacelle. The maximum noise treatment required the introduction of considerable jet suppression and extensive acoustic treatment, both in the inlet and fan duct, to reduce the turbomachinery noise. The different engine treatments are discussed in greater detail in reference 1. The traded noise level calculated according to FAR Part 36 rules was used as a single noise level comparison criteria.

The impact of TOGW of achieving lower noise levels with engine nacelle noise treatment is shown in figure 12. The corresponding data for the integrated four-engine configuration 5-3 are included in this figure.

Because of the second-segment, engine-out, climb gradient requirement, low-speed aerodynamic data without the leading-edge devices were used for the two-engine airplane configuration. As shown in reference 1, deleting the leading-edge devices gives substantially better lift-to-drag ratio for flap deflections that are less than maximum. The aerodynamic data with the leading edges deployed were used in the previous study of the four-engine airplane configuration 5-3. This configuration was reanalyzed using the "without leading edge device" aerodynamic data. The results as shown in figure 12 indicate a slightly reduced TOGW penalty for achieving lower noise levels. The variations of TOGW with noise level are nearly identical for both the two-engine arrangement 5-4-1 and the integrated-engine arrangement 5-3. For equal community noise levels, the gross weight of the alternate configuration is approximately 2% higher than that of the integrated-engine arrangement.

The range capability of configuration 5-4-1a was evaluated by increasing the total fuel. The results as shown in figure 13 indicate that at the comparable gross weights, the range of the two-engine airplane is approximately 185 km (100 nmi) less than that of the integrated four-engine configuration.

Range: 5560 km (3000 nmi)
Payload: 18 143 kg (40 000 lb)
Design Mach = 1.2
Initial cruise altitude capability: 11 887 m (39 000 ft)
Takeoff field length: ≤ 3505 m (11 500 ft)
BPR = 1.0 engines

Takeoff gross weight,
(lb)

Airframe noise
may be limiting

Increased treatment

With L.E. device
Without L.E. device

Model 5-4-1a   Model 5-3a

Traded noise, ΔEPNdB

FIGURE 12.—IMPACT OF NOISE TREATMENT ON YAWED-WING AIRPLANE
TAKEOFF GROSS WEIGHTS

35
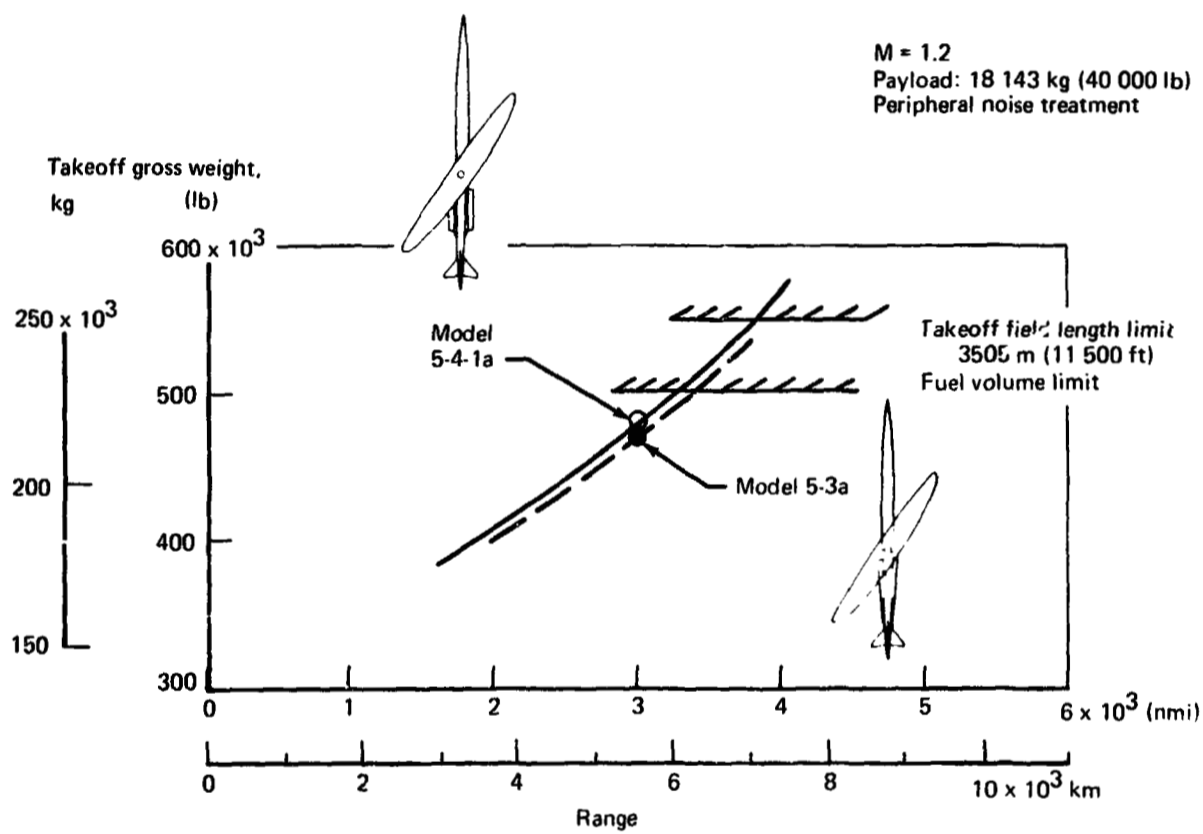
FIGURE 13.—MODEL 5-4-1a RANGE CAPABILITY STUDY

SIZED AIRPLANE DEFINITION—MODEL 5-4-1a

Model 5-4-1a has been developed from the "uncycled baseline" configuration with the aforementioned parametric performance analysis program. The configuration drawing on figure 14, the weight statement on table 7, and the drag summary on table 8 illustrate the configuration that was derived by use of the mission se⁻'ars.

FIGURE 14.--MODEL 5-5 (5-4-1a)

37

TABLE 7.—SIZED AIRPLANE WEIGHT STATEMENT, MODEL 5-4-1a

	Weight, kg	Cg body station, m	Weight, lb	Cg body station, in.
Wing	30 620	56.90	67 500	2240
Horizontal tail	1 210	86.87	2 680	3420
Vertical tail	670	86.61	1 490	3410
Body	25 210	48.51	55 580	1910
Main landing gear	5 900	70.36	13 000	2770
Nose landing gear	2 720	29.21	6 000	1150
Nacelle and strut	6 740	67.31	14 860	2650
Total structure	73 070	55.79	161 110	2197
Engine	11 000	68.32	24 250	2690
Engine accessories				
Engine controls	630	68.33	1 400	2690
Starting system				
Fuel system	2 270	59.94	5 000	2360
Thrust reverser (in nacelle)				
Total propulsion group	13 900	66.96	30 650	2636
Accessory drive system	490	69.33	1 080	2690
Instruments	480	21.08	1 050	830
Surface controls	3 030	59.44	6 690	2340
Hydraulics	1 970	60.96	4 330	2400
Pneumatics	660	60.96	1 450	2400
Electrical	1 810	50.29	2 980	1980
Electronics	1 390	21.59	3 070	850
Flight provisions	430	19.81	950	780
Passenger accommodations	5 570	44.45	12 280	1750
Cargo handling	750	41 91	360	1650
Emergency equipment	340	44.45	740	1750
Air conditioning	1 810	48.51	4 000	1910
Insulation	1 330	41.91	2 930	1650
Auxiliary power unit	610	86.11	1 350	3390
Water ballast system	110	24.89	250	980
Total fixed equipment	20 780	48.43	45 810	1907
Exterior paint	90	50.29	200	1980
Options	1 140	50.29	2 500	1980
Manufacturer's empty weight	108 980	55.75	240 270	2195
Standard and operational items	5 140	44.45	11 330	1750
Operational empty weight	114 120	55.24	251 600	2175
Maximum taxi weight	217 000		478 400	

Note: The weight and balance data for the mission sized configuration 5-4-1a were derived from the uncycled baseline configuration 5-4-1 by the weight scales used in the design selection program. Detailed weight and balance analyses were not performed on this particular configuration.

TABLE 8.—SCALED CRUISE DRAG SUMMARY, MODEL 5-4-1a
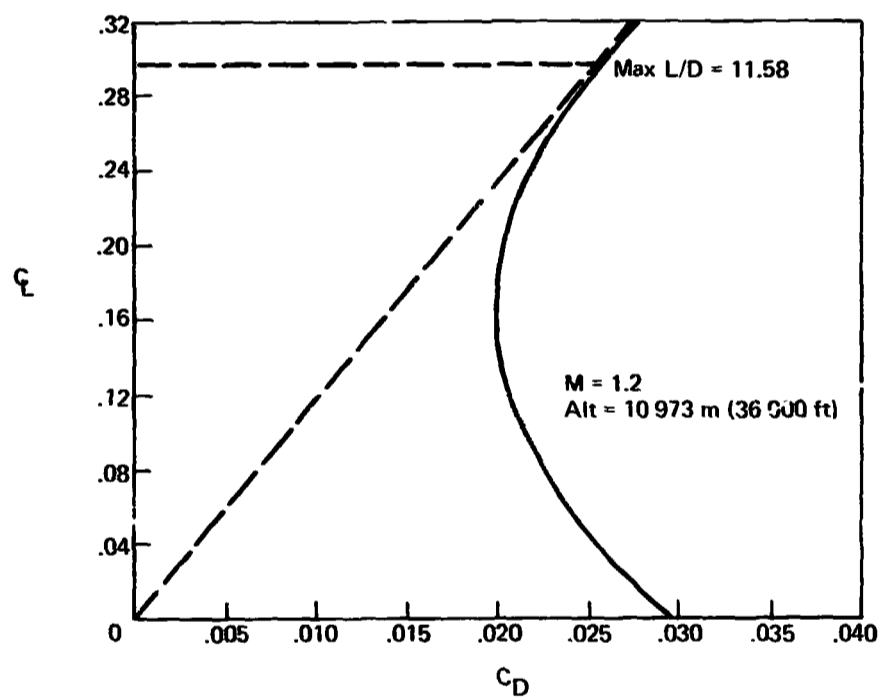
Component	$\dfrac{A_{wet}}{S}$	Ref. length		c_{D_F}	c_{D_W}	Comment
		m	ft			
Body	2.434	86.47	283.7	0.00341	0.00167	"No engine" body
(W·B)$_{interf}$					-.00004	"No engine" wing + body
Wing	1.935	9.60	31.48	.00364	.00163	S_{ref} = 319.6 m^2 (3440 ft^2)
Nacelles + (W·N)$_{interf}$	0.524	14.05	46.1	.00094	.00076	All wave drag relative to "no engine" airplane
Horizontal tail	.170	3.23	10.6	.00038	.00052	S_H = 27.4 m^2 (295 ft^2)
Vertical tail	.159	4.74	15.7	.00033	.00038	S_V = 25.5 m^2 (275 ft^2)
Miscellaneous					.00071	Roughness and protuberances
Struts	.149	16.70	54.8	.00026	.00021	Thrust SLS ÷ 330 500 N (74 300 lb)/engine
Totals	5.371			.00896	.00584	Sized Airplane

39

PLACARD STUDY

The cruise speed placard selected for the initial studies reported in reference 1 was 180 m/s (350 kn) equivalent airspeed (EAS) and Mach 1.2, as shown in figure 15. Based on this selection, the strength design conditions for the yawed wing of model 5-3-2 included:

- Gust loads at 6096 m (20 000 ft) and 180 m/s (350 kn) EAS

- 2.5-g maneuver loads at the design dive speed of 216 m/s (420 kn) EAS

These design points are also indicated on figure 15.

This selected speed placard limited Mach = 1.2 cruise to altitudes above 11 890 m (39 000 ft). This design constraint prohibited the single-fuselage yawed-wing configuration 5-3-2 from achieving the minimum gross weight as indicated by the "eye" on the design selection chart of figure 16. This minimum gross weight design has a cruise altitude that is less than the 11 890 m (39 000 ft) limit.

To allow cruising at Mach 1.2 at a lower altitude, the structural design maximum cruise speed would have to be increased. This could result in an increase in the weight of the wing structure. The object of the placard study was to determine the performance trade between structural weight, engine size, and cruise efficiency for variations in structural design maximum cruise speed.

PLACARD STUDY APPROACH

The wing structural requirements determined from the strength design conditions used for model 5-3-2 development provided a design that was sufficiently strong for all speed-altitude conditions indicated by the structural design speed placard in figure 15. The fact that design gust velocities decrease above an altitude of 6096 m (20 000 ft), as shown in figure 17, was not considered in the previous analyses. The possibility exists, therefore, that the wing structure for model 5-3-2 could be of sufficient strength to permit operation at equivalent airspeeds exceeding 180 m/s (350 kn) at altitudes above 6096 m (20 000 ft).

To explore this possibility, wing structural loads were calculated for a large number of additional gust-critical flight conditions. Based on these loads, the maximum cruise speed-altitude envelope above 6096 m (20 000 ft) was determined for the strength design wing of model 5-3-2. Adding a standard upset and a flutter and divergence margin to this modified maximum cruise speed
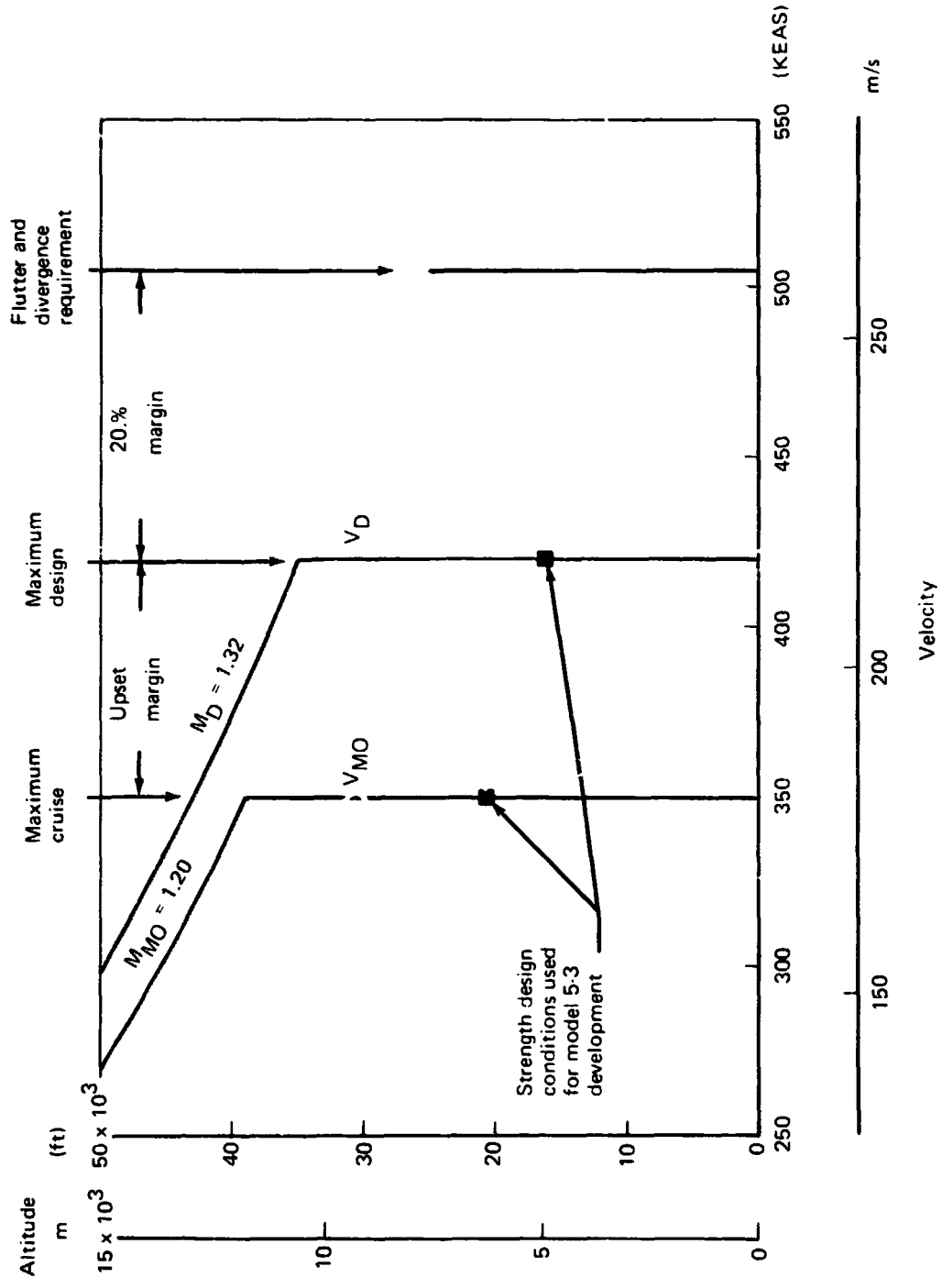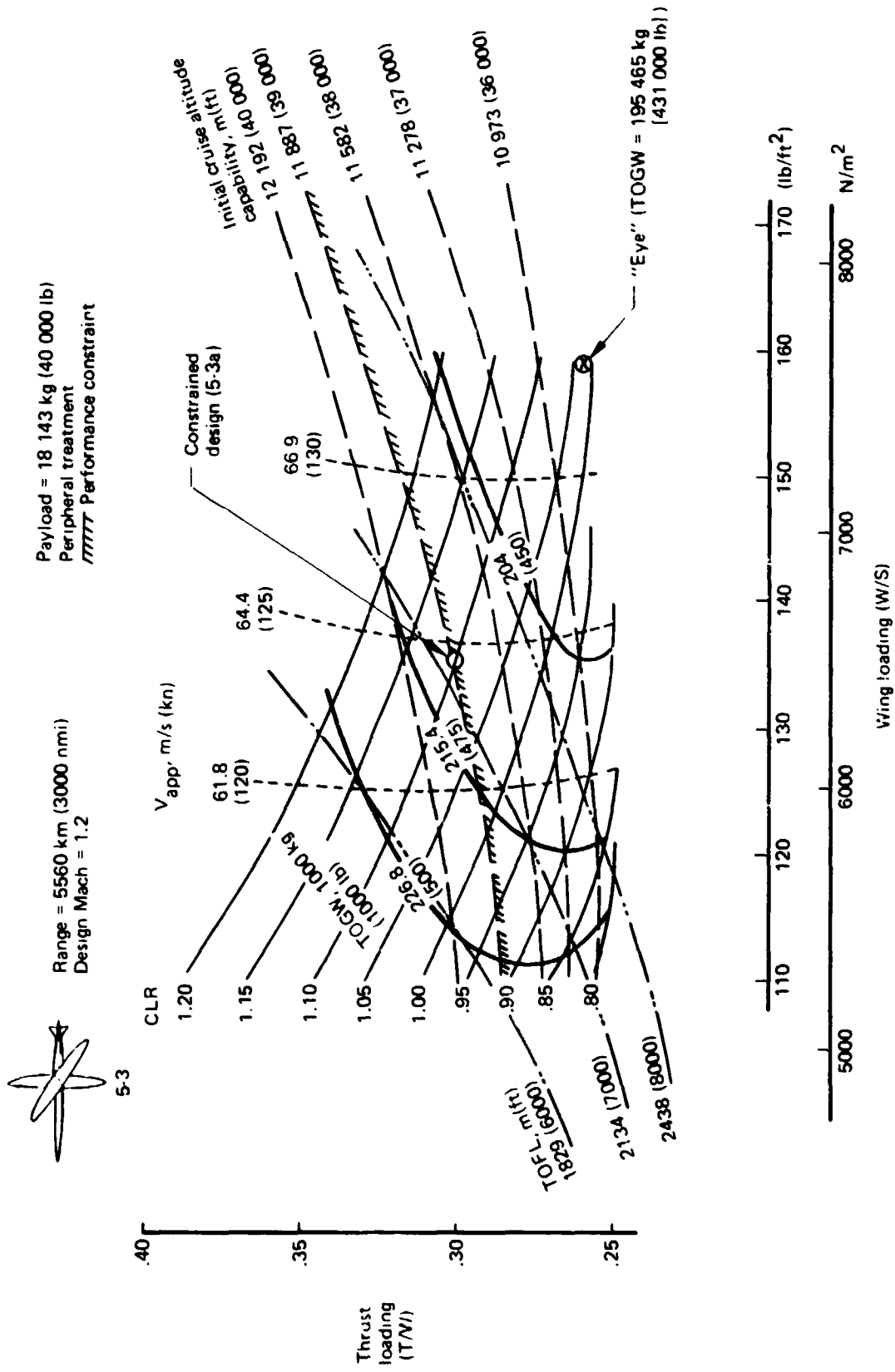
FIGURE 15.—MODEL 5-3 DESIGN SPEED PLACARD
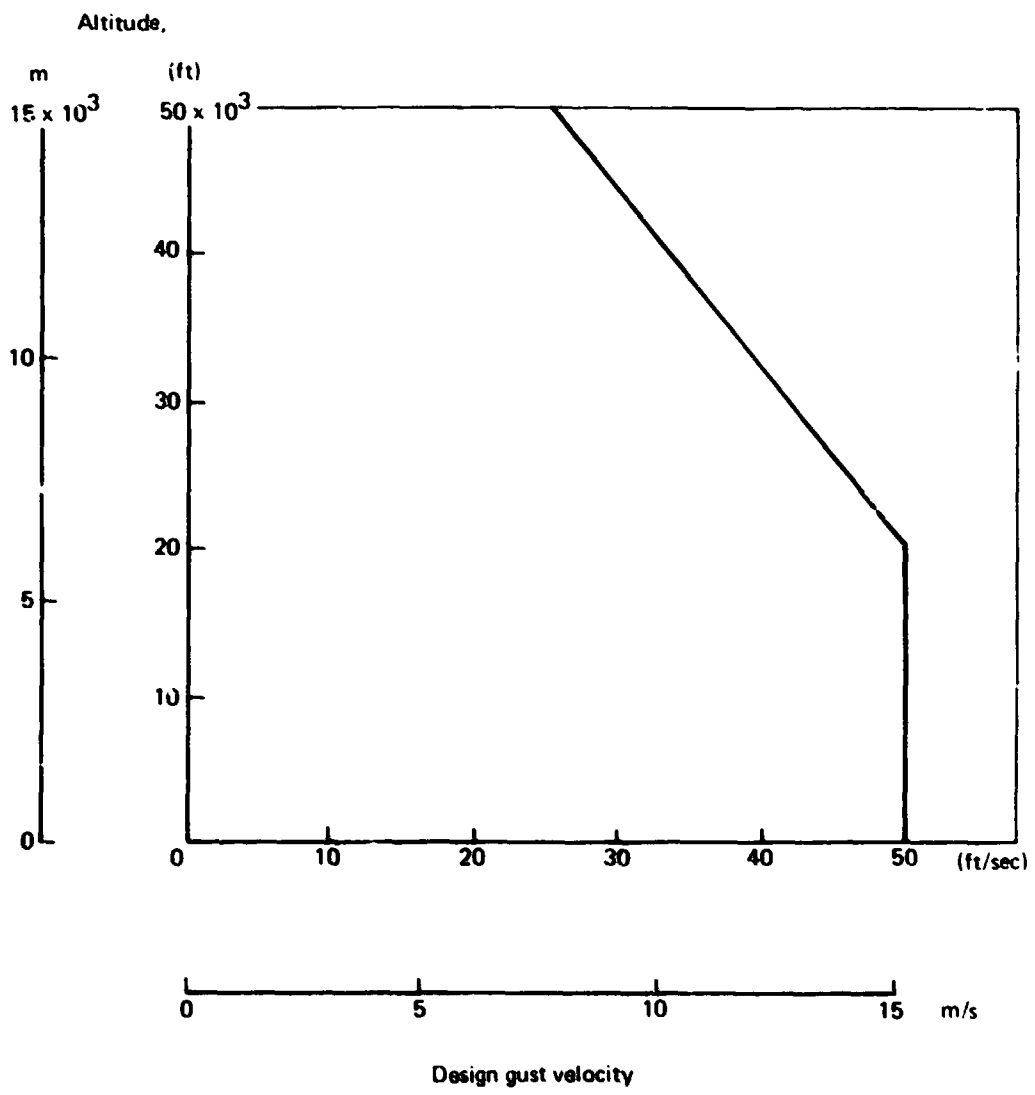
FIGURE 16.—MODEL 5-3 DESIGN SELECTION CHART

43

Altitude,

FIGURE 17. — DESIGN GUST VELOCITIES

resulted in the maximum structural design speeds and the minimum flutter and divergence clearance speeds shown in figure 18.

Calculations were then made to determine the structural requirements corresponding to the 2.5-g maneuver-critical conditions along the modified maximum design speed placard. In addition, the divergence speed of the strength designed wing was calculated to be 590 KEAS, as shown in figure 18.

The results of these investigations indicate that the modified speed placard of figure 18 could be achieved with only a modest increase in the weight of the wing. The wing for model 5-3-2 would require an increase of 200 kg (440 lb) of structural material. This modified speed placard permits Mach 1.2 cruise altitudes as low as 10 360 m (34 000 ft).

GROSS WEIGHT REDUCTION

The design selection charts for model 5-3 (fig. 15) and for the alternate configuration, model 5-4-1 (fig. 10), indicate that the minimum-sized airplane takeoff gross weight decreases for initial cruise altitude limit capability below the initial constrained cruise altitude limit of 11 890 m (39 000 ft). Figure 19 shows this variation of takeoff gross weight with initial cruise altitude capability for both of these configurations. The required takeoff gross weight is reduced as the maximum initial cruise altitude capability is lowered since smaller engines and less wing area are required. The minimum TOGW corresponding to the eye of the design selection chart can be achieved by both models 5-3 and 5-4-1 without violating the modified structural placard limits. However, the two-engine arrangement cannot quite achieve the gross weight indicated by the eye without violating the takeoff field length design constraint of 3505 m (11 500 ft). Cruising at the lower altitudes decreases the takeoff gross weight for the integrated yawed-wing configuration and the alternate configuration by 8% and 6%, respectively.

EFFECT OF DESIGN CRUISE SPEED REDUCTION

The wing designs for all of the airplanes represented by the TOGW curves on figure 19 have sufficient strength to permit cruise at altitudes as low as 10 360 m (34 000 ft). The required gross weights for initial cruise altitude capability above 10 360 m (34 000 ft) could be reduced by lowering the design cruise speeds so that the design speed matches the Mach 1.2 cruise speed. If the design operating speed placard (fig. 18) were reduced by an equal amount at all altitudes a structural weight saving would be realized.
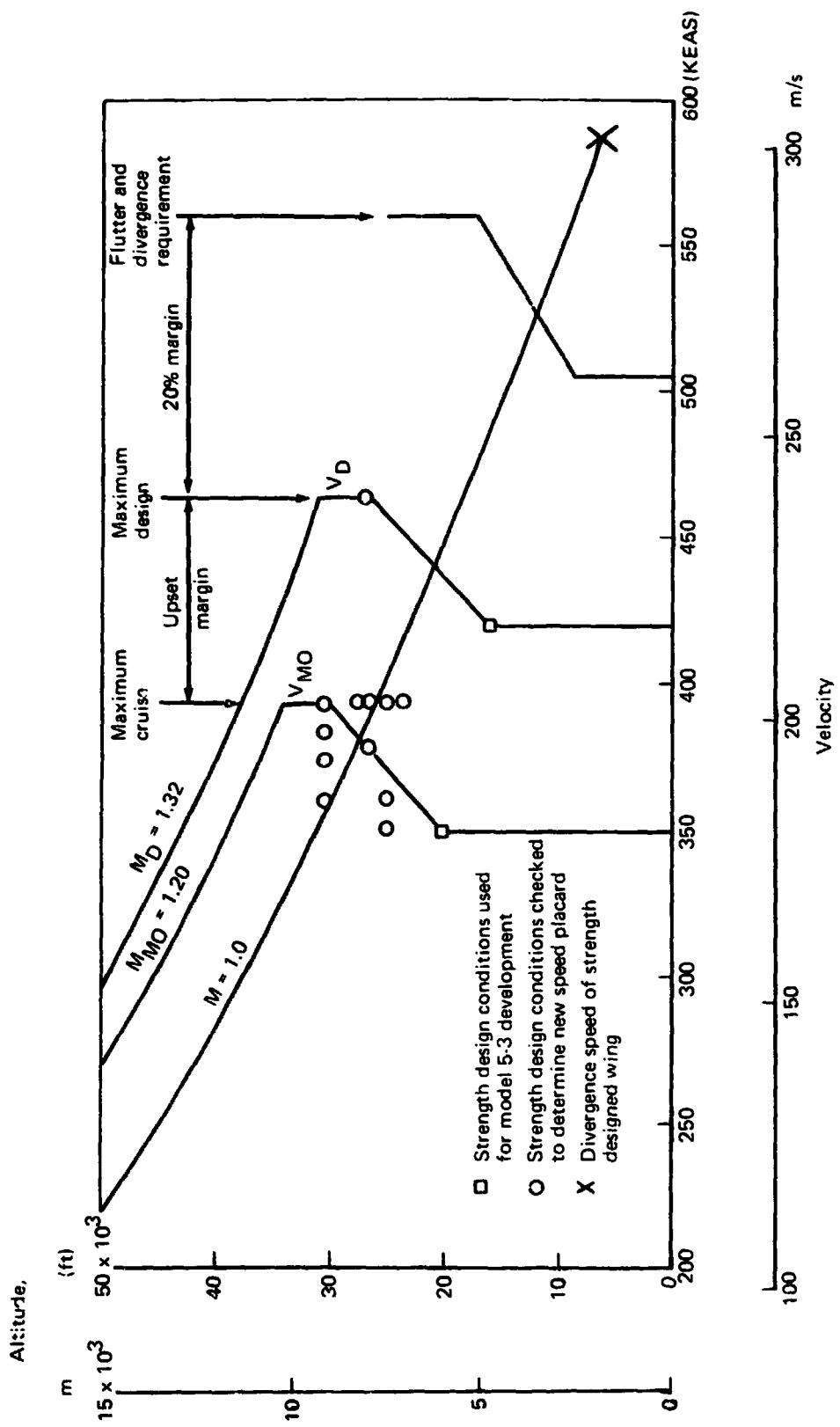
FIGURE 18.—MODIFIED STRUCTURAL DESIGN SPEED PLACARD

Design Mach = 1.2
Payload = 18 140 kg (40 000 lb)
Range = 5560 km (3000 nmi)
Peripheral engine treatment
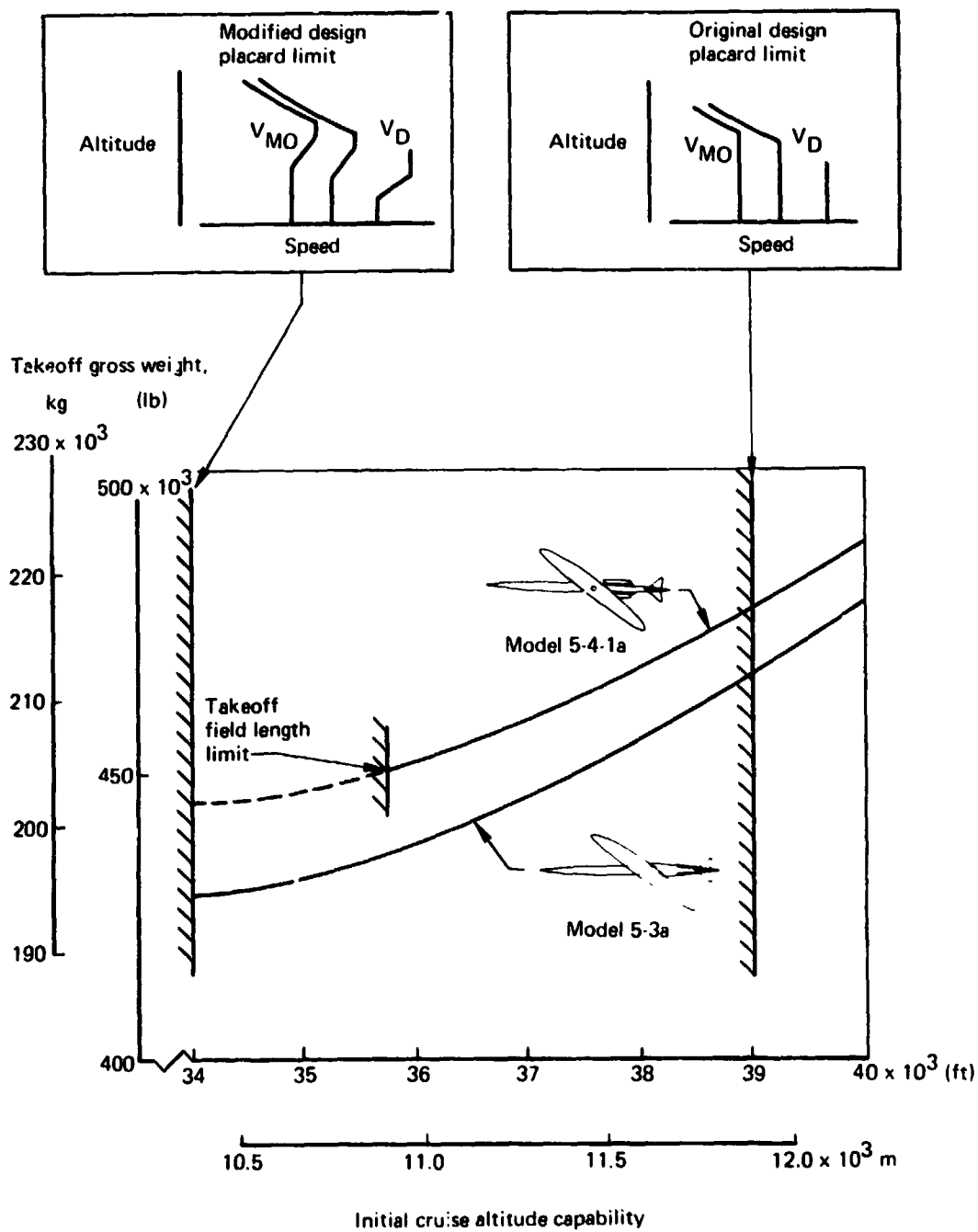
FIGURE 19.—GROSS WEIGHT VARIATION WITH INITIAL CRUISE ALTITUDE CAPABILITY

The effect of lowering the design speeds to match the Mach 1.2 initial cruise altitude capability was investigated by reducing the design speed placard by an equal amount at all altitudes, as shown in the upper left portion of figure 20. The optimum design speeds that provide this match is shown in the upper right portion of figure 20. The wing structural material requirements decreased by 55.8 kg (125 lb) for each 0.5 m/s (1 kn) reduction in the design cruise speed. The wing weight savings produced an even greater reduction in the sized airplane gross weights.

The net effect of reducing the design cruise speed to match the Mach = 1.2 initial cruise speed on the required takeoff gross weight is shown in figure 20. Appreciable reductions in gross weight were achieved. Lowering the design speed has a slight effect on the climb performance. A reduction of the maximum cruise equivalent speed by 12.9 m/s (25 kn) would lower the rate of climb during climb by approximately 6% since the best climb speed is approximately equal to the maximum design cruise speed for commercial transports.

FIGURE 20.—MINIMUM GROSS WEIGHT VARIATION WITH INITIAL CRUISE
ALTITUDE CAPABILITY

AEROELASTIC STABILITY AND CONTROL ANALYSES

During the initial study period reported in reference 1, a dynamic stability analysis was made of a rigid yawed-wing airplane. This previous study showed that aerodynamic coupling causes significant changes in the behavior of the aircraft following a control deflection. With the wing in its yawed position, the response to an elevator deflection was shown to be a combination of pitch, roll, and yaw. Similar coupled motions resulted from aileron and rudder deflections.
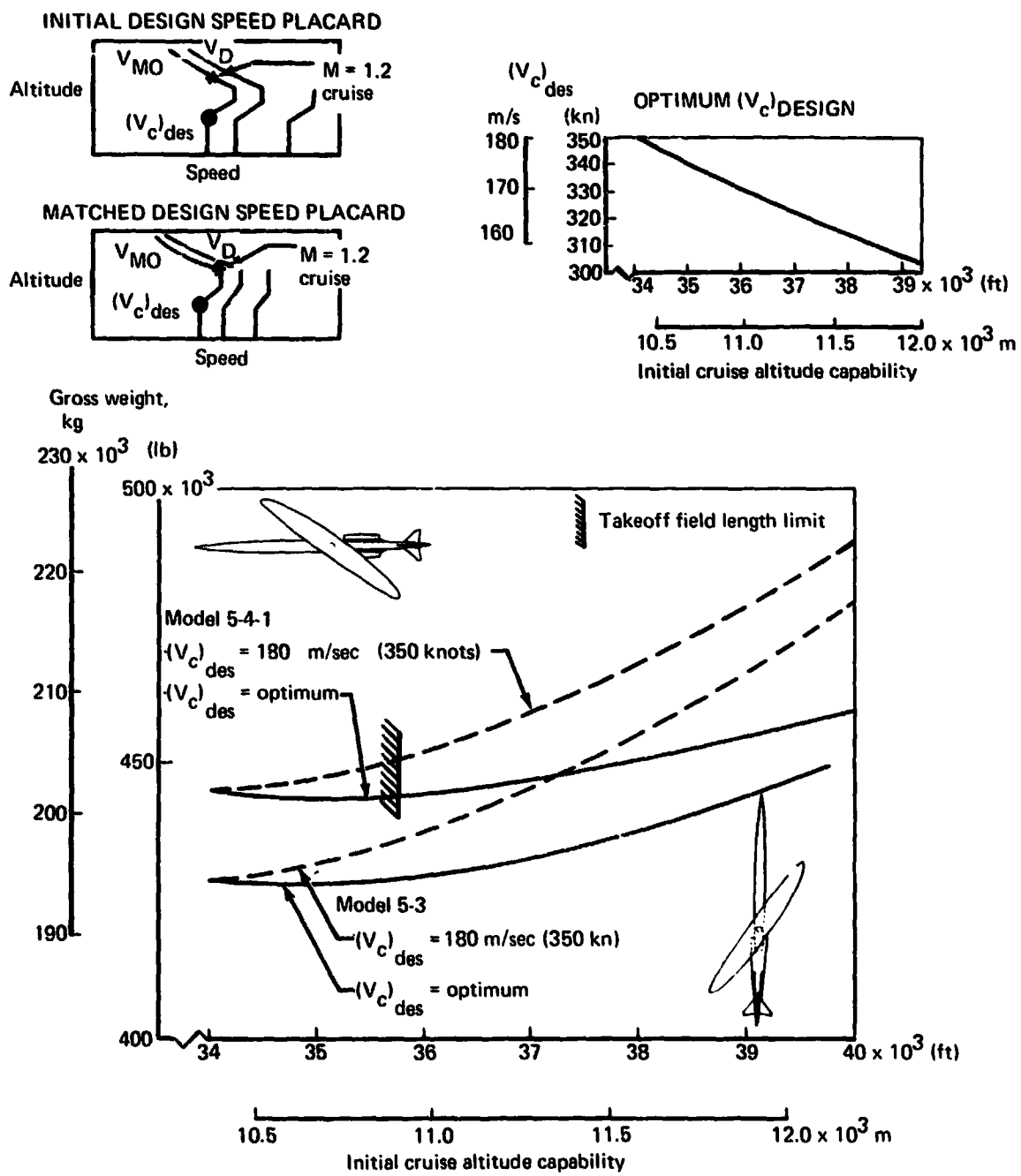
This coupling of the longitudinal, lateral, and directional motions associated with the yawed-wing configuration could present unique problems in the design and mechanization of the flight control system. The effect of flexibility could be significant because of the different aeroelastic tendencies of the forward and aft wings.

The objectives of the study reported herein were to: (1) determine the dynamic response characteristics of the integrated-engine, yawed-wing configuration model 5-3 with a flexible wing but rigid body and empennage; and (2) identify control system characteristics based on the results of the elastic airplane analyses.

STUDY APPROACH

In the previous study (ref. 1) the airplane was assumed to be rigid and the response of the airplane to discrete control inputs was computed. A digital computer program was used to solve the complete six-degree-of-freedom equations of motion. This technique was again employed for this study, with the effects of flexibility included as additions to the basic aircraft stability derivatives. The main configuration difference from the previous study was the wing aspect ratio. The aspect ratio of the wing in the study reported herein was 10.2 instead of the aspect ratio of 12.7 used in the previous study.

The stability and control analysis documented herein and that of reference 1 were conducted with the aircraft left wing forward.

A quasi-steady approach neglecting unsteady aerodynamic effects was used to calculate the wing aerodynamic stability derivatives in both studies. With this approach, the flow over the wing undergoing pitch or roll motions is calculated as the flow on an equivalent cambered and twisted wing. The equivalent wing produces the same normal velocity distribution in straight and level flight as on the actual wing in pitch or roll. This approach is described in references 3 and 4.

In the previous study the wing stability derivatives were calculated by aerodynamic strip theory. The current study used linear aerodynamic planar surface theory. The use of the planar surface theory accounted for the effect of the forward wing upwash on the aft wing. This increased the aerodynamic loading on the trailing wing. The shift in span loading produced a large negative (left-wing-down) rolling moment resulting from an increase in angle of attack and a negative (nose-down) pitching moment. The latter increased the static stability of the airplane. These two stability contributions were not included in the previous study.

The ground rules were the same as for the previous study; namely, that 1985 level technology provides fly-by-wire controls, that adequate control authority exists throughout the flight envelope, and that flight in regions of pitchup or possible lock-in stall is prevented. In addition, the aircraft's stability augmentation system was assumed capable of providing whatever degree of static margin that was needed to stabilize the aircraft. The airplane was flown open-loop in this study; that is, there are no attitude or rate-dependent control deflections tending to stabilize the aircraft, other than by controlling static margin.

The nominal configuration and flight condition for the simulation were:

Mach number	= 0.8
Altitude	= 6096 m (20 000 ft)
Gross weight	= 181 440 kg (400 000 lb)
Wing sweep	= 0.783 rad (45°)
Cg location	= 0.355 $\bar{c}_w$ (body station 57.8 m/2271 in.)

The configuration that was analyzed corresponded to the baseline configuration 5-3 (fig. 21) with the exception that the left wing was yawed forward to be consistent with the original dynamic stability analysis of reference 1.

The aircraft was perturbed from straight and level flight by single-axis control deflections of the following types:

δ_e	pulse and step	(elevator)
δ_r	pulse	(rudder)
δ_a	step	(aileron)

FIGURE 21.—SINGLE FUSELAGE, YAWED WING (8:1 ELLIPSE), MODEL 5-3

Note: The stability analysis has been done with the left wing forward

The responses were analyzed and compared to determine: (a) the rigid vehicle responses, and (b) the effect of wing flexibility on the configuration of this study.

.

STABILITY DERIVATIVE CALCULATION

In addition to the usual stability derivatives exhibited by conventional aircraft with bilateral symmetry, the yawed wing provides derivatives that couple the longitudinal and lateral-directional aerodynamics. The stability derivatives consisted of contributions from the wing, body, empennage, and control surfaces. The body, control surfaces, and empennage contributions were calculated from a combination of linear aerodynamic theory and empirical methods (ref. 5).

The wing rigid derivatives were calculated by linear theory lifting surface methods. Flexibility increments were obtained using a wing structural synthesis program (ORACLE). ORACLE includes an aeroelastic loads analysis based on beam theory and lifting line aerodynamics as described in reference 6.

For the ORACLE program solutions, the wing was divided into twelve chordwise panels (table 9). The wing was assumed to be clamped at the fuselage centerline. Stability derivatives were obtained from summation of loads on the wing panels.

Drag forces on the wing panels were considered only for computing yawing moments. Drag forces were neglected in computing pitching moments. The drag forces were calculated assuming 90% of full leading-edge suction was achieved.

Wing side force components (in the y-direction) were neglected.

The wing was assumed to be weightless except in computations of the vertical acceleration derivatives.

Angle-of-Attack (α) Derivatives

The yawed-wing camber and twist have been designed to produce a symmetric load distribution for the 1-g cruise condition. Angle-of-attack perturbations from the design conditions result in incremental spanwise lift distributions that correspond to the lift generated on a yawed flat wing. Spanwise load distributions are shown in figure 22 for the rigid wing yawed 0.783 rad (45°). The design 1-g elliptic load distribution and the load distribution for a flat yawed elliptic wing are shown. The flat wing distribution represents the shape of the incremental lift that is developed on the rigid wing as the angle of attack departs from the design attitude.

TABLE 9.—WING PANEL WEIGHTS

Wing panel geometry
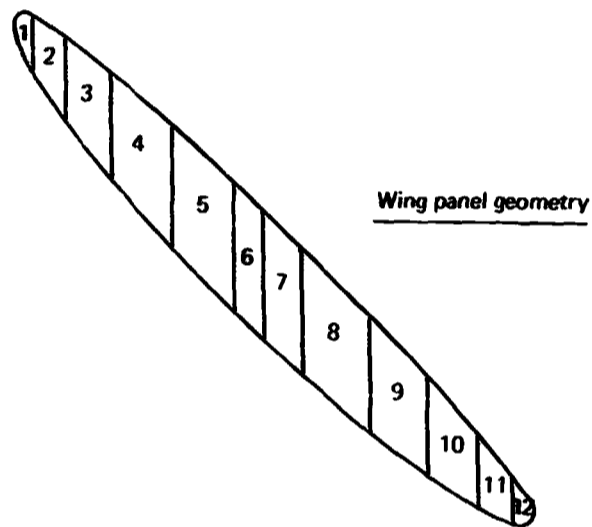
Wing	Panel no.	Structure			Fuel		
		Weight, kg (lb)	Body station, m (in.)	Span fraction	Weight,[a] kg (lb)	Body station, m (in.)	Span fraction
Left	1	150 (331)	36.96 (1455)	0.017	0 (0)	37.03 (1458)	0.016
	2	738 (1 627)	39.29 (1547)	.062	1 149 (2 534)	39.65 (1561)	.072
	3	1 924 (4 242)	42.95 (1691)	.135	4 885 (10 770)	43.18 (1700)	.148
	4	3 634 (8 012)	47.62 (1875)	.235	11 473 (25 294)	47.65 (1876)	.247
	5	5 536 (12 204)	53.04 (2088)	.351	18 472 (40 723)	52.86 (2081)	.365
	6	3 236 (7 135)	57.66 (2270)	.452	11 297 (24 905)	56.62 (2229)	.452
Right	7	3 236 (7 135)	57.91 (2280)	.515	11 297 (24 905)	57.91 (2280)	.518
	8	5 536 (12 204)	60.40 (2378)	.615	18 472 (40 723)	59.56 (2345)	.619
	9	3 634 (8 012)	64.52 (2540)	739	11 473 (25 294)	63.91 (2516)	.739
	10	1 924 (4 242)	69.57 (2739)	.817	4 885 (10 770)	69.0 (2713)	.841
	11	738 (1 627)	73.91 (2910)	.931	1 149 (2 534)	73.38 (2889)	.922
	12	150 (331)	77.11 (3036)	.984	0 (0)	76.68 (3019)	.982

[a]41% of fuel weight used at airplane gross weight = 181 440 kg (400 000 lb)
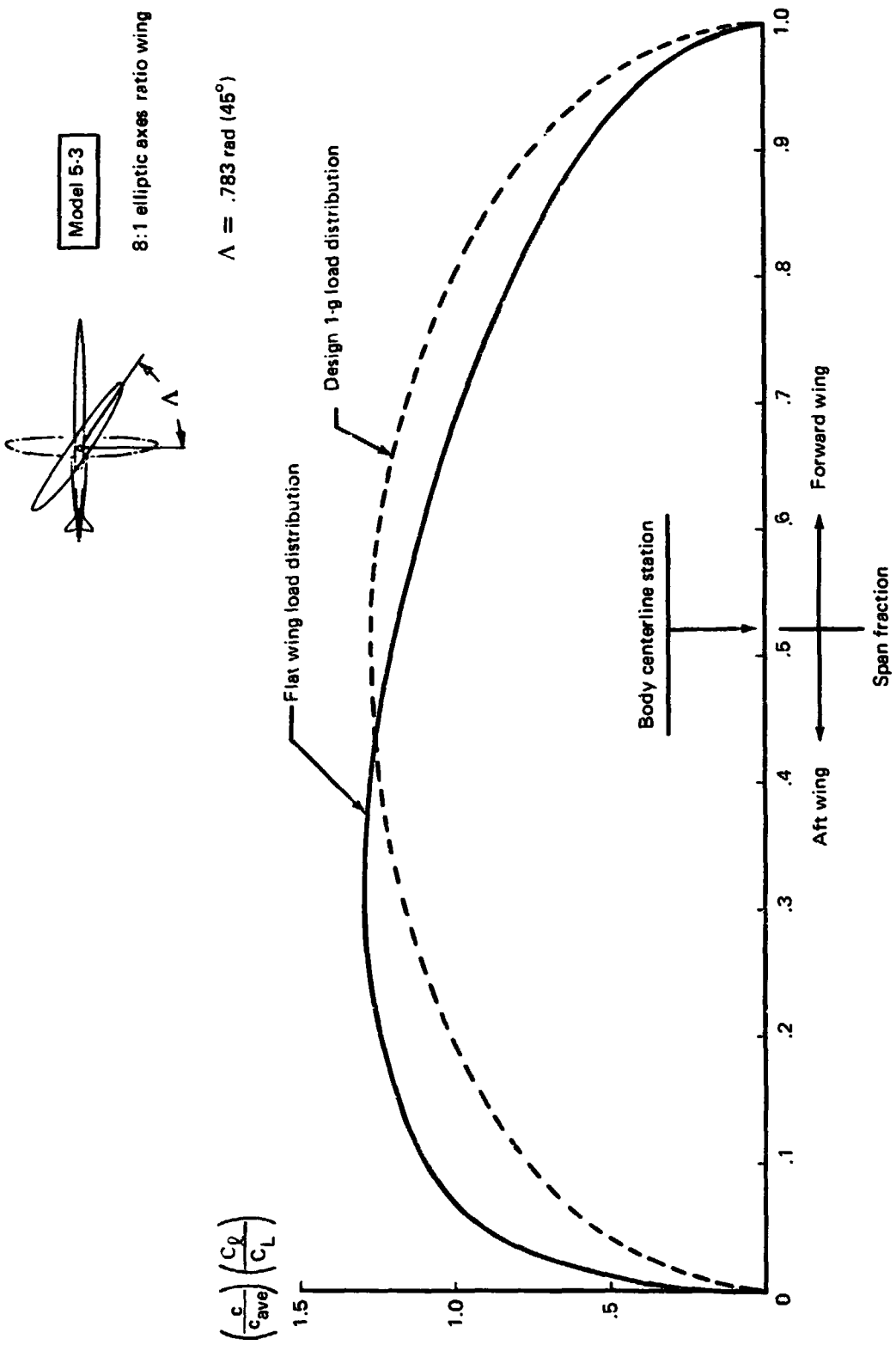
FIGURE 22.— YAWED WING RIGID SPANWISE LOAD DISTRIBUTION

Model 5-3

8:1 elliptic axes ratio wing

$\Lambda = .783$ rad $(45°)$

Design 1-g load distribution

Flat wing load distribution

Body centerline station

Span fraction

Aft wing

Forward wing

$\left(\dfrac{c}{c_{ave}}\right)\left(\dfrac{C_\ell}{C_L}\right)$

56

The unsymmetric shape of the flat wing lift distribution is the result of the upwash field generated by the forward wing increasing the local angle of attack that the aft wing "feels." The effective center of pressure that lies on the aft wing produces pitch and rolling moments as the angle of attack varies.

The bending of the forward wing increases its twist and therefore its lift. Conversely, the bending of the aft wing decreases its twist and therefore its load distribution. Flexibility, therefore, moves the center of pressure forward and inward toward the body. The effects of the upwash field and of flexibility tend to cancel each other.

The variations of lift, C_{z_α}, rolling moment, C_{ℓ_α}, pitching moment, C_{m_α}, and yawing moment, C_{n_α}, were determined from the flat wing load distributions. The yawing moment was calculated from the sectional drag force assuming 90% of full leading-edge suction.

Sideslip (β) Derivatives

Calculations were made for a wing positioned at 0.87 rad (50°) yaw to simulate the sideslip angle of 0.09 rad (5°), and results were compared with those from the wing positioned at 0.783 rad (45°). The cruise load distributions were used in both cases. The effect on the wing lift distribution of crossflow from the body was neglected in determining the flexibility increments.

Aileron Deflection (δ_a) Derivatives

Calculations were made for the rigid and flexible wings, with and without aileron deflection, at constant angle of attack at the wing root.

The ailerons are located on the wings as shown in figure 21. The torsional flexibility near the tips of the wing results in a loss in control effectiveness so that R_E/R_R, the ratio of elastic wing, $C_{\ell_{\delta_a}}$, to rigid wing, $C_{\ell_{\delta_a}}$, is less than 1.0.

Improved roll control effectiveness could be obtained by moving the ailerons inboard where the wing is stiffer in torsion. Also, more wing area would be under the influence of pressure changes caused by aileron deflection.

Vertical Acceleration (n) Derivatives

The wing panel weights data were included for computing these derivatives. The wings were assumed to have 41% of full wing fuel with an airplane gross weight of 181 440 kg (400 000 lb).

The load distributions were obtained for the flexible wing with and without wing structural and fuel weights at a condition of level flight. Differences between these solutions were used to compute the vertical acceleration stability derivatives.

Roll (p) Derivatives

Quasi-steady calculations were made to include the effect of roll rate about the x-axis for the roll derivatives. The angle of attack at each wing panel was changed by:

$$\Delta \alpha_p = \frac{py}{V}$$

where

$\Delta \alpha_p$ = change in angle of attack due to roll rate

p = roll rate

y = spanwise distance from x-axis to the midchord of a wing panel

V = true airspeed

calculations were made for the rigid and the flexible wing, with and without roll rate. The differences in wing loads between these solutions were found. These differences were used to compute C_{z_p}, C_{ℓ_p}, and C_{m_p}.

For computation of C_{n_p}, the fore-and-aft inclination of panel lift vectors with change in local angle of attack must be considered (ref. 3). For positive roll rate, panel lift vectors are inclined forward on the right wing and backward on the left wing.

The change in drag due to roll rate on each wing panel, including inclination of lift vectors, was found from the equation

$$\Delta D = 0.2[L_0(\Delta \alpha_p) + (\Delta L)\alpha_0] - L_0(\Delta \alpha_p)$$

where

ΔD = change in panel drag

L_0 = initial panel lift without roll rate

58

$\Delta \alpha_p$ =   change in panel α due to roll rate

ΔL =   change in panel lift due to roll rate

α_o =   initial panel angle of attack without roll rate

The last term of the equation accounts for the inclination of the lift vectors with roll rate.

Yawing moments were calculated from these panel drag forces to find the value of $C_{n_p^\wedge}$.

Pitch (q) Derivatives

For the pitch derivatives, quasi-steady calculations were made to include the effect of pitch rate about the y-axis. The angle of attack at each wing panel was changed by

$$\Delta \alpha_q = \frac{q(\Delta x)}{V}$$

where

$\Delta \alpha_q$ =   change in angle of attack due to pitch rate

q   =   pitch rate

Δx =   the distance aft from the y-axis to the 75% chord point at the center of the panel

V   =   true airspeed

Calculations were made for rigid and flexible wings, with and without pitch rate, and the differences in wing loads between these solutions were found. These differences were used to compute $C_{z_q^\wedge}$, $C_{\ell_q^\wedge}$, and $C_{m_q^\wedge}$.

For computation of $C_{n_q^\wedge}$, the fore-and-aft inclination of panel lift vectors with change in local angle of attack was considered similarly as for computation of $C_{n_p^\wedge}$. These effects can be neglected on symmetric wings with a pitch rate, but cannot be neglected on a yawed wing. For positive pitch rate (nose up) and left wing forward, panel lift vectors are inclined forward on the right wing and backward on the left wing.

The change in drag due to pitch rate on each panel was found from the equation

$$\Delta D = 0.2[L_o(\Delta\alpha_q) + (\Delta\alpha)\alpha_o] - L_o(\Delta\alpha_q)$$

where

ΔD = change in panel drag

L_o = initial panel lift without pitch rate

$\Delta\alpha_q$ = change in panel α due to pitch rate

ΔL = change in panel lift due to pitch rate

α_o = initial panel angle of attack without pitch rate

The last term of the equation accounts for the inclination of lift vector with pitch rate.

Yawing moments were calculated from these drag forces to find the value of C_{n_q}.

Yaw Rate (r) Derivatives

A positive yaw rate about the z-axis causes the local velocity to increase on the left wing and to decrease on the right wing. The ORACLE program cannot handle a case where the forward velocity varies along the wing span. The r derivatives for a rigid wing were obtained by calculation revisions to the ORACLE solution without yaw rate. The initial spanwise lift distribution was symmetric.

Loads on the wing panels were revised by multiplying by the ratio of dynamic pressure with yaw rate to dynamic pressure without yaw rate. The sideward velocity components at the panels of the swept wing were considered negligible.

ΔC_{z_r} was found as follows:

$$\Delta C_{z_r} = \left(C_{z_r}/C_{z_\beta}\right)_{rigid} \left(\Delta C_{z_\beta}\right)$$

60

where $\left(C_{z_r}/C_{z_p}\right)_{rigid}$ is ratio of C_{z_r} to C_{z_p} for the rigid wing. This was considered acceptable since the incremental lift distribution due to yaw rate was very similar to the incremental lift distribution due to roll rate.

ΔC_{ℓ_r}, ΔC_{m_r}, and ΔC_{n_r} were found by a similar method.

In the method above, it was assumed that the ratios of elastic loads to rigid loads were the same for roll and yaw derivatives.

Wing Stiffness and Weights

Wing bending and torsional stiffnesses used in this study are shown in figure 23.
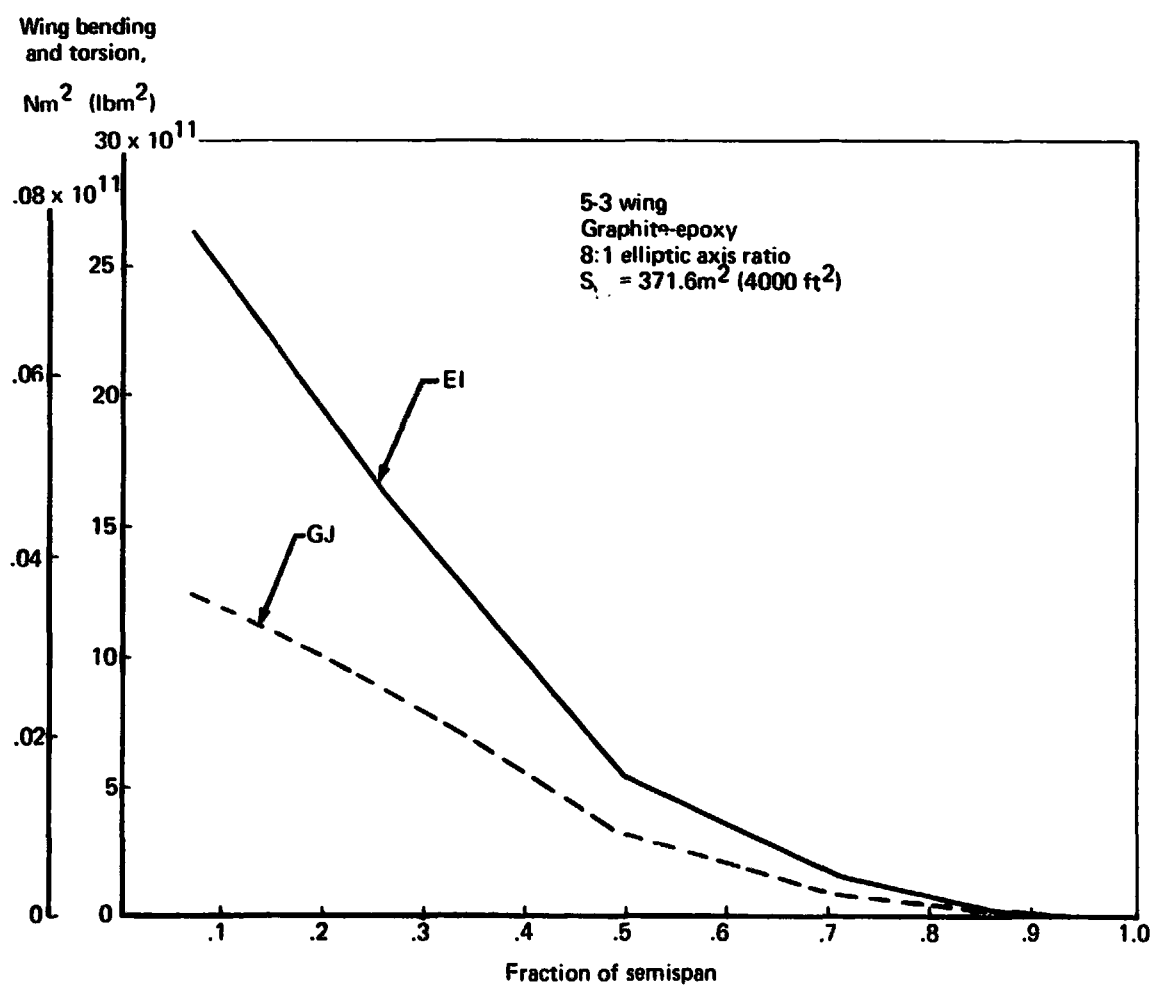

FIGURE 23.—WING STIFFNESS

These stiffnesses are referred to a load reference axis, which is located midway between the front and rear spars of the wing. The location of the wing spars can be seen in figure 21.

Wing panel weights data used in this study are shown in table 9. The wing planform is such that, when pivoted about the point at 50% root chord with left wing forward, the right wing has a longer span than the left wing.

Stability Derivative Values

The calculated stability derivatives for model 5-3 are summarized in table 10. The reference geometry and mass properties data descriptive of the 5-3 configuration are presented in table 11.

The airplane static stability is a combination of the aerodynamic contribution and "artificial" stability provided by the stability augmentation system and varied during this study. The factors comprising the aerodynamic contribution are due to the wing, tail, and wing offset due to pivot location. The aerodynamic center buildup is as shown in the following table (rigid airplane, wing swept $\pi/4$ rad ($45°$)).

$$\bar{X}_{a.c._{wing}} = 0.25\, \bar{c}_{w_{\Lambda=0}}$$

$$\bar{X}_{a.c._{tail}} = 0.122\, \bar{c}_{w_{\Lambda=0}}$$

$$\bar{X}_{a.c._{pivot\ and\ \Lambda=\pi/4\ rad\ (45°)}} = 0.365\, \bar{c}_{w_{\Lambda=0}}$$

$$\bar{X}_{a.c._{SAS}} = 0.40\, \bar{c}_{w_{\Lambda=0}}$$

$$Net\ \bar{X}_{a.c.} = 1.137\, \bar{c}_w$$

The 40% $\bar{c}_w$ aft shift in aerodynamic center by an assumed level of artificial stability augmentation was included so that the study could proceed in a timely manner. Configuration changes that would include the combined effects of changes in center-of-gravity location, tail volume coefficient, and a lesser amount of stability augmentation is the recommended way to achieve the same overall stability level. The center of gravity is $\bar{X}_{cg} = 0.355\, \bar{c}_{w_{\Lambda=0}}$ (fuselage station 2271) so the rigid static margin for this nominal case is 0.782, or 78.2% $\bar{c}_{w_{\Lambda=0}}$.

Significant aspects of wing flexibility contributions to aircraft stability are:

● Reduced static longitudinal stability

TABLE 10.—YAWED WING CONFIGURATION 5-3 AERODYNAMIC DATA (Λ_w = 0.783 RAD (45°), LEFT WING FORWARD)

Notes: M = 0.80, h = 6096 m (20 000 ft)

The aerodynamic coefficients are referenced to the conventional stability axes system

Parameter	Unit	Rigid	Flexible	Parameter	Unit	Rigid	Flexible
C_{x_o}	—	-0.0151	-0.0151	$C_{z_{\hat r}}$	1/rad	0	-0.13
C_{z_o}	—	.047	.068	$C_{m_{\hat r}}$	1/rad	0.379	.436
C_{z_α}	1/deg	-.074	-.079	$C_{y_{\hat p}}$	1/rad	-.044	-.044
C_{m_o}	—	.216	.108	$C_{n_{\hat p}}$	1/rad	-.0085	-.0119
C_{m_α}	1/deg	-.058	-.029	$C_{\ell_{\hat p}}$	1/rad	-.400	-.444
C_{n_α}	1/deg	.000147	-.000131	$C_{z_{\hat p}}$	1/rad	0	.61
C_{ℓ_α}	1/deg	-.00518	-.001	$C_{m_{\hat p}}$	1/rad	-2.66	-3.12
C_{y_β}	1/deg	-.0044	-.0044	$C_{n_{\delta_a}}$	1/deg	0	-.0000011
C_{n_β}	1/deg	.00061	.00059	$C_{\ell_{\delta_a}}$	1/deg	-.00117	-.00115
C_{ℓ_β}	1/deg	-.00123	-.00086	$C_{m_{\delta_a}}$	1/deg	-.00780	-.00785
C_{z_β}	1/deg	-.00398	-.00450	$C_{z_{\delta_a}}$	1/deg	0	.00094
C_{m_β}	1/deg	-.00066	.00189	$C_{y_{\delta_r}}$	1/deg	.00197	.00197
$C_{z_{\hat\alpha}}$	1/rad	-1.03	-1.03	$C_{n_{\delta_r}}$	1 deg	-.00136	-.00136
$C_{m_{\hat\alpha}}$	1/rad	-4.78	-4.78	$C_{\ell_{\delta_r}}$	1/deg	.00026	.00026
$C_{z_{\hat q}}$	1/rad	-2.02	1.58	$C_{z_{\delta_e}}$	1/deg	-.00188	-.00188
$C_{m_{\hat q}}$	1/rad	-27.1	-28.7	$C_{m_{\delta_e}}$	1/deg	-.0088	-.0088
$C_{n_{\hat q}}$	1/rad	-.1630	-.1595	C_{z_n}	1/g	0	.0026
$C_{\ell_{\hat q}}$	1/rad	-2.66	-2.79	C_{m_n}	1/g	r,	-.024
$C_{y_{\hat r}}$	1/rad	.229	.229	C_{ℓ_n}	1/g	0	-.0036
$C_{n_{\hat r}}$	1/rad	-.1650	-.1654	C_{n_n}	1/g	0	.00009
$C_{\ell_{\hat r}}$	1/rad	.0885	.0950				

TABLE 11.—YAWED WING CONFIGURATION 5-3 REFERENCE GEOMETRY AND
MASS PROPERTIES DATA (Λ_w = 0.783 RAD (45°), LEFT WING FORWARD)

Notes: Tail volume coefficients based on $\bar{c}_w/4$ to $\bar{c}_{tail}/4$.
The moments of inertia and products of inertia are
referenced to the conventional body axes system.

Parameter	English units		SI units	
S_w	ft^2	4000	m^2	371.6
$b_\Lambda = 45°$	ft	143	m	43.5
$\bar{c}_\Lambda = 0$	ft	21.5	m	6.55
AR	–	10.2	–	10.2
S_H	ft^2	372	m^2	34.6
S_V	ft^2	347	m^2	32.2
V_H	–	.44	–	.44
V_V	–	.0432	–	.0432
W	lb	400 000	kg	181 440
Cg^a	in.	2271	m	57.8
I_{xx}	$lb\text{-}sec^2\text{-}ft$	5.18×10^6	$kg\text{-}sec^2\text{-}m$	$.712 \times 10^6$
I_{yy}	$lb\text{-}sec^2\text{-}ft$	41.8×10^6	$kg\text{-}sec^2\text{-}m$	5.78×10^6
I_{zz}	$lb\text{-}sec^2\text{-}ft$	46.6×10^6	$kg\text{-}sec^2\text{-}m$	6.43×10^6
I_{xy}	$lb\text{-}sec^2\text{-}ft$	-3.4×10^6	$kg\text{-}sec^2\text{-}m$	$-.469 \times 10^6$
I_{xz}	$lb\text{-}sec^2\text{-}ft$	0.49×10^6	$kg\text{-}sec^2\text{-}m$	$.067 \times 10^6$

[a]Fuselage station

- Reduced pitch/roll coupling

- Reduced lateral stability (dihedral effect)

- Contribution of normal load factor derivatives to longitudinal and lateral stability

MODEL 5-3 DYNAMIC STABILITY BOUNDARY

A significant difference between this study and the previous study (ref. 1) is the inclusion of aerodynamic coupling terms caused by the increased aerodynamic loading that occurs on the trailing wing. This shift in span loading produces a change in rolling moment and nose-down pitching moment with angle of attack. In the reference 1 study, these effects were included only for their influence on steady trim conditions by the addition of a suitable twist distribution. They were not included as perturbation effects (stability derivatives) at that time. The pitch/roll coupling term, C_{ℓ_α} (rolling moment due to angle of attack), and the change in longitudinal stability, C_{m_α}, result from the combined effect of a change in the wing spanwise load distribution (an aerodynamic upwash effect) and the corresponding change in the location of the wing aerodynamic center relative to the fuselage (a geometric effect that is dependent on the wing pivot location).

The incorporation of the pitch/roll coupling term, C_{ℓ_α}, caused a large decrease in overall vehicle stability, compared to the previous study, reference 1. Small control deflections, which previously resulted in mild, convergent oscillations (ref. 1), now caused large and often divergent aircraft motions.

In order to establish the static stability levels required for dynamic stability, a series of responses to an elevator pulse were calculated with the six-degree-of-freedom simulation.

A matrix of responses was obtained by varying pitch/roll coupling at constant static longitudinal stability and by varying static longitudinal stability while maintaining constant pitch/roll coupling. These parametric data are shown in figure 24. The stability boundary was established for the rigid airplane at the longitudinal stability–pitch/roll coupling levels, which produced convergent short-period responses to an elevator pulse. The flexible vehicle does not readily lend itself to this type of evaluation as variations in pitch/roll coupling (achieved by wing pivot relocation) would be reflected in variations of the additional flexible derivatives. The flexible vehicle divergent/convergent boundary, therefore, was established at the level of C_{ℓ_α} representative of the 5-3 configuration by varying static longitudinal stability. Vehicle stability characteristics falling to the left of the boundaries produced divergent time responses while those to the right produced convergent responses.
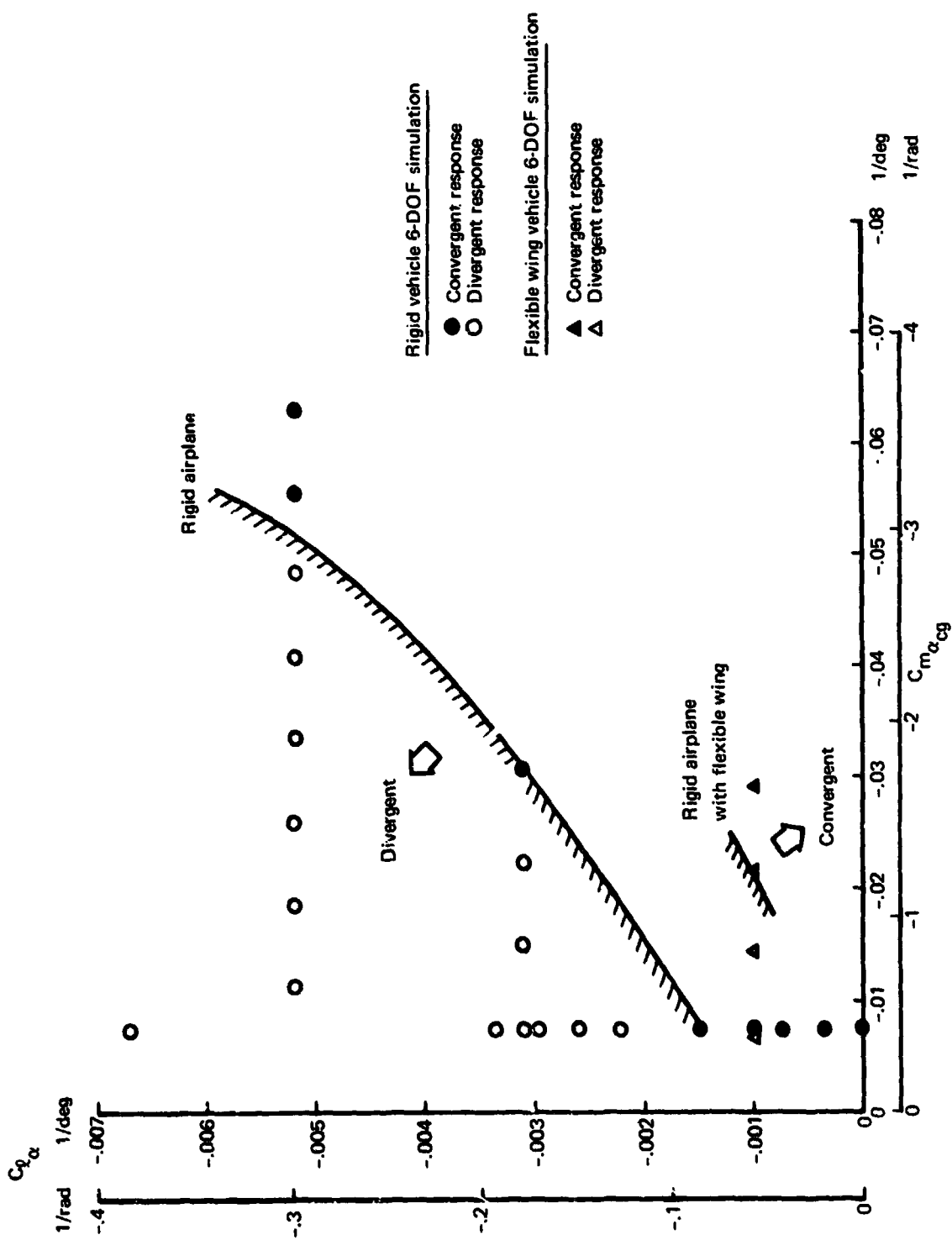
FIGURE 24.—DYNAMIC STABILITY BOUNDARY DEFINITION FOR CONFIGURATION 5-3

The aerodynamic characteristics for the rigid and flexible 5-3 airplane, as initially configured, and those of a NASA/Ames asymmetric wing radio control model (ref. 7) are shown with the stability boundaries of model 5-3 in figure 25. The radio control model stability characteristics were included in this study because of its demonstrated positive dynamic stability characteristics. The radio control model was stable because of its extremely forward cg location, forward wing pivot location, and large tail volume.

These data illustrate that vehicle modifications that reduce the pitch/roll coupling (C_{ℓ_α}) or increase the longitudinal stability (C_{m_α}) allow model 5-3 to achieve positive dynamic stability. The required stability levels may be obtained by forward center-of-gravity location, wing pivot geometry modification, increased horizontal tail volume, and a stability augmentation system. Some examples of configuration changes that would produce stable oscillatory response characteristics for the rigid airplane and for the rigid airplane with flexible wing are as follows:

● Rigid airplane:

1) A 35% $\bar{c}_w$ increase in static margin by a combination of artificial SAS, cg shift, or tail volume increase.

2) A 10% $\bar{c}_w$ forward shift in cg location and a relocation of the wing pivot from 50% c_R to 25%. Movement of the wing pivot forward from 50% c_R to 25% c_R decreases the pitch/roll coupling and thereby reduces the requirements for improved static margin.

● Rigid airplane with flexible wing:

1) A 30% $\bar{c}_w$ increase in static margin by a combination of artificial SAS, cg shift, or tail volume increase.

2) Configuration changes similar to item 2) for the rigid airplane.

As discussed earlier in the establishment of the dynamic stability boundaries, it was not feasible to estimate the effects of both cg and wing pivot location for the flexible airplane; however, it is assumed that the beneficial results obtained through this process on the rigid vehicle will also apply to the flexible vehicle. These data further indicate that the rigid 5-3 vehicle encounters no stability problems at the static stability levels representative of the NASA radio control model.

The results of this parametric study indicate that sufficient pitch stability augmentation greatly improved the response characteristics, so the main part of the study was performed with
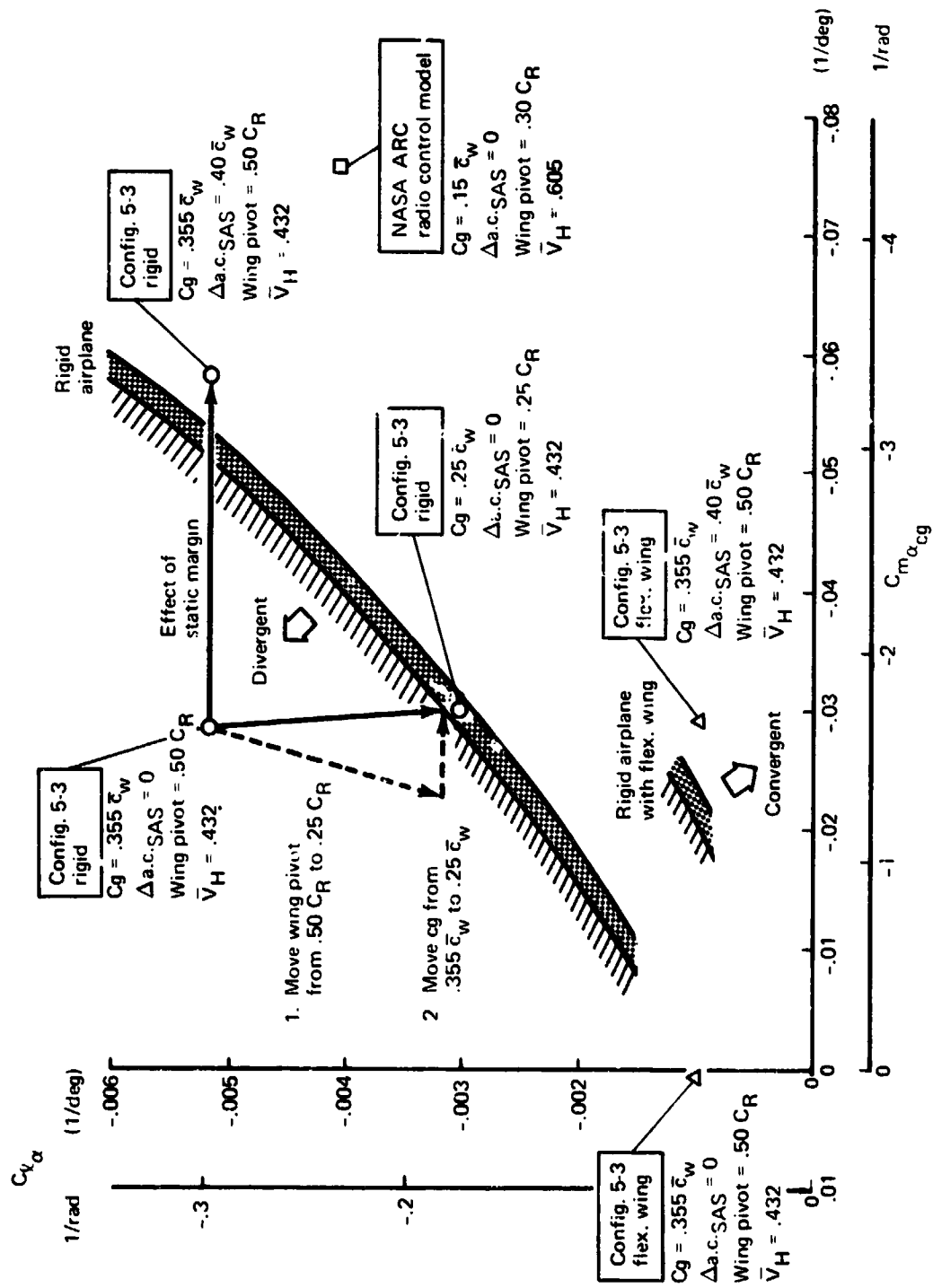
FIGURE 25.—CONFIGURATION MODIFICATION FOR CONVERGENT RESPONSES

68

values of C_{m_α} required for dynamic stability. This required an aft shift in aerodynamic center of 40% $\bar{c}_w$ due to an assumed artificial stability augmentation system. The recommended approach would be to improve the overall stability level of the airplane by design changes. The changes as previously mentioned would include the combined effects of changing the pivot location, center-of-gravity location, tail volume coefficient, and a lesser amount of stability augmentation. These design changes were beyond the scope of the study.

The effects of static lateral stability $\left(C_{\ell_\beta}\right)$ on the dynamic response characteristics of configuration 5-3 were investigated in an abbreviated study. Responses to an elevator pulse were obtained for the rigid airplane by reducing the assumed level of pitch stability augmentation to 20% $\bar{c}_w$. With the nominal value of C_{ℓ_β} identified in table 10, the airplane had an oscillatory divergent response. The dihedral effect, C_{ℓ_β}, was then set to zero and the responses to an elevator pulse were again determined. The results indicated that this reduction in dihedral effect produced a stable, highly damped response with the reduced longitudinal stability level, which previously had exhibited an oscillatory divergent response. However, the reduced level of C_{ℓ_β} produced a steady bank angle as a result of the elevator input.

These results indicate that the response of configuration 5-3 can be improved by a reduction in the dihedral effect, C_{ℓ_β}, that could be achieved by means of a stability augmentation system or configuration changes such as the addition of a ventral fin. These response data are included in the following sections.

DYNAMIC RESPONSES FOR MODEL 5-3

Table 12 presents the matrix of time responses documented in this study.

The influence of static longitudinal stability on the dynamic stability of the response is demonstrated by figures 26 and 27. Comparison of figures 27 through 30 versus figures 31 through 36 shows the influence of wing flexibility. The influence of dihedral effect $\left(C_{\ell_\beta}\right)$ is shown in figures 37 and 38.

Divergent short-period time responses to an elevator pulse are shown in figure 26 for the rigid vehicle, with static longitudinal stability augmented by 30% (0.30 $\bar{c}_w$). Comparison of these data with the convergent responses of figure 27 for the rigid vehicle with 40% augmentation demonstrates the effect of increased longitudinal static margin on vehicle stability. As stated previously, the assumed stability augmentation level was employed to perform the stability analysis. Configuration modifications such as those previously identified are recommended.
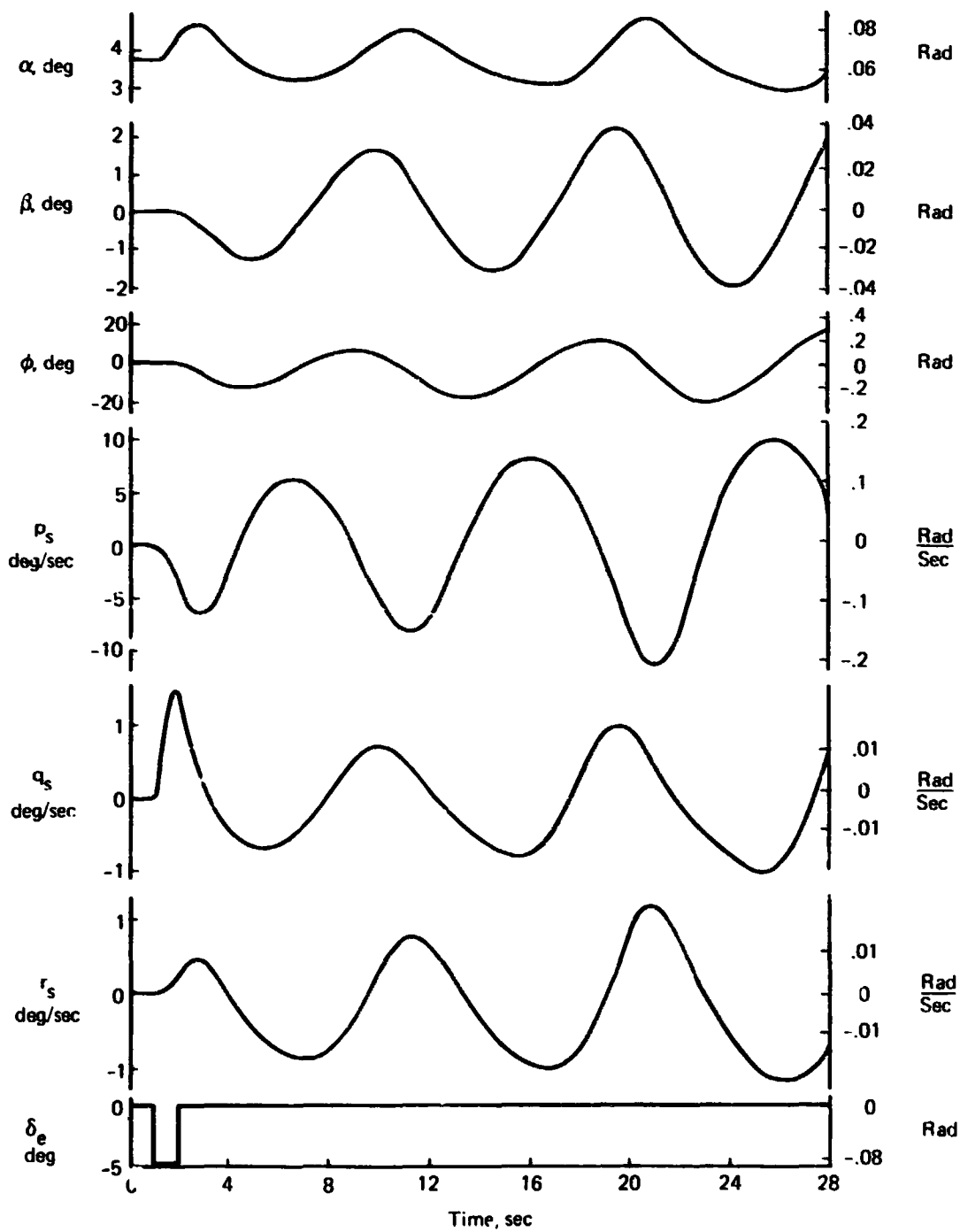
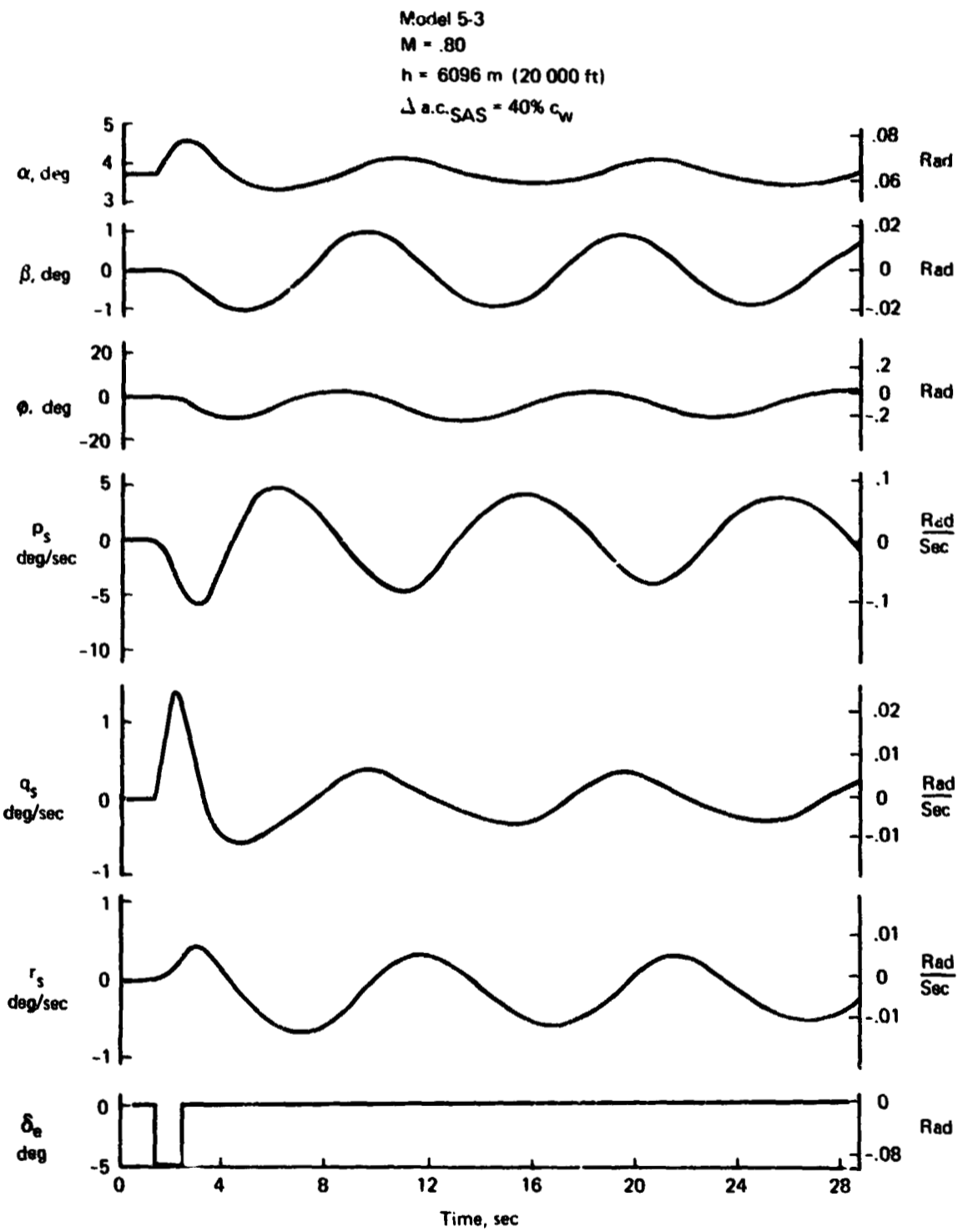FIGURE 26.- RIGID AIRPLANE, DIVERGENT RESPONSE TO ELEVATOR PULSE

FIGURE 27.—RIGID AIRPLANE, RESPONSE TO ELEVATOR PULSE (SHORT PERIOD)

71

TABLE 12.—TIME RESPONSE MATRIX

Config	Stab. aug	Control surface input					
		$\delta_e$pulse short period	δ_e pulse phugoid	δ_r pulse	$\delta_{e_{step}}$	$+\delta_{a_{step}}$	$-\delta_{a_{step}}$
		Figure no.					
Rigid	30%	26	–	–	–	–	–
Rigid	40%	27	–	28	29	30	–
Flexible	40%	31	32	33	34	35	36
Rigid[a]	20%	37	–	–	–	–	–
Rigid[a]	20%	38	–	–	–	–	–

[a]Lateral stability evaluations

Figures 28, 29, and 30, respectively, present time responses for the rigid vehicle with 40% stability augmentation to rudder pulse, elevator step, and aileron step control surface inputs. These data, together with those of figure 27, establish the rigid vehicle responses in order to illustrate the effect of the flexible wing upon vehicle dynamic stability.

Flexible vehicle (wing flexibility only is included) time responses to elevator pulse (short-period motion), elevator pulse (phugoid motion), rudder pulse, elevator step, positive aileron step, and negative aileron step control surface inputs are shown, respectively, in figures 31 through 36. The flexible vehicle responses are those of the basic airplane w ' longitudinal stability augmented by 40% so that the flexible wing contribution to stability ectly evidenced by comparison of the above figures with figures 26 through 30.

Comparison of figures 27 (rigid airplane) and 31 (rigid airplane with flexible wing) demonstrates that an effect of wing flexibility on the short-period longitudinal response due to a 0.087 rad (5°) elevator pulse is to increase vehicle damping and reduce the magnitude of longitudinal and lateral-directional attitude and rate excursions. Wing flexibility reduced pitch/roll coupling subsequent to the elevator pulse by approximately 50%, as evidenced by the reduction in roll response.

The flexibility contribution to the dutch roll response resulting from a 0.087 rad (5°) rudder pulse is shown in figures 28 (rigid) and 33 (flexible). The flexible vehicle is seen to be more highly
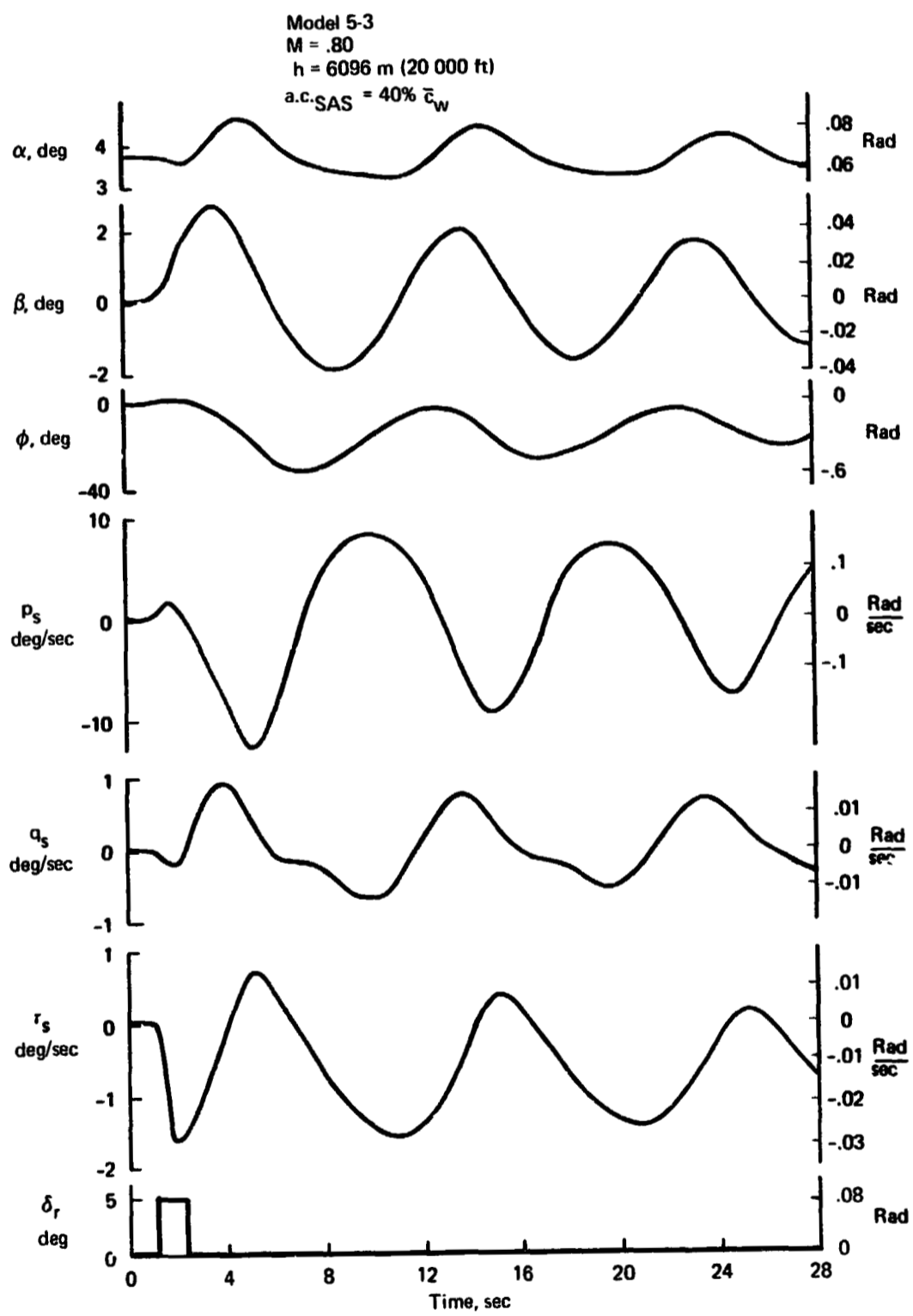
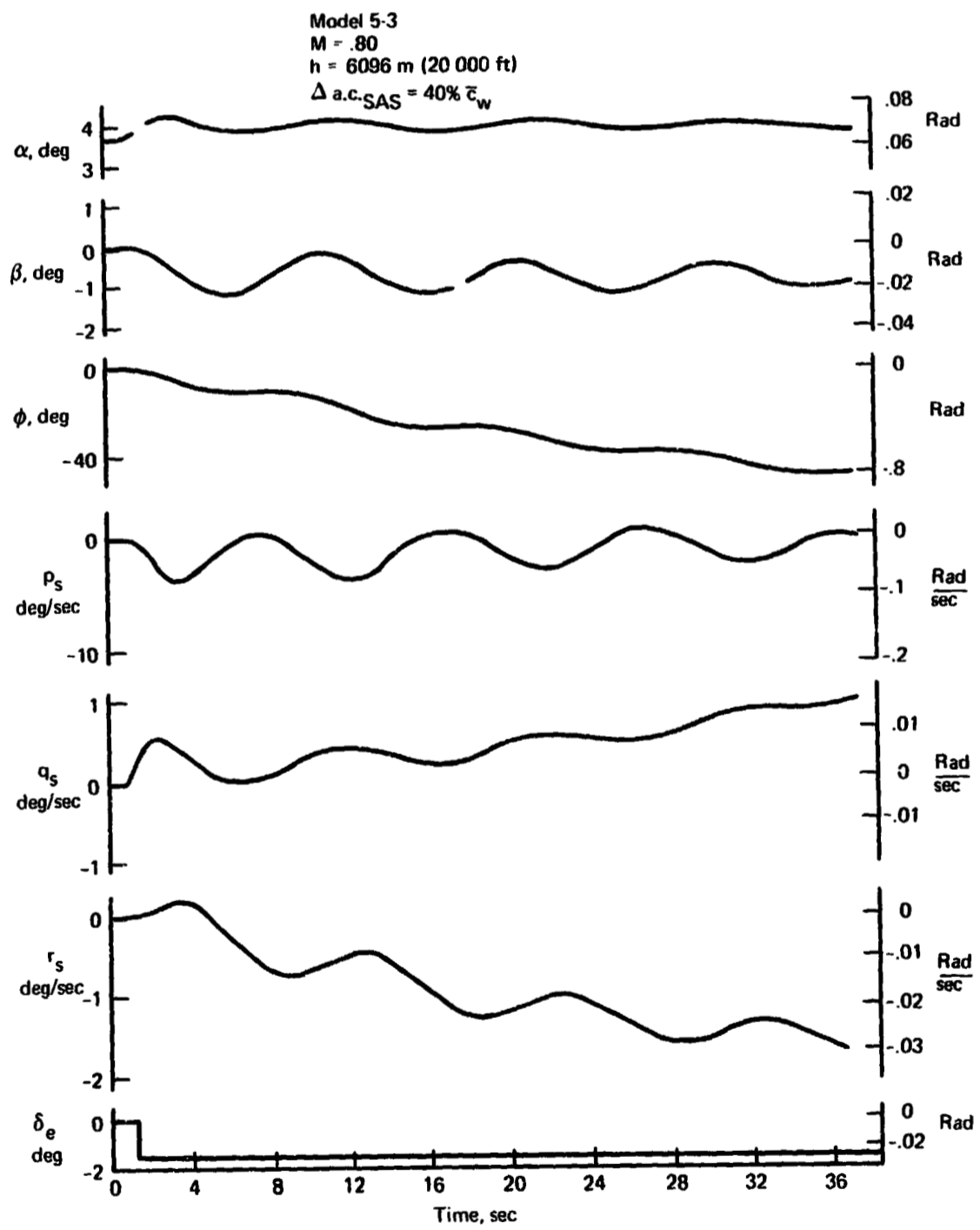FIGURE 28.—RIGID AIRPLANE, RESPONSE TO RUDDER PULSE
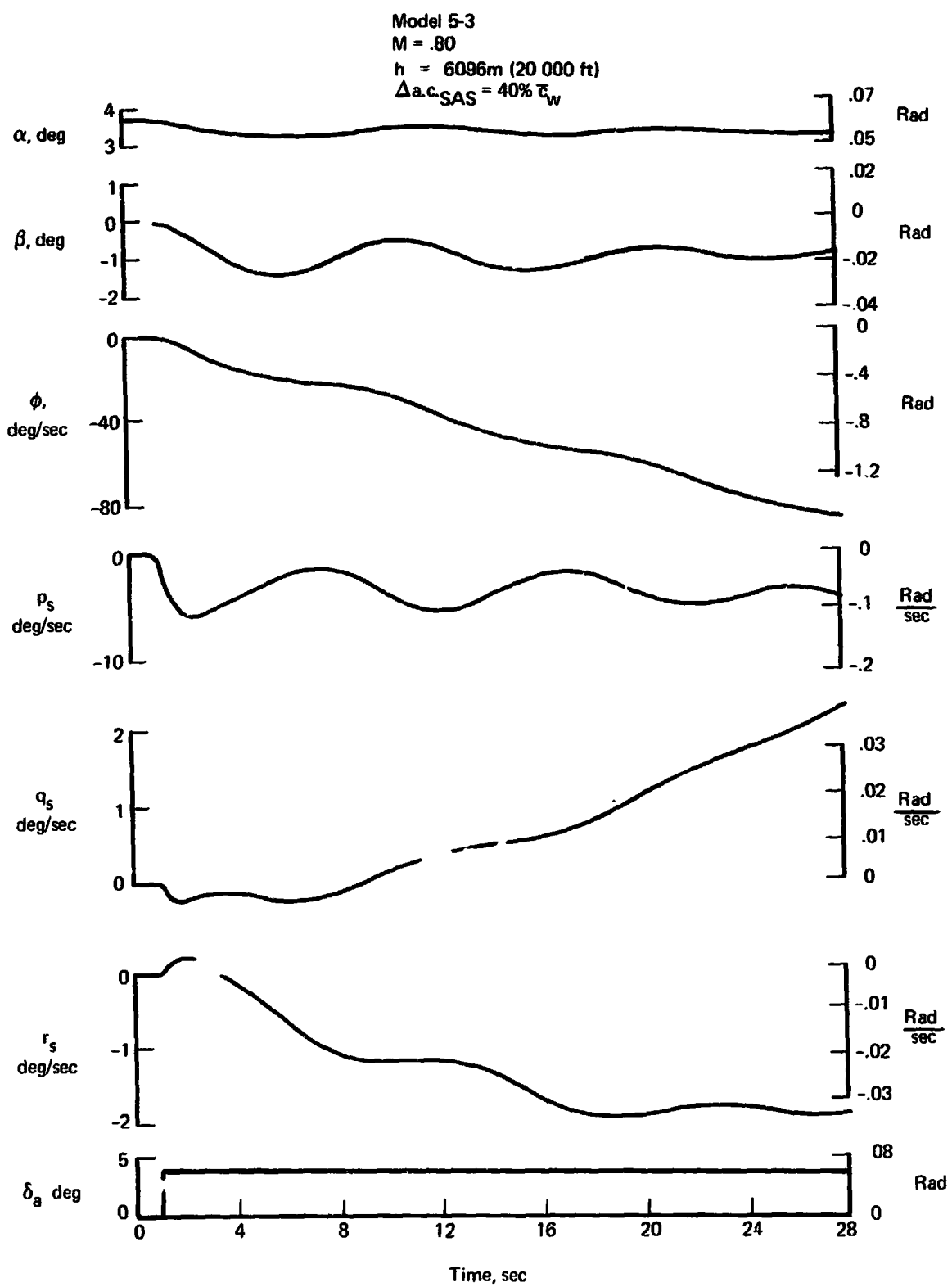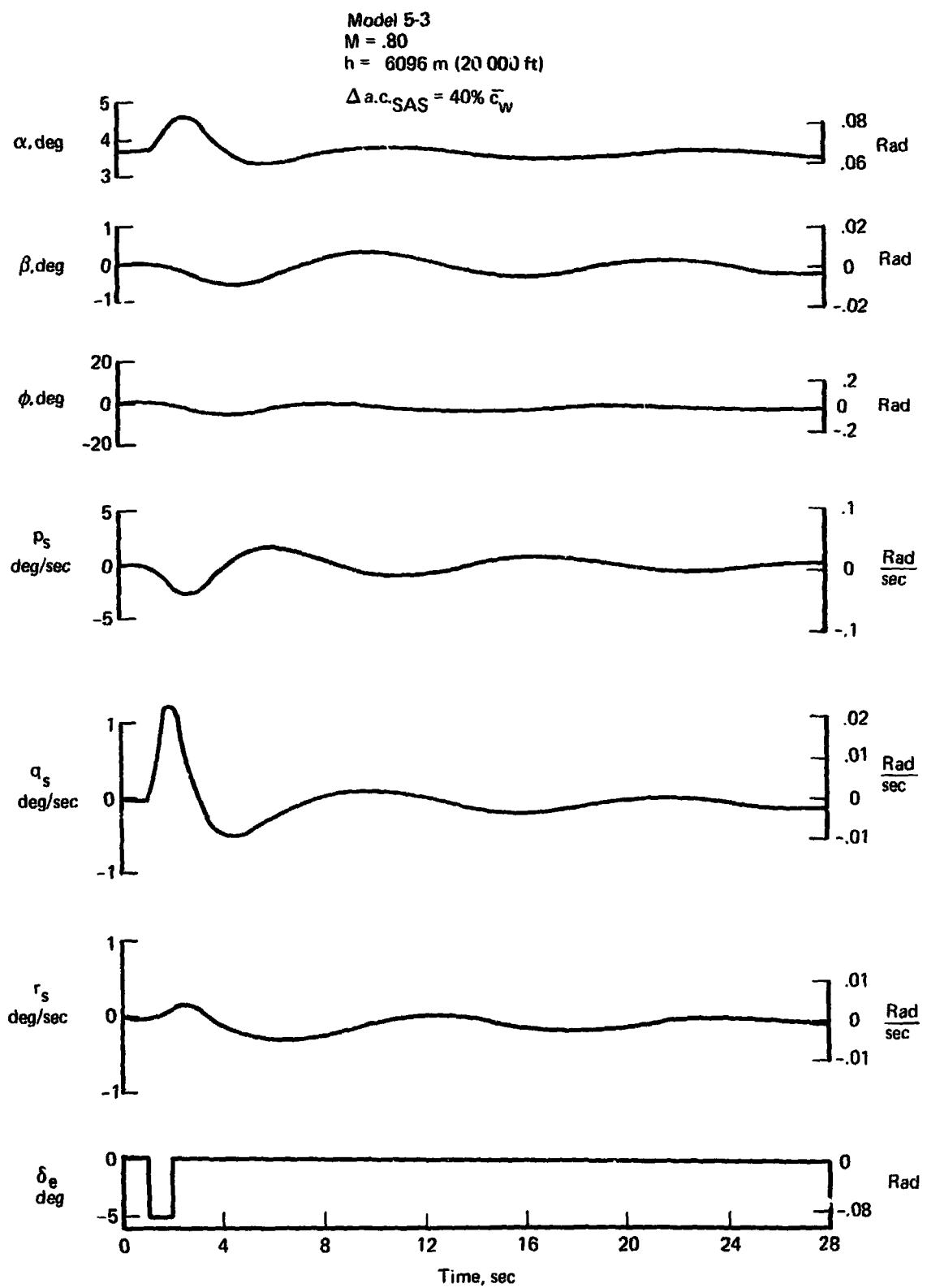
73

FIGURE 29.—RIGID AIRPLANE, RESPONSE TO ELEVATOR STEP

FIGURE 30.—RIGID AIRPLANE, RESPONSE TO POSITIVE AILERON STEP

FIGURE 31.—RIGID AIRPLANE WITH FLEXIBLE WING, RESPONSE
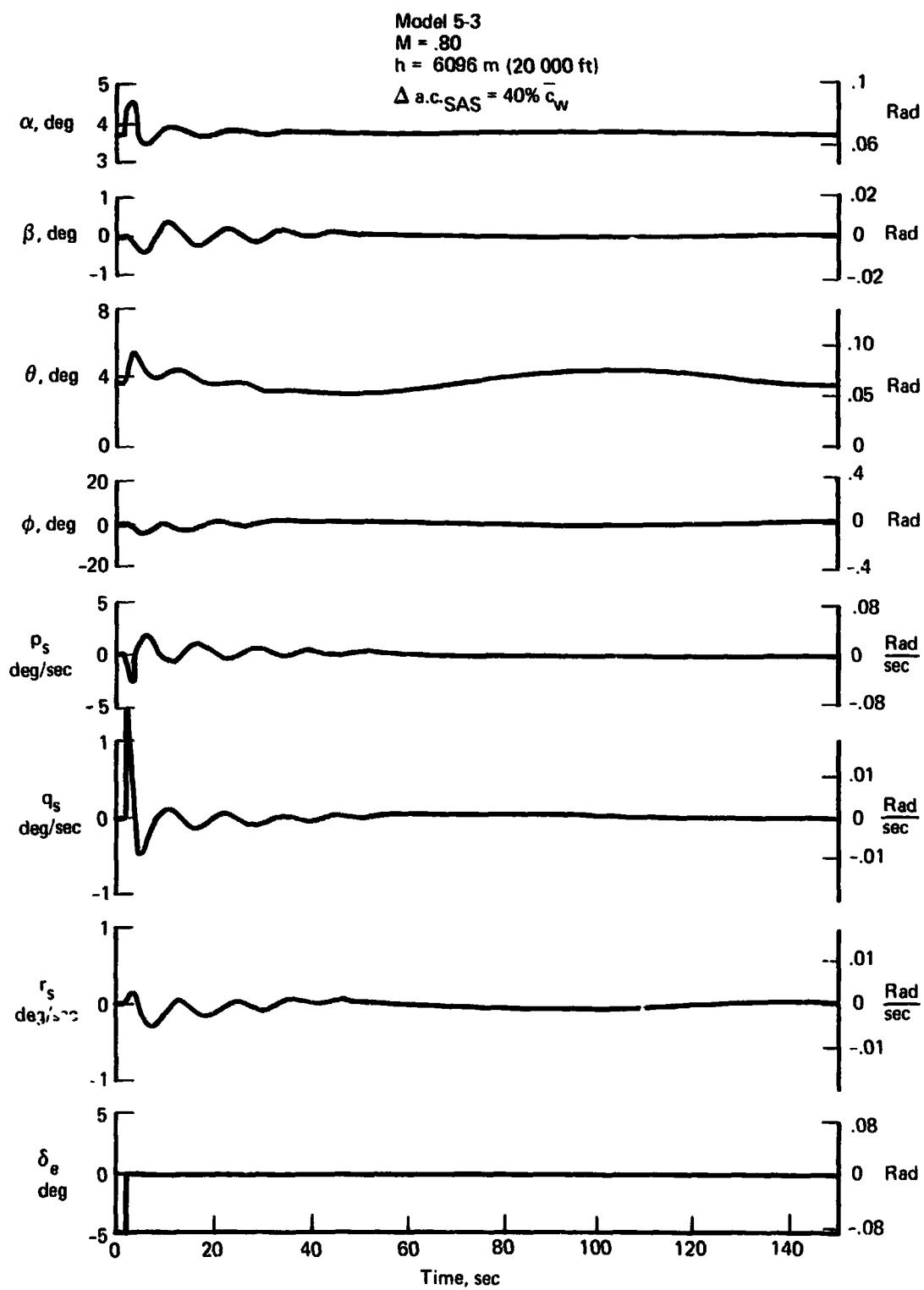TO ELEVATOR PULSE (SHORT PERIOD)

FIGURE 32.—RIGID AIRPLANE WITH FLEXIBLE WING, RESPONSE TO ELEVATOR PULSE
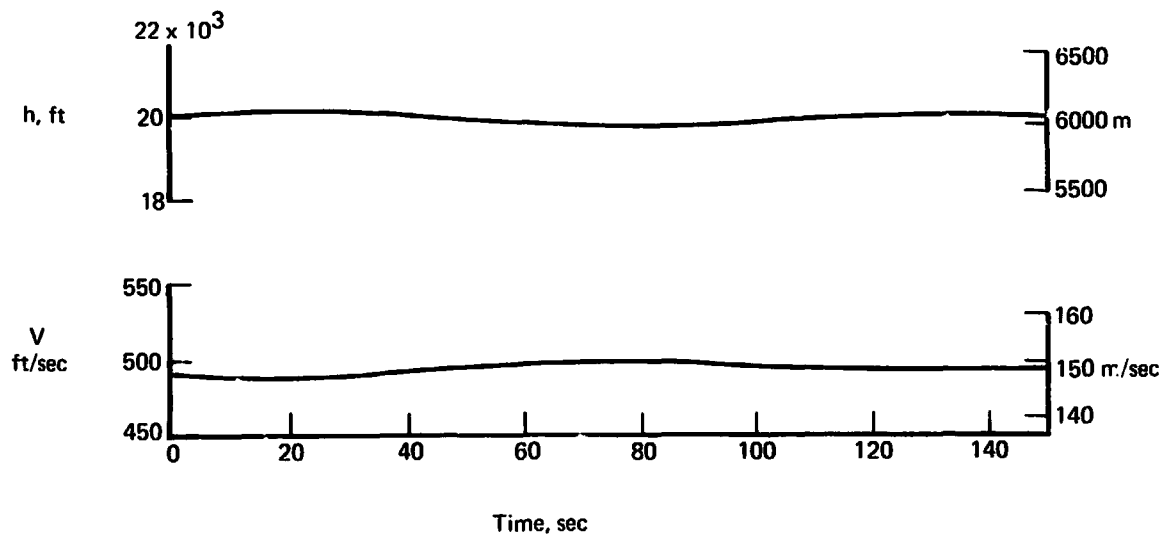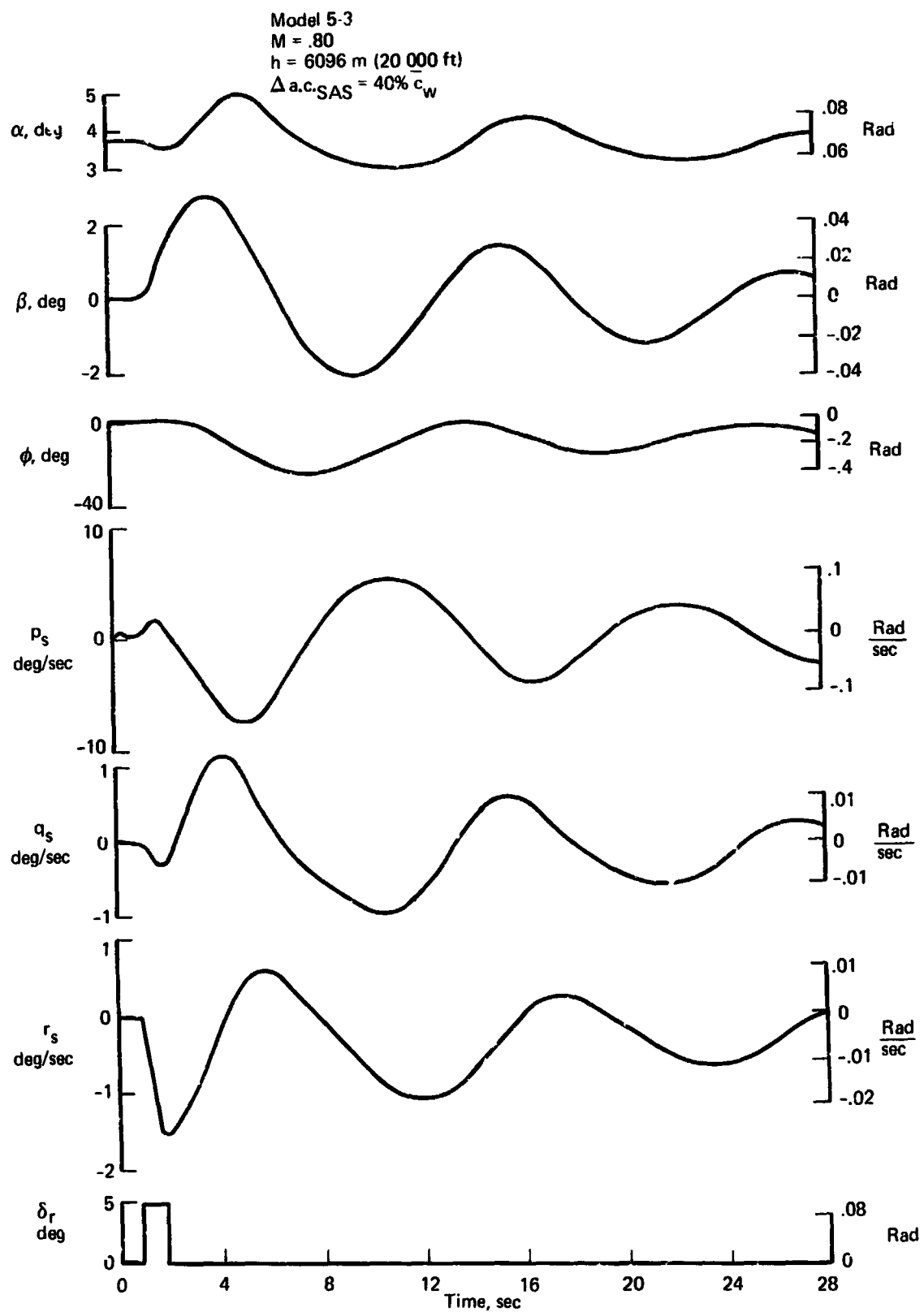(PHUGOID)

FIGURE 32.—(CONCLUDED)

FIGURE 33.—RIGID AIRPLANE WITH FLEXIBLE WING, RESPONSE TO RUDDER PULSE
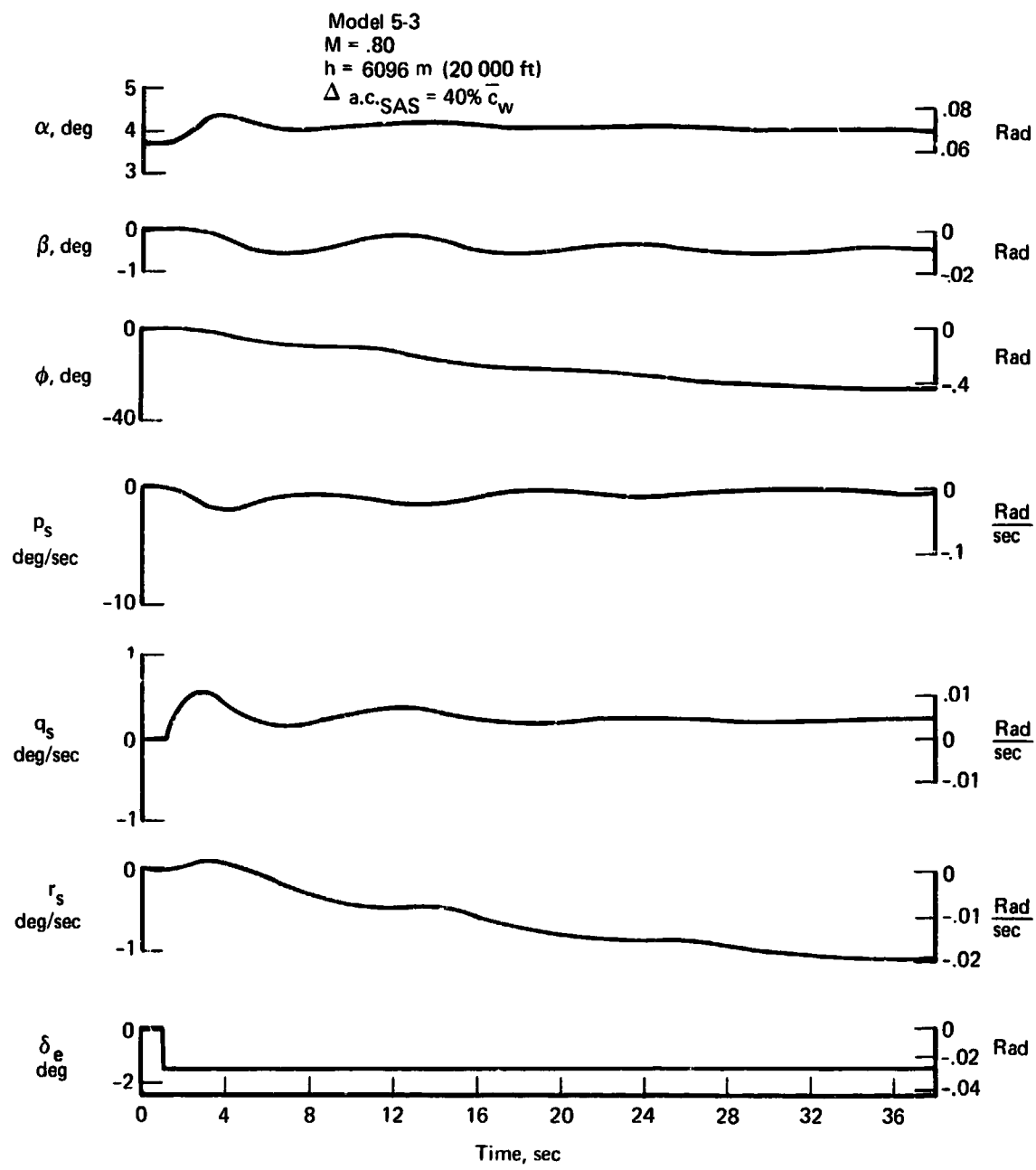
79

FIGURE 34.—RIGID AIRPLANE WITH FLEXIBLE WING, RESPONSE TO ELEVATOR STEP

80
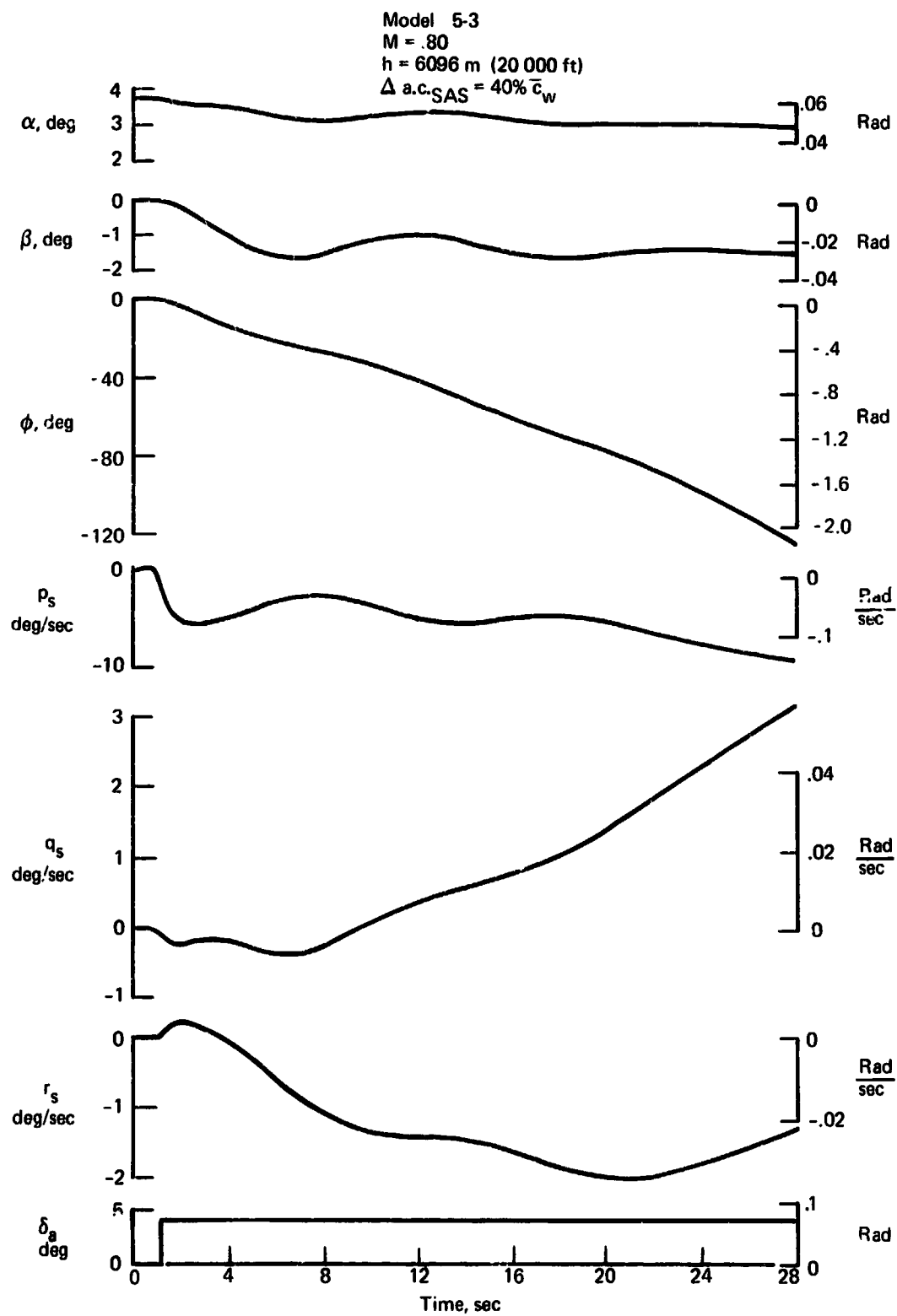
FIGURE 35.—RIGID AIRPLANE WITH FLEXIBLE
WING, RESPONSE TO POSITIVE AILERON STEP

81

Model 5-3
M = .80
h = 6096 m (20 000 ft)

Δ a.c.$_{SAS}$ = 40% $\bar{c}_w$

α, deg

β, deg

ϕ, deg

p_s deg/sec

q_s deg/sec
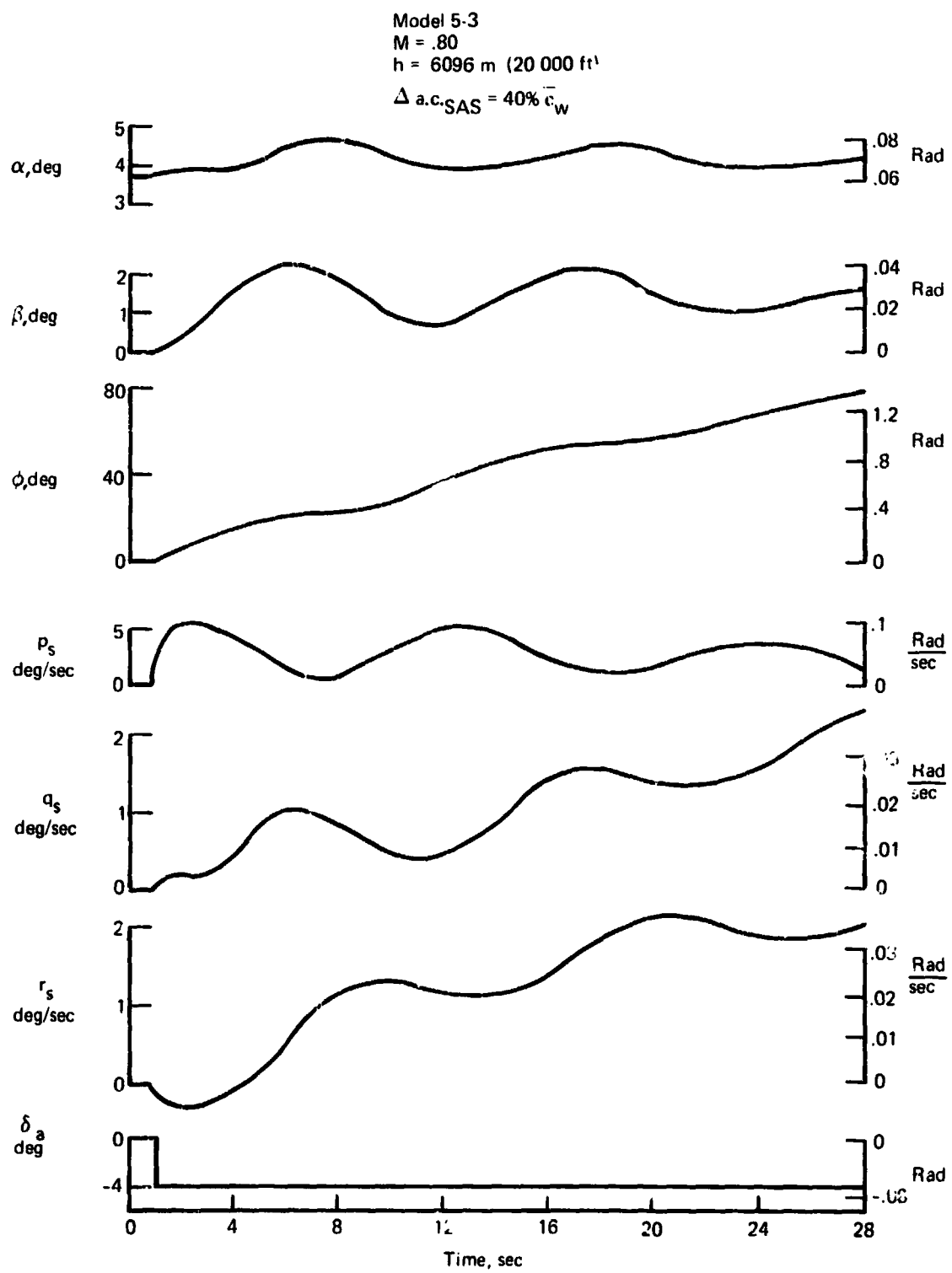
r_s deg/sec

δ_a deg

Time, sec

FIGURE 36.—RIGID AIRPLANE WITH FLEXIBLE WING, RESPONSE TO NEGATIVE AILERON STEP

damped and to experience lower attitude and rate excursions with the exception of angle of attack, which peaks near the same values, rigid and flexible.

Response to a 0.026 rad (1.5°) elevator step is presented in figures 29 (rigid) and 34 (flexible). In both cases the airplane retrims at an increased angle of attack and rolls left wing down due to the pitch/roll coupling derivative, C_{ℓ_α}. The greater extent of rigid airplane coupling is evidenced by the larger sideslip excursions and the larger maximum roll angle attained by the rigid vehicle. The three-axes rate excursions indicate that the flexible wing vehicle is more highly damped and experiences lower peak-to-peak angular rates.

Figures 30 and 35, respectively, illustrate rigid and flexible wing vehicle responses to a positive 0.07 rad (4°) step aileron input. Both vehicles attain similar equilibrium angles of attack and sideslip The flexible airplane demonstrates a higher roll rate than the rigid and consequently achieves a larger roll attitude. This results from the fact that the larger pitch/roll coupling of the rigid vehicle retards its rolling motion relative to the flexible vehicle as each airplane attains an equilibrium angle of attack   the steady-state trim value $\left(-C_{\ell_\alpha}\right)$ $(-\Delta\alpha) = +C_\ell$. The pitch trim change results from the coupling term, $C_{m_{\delta_a}}(-)$.

The influence of dihedral effect, C_{ℓ_β}, is shown in figures 37 and 38 for the rigid airplane. Responses to a 0.087 rad (5°) elevator pulse were determined with the static longitudinal stability augmented by 20% (0.20 $\bar{c}_w$) for the nominal 5-3 configuration $\left(C_{\ell_\beta} = -0.00123/\text{deg}\right)$, figure 37, and for the airplane with C_{ℓ_β} set to zero, figure 38. The results in figure 37 demonstrate that airplane is dynamically unstable with this static stability level. Reduction of the dihedral effect, C_{ℓ_β}, to zero (fig. 38) resulted in a dynamically stable response to the control surface deflection. This figure further illustrates that the reduced dihedral effect produced a large steady-state roll attitude subsequent to damping of the pitch transient.

FLIGHT CONTROL SYSTEM MECHANIZATION

In addition to the stability augmentation function performed by the feedback control system of a conventional (i.e., symmetric) airplane, the control system of the yawed-wing airplane would have two important tasks brought about by the coupling of longitudinal and lateral-directional modes of motion. The system would:

1) Decouple the aeradynamics and suppress uncommanded motion about each of three axes;

2) Give positive and satisfactorily quick response to pilot inputs. again decoupled so the pilot may obtain response about a single axis from a single, appropriate control deflection command.
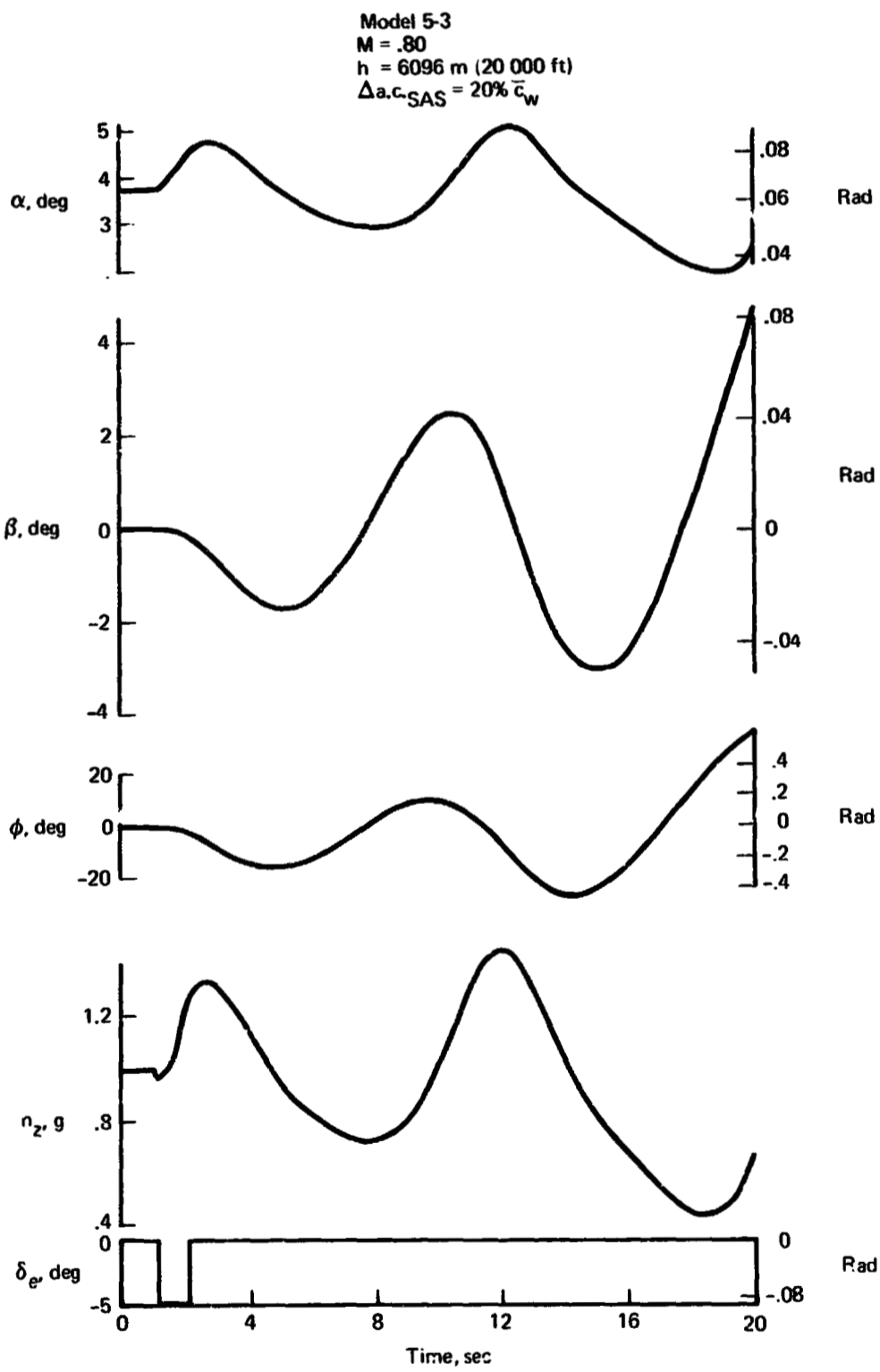
FIGURE 37.—RIGID AIRPLANE, DIVERGENT RESPONSE TO ELEVATOR
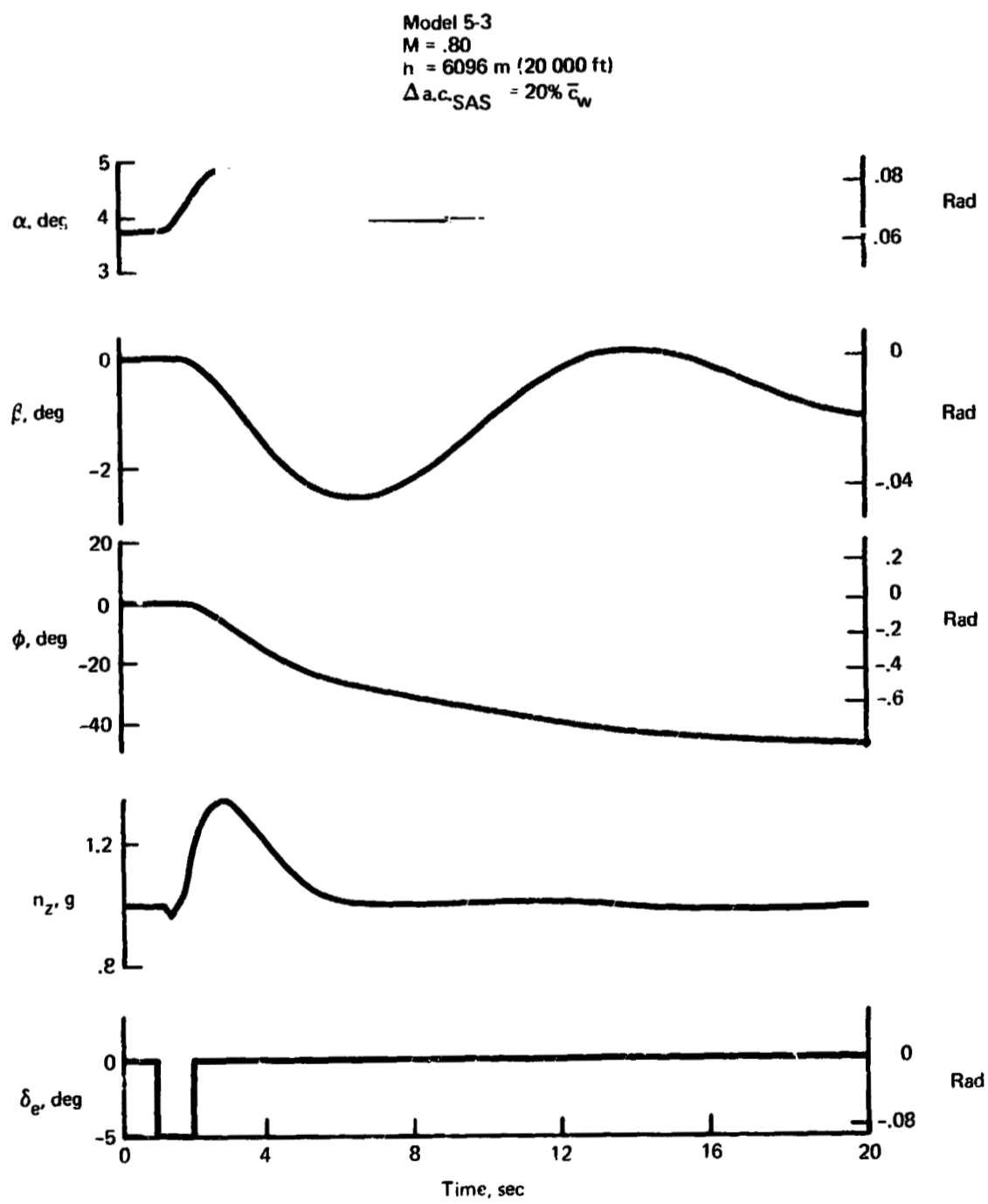PULSE—C_{l_β} = -0.00123/DEG

FIGURE 38.—RIGID AIRPLANE, RESPONSE TO ELEVATOR PULSE—$C_{\varrho_\beta} = 0$

Analysis of the response time histories shows that the presence of the rolling moment due to angle of attack derivative, C_{ℓ_α}, causes large bank angle response to occur in the phugoid and short-period modes, as well as in the lateral-directional modes. This is shown in figures 39 and 40, where the relative magnitudes and phases of the predominant responses to an elevator pulse are shown as phasors revolving counterclockwise at the system frequency, ω_n. The same is shown in figure 41 for the response to a rudder pulse.

These responses differ from those of a laterally symmetric airplane. In figure 39, the short period, which usually contains only angle of attack, α, and pitch angle, θ, is now seen to contain large amounts of roll, ϕ, and sideslip, β, due to the effect of the quantity, $C_{\ell_\alpha}\Delta\alpha$. The phugoid, shown in figure 40, usually contains only u and θ but now has large amounts of ϕ and yaw, ψ. The response usually seen for the dutch roll, figure 41, consists mainly of β and ϕ, but now contains small amounts of α and θ.

These phasor plots suggest that these modes, which can be excited by turbulence as well as by control deflections, can be controlled and unwanted motion suppressed by appropriate specific cross-axis feedback to the control surfaces. For example, it can be seen in figure 39 that roll rate, $\hat{p}$, and minus angle of attack, $-\alpha$ (which is $180°$ out of phase with α), both lead the bank angle in phase and are therefore natural quantities for defining aileron deflections to counteract the roll.

The undesirable excitation of certain degrees of freedom by control application can also be lessened by cross-coupling the control commands. This would be useful in cases such as figure 31, in which the roll rate, p_s, resulting from an elevator deflection could be suppressed by appropriate coupling of the aileron to the elevator.

The control system mechanization accomplishing the above uncoupling and stabilization should contain the following three subsystems:

1)   Attitude and rate feedback to ensure good response to control inputs (attitude or rate command from the pilot) and to assist in cross-axis stabilization;

2)   Specific cross-axis response feedback to decouple the lateral-directional variables from the longitudinal variables;

3)   Specific cross-axis control coupling to prevent unwanted excitation of the modes.

The 5-3 configuration should undergo design modifications in terms of cg location, wing pivot, and tail size before the control system is evaluated and gains are determined.

FIGURE 39.—FLEXIBLE AIRPLANE, SHORT PERIOD RESPONSE TO δ_e PULSE

$\frac{\pi}{2}$ rad (90°)

Model 5-3
M = 0.8
h = 6096 m (20 000 ft)
Δ a.c._SAS = 40% $\bar{c}_w$

Phase
lead

ψ

112°

$\hat{u}$

84°

$\hat{\theta}$

π rad
(180°)

1.0   2.0   3.0

0 rad
(0°)

155°

ϕ

$\frac{3\pi}{2}$ rad (270°)
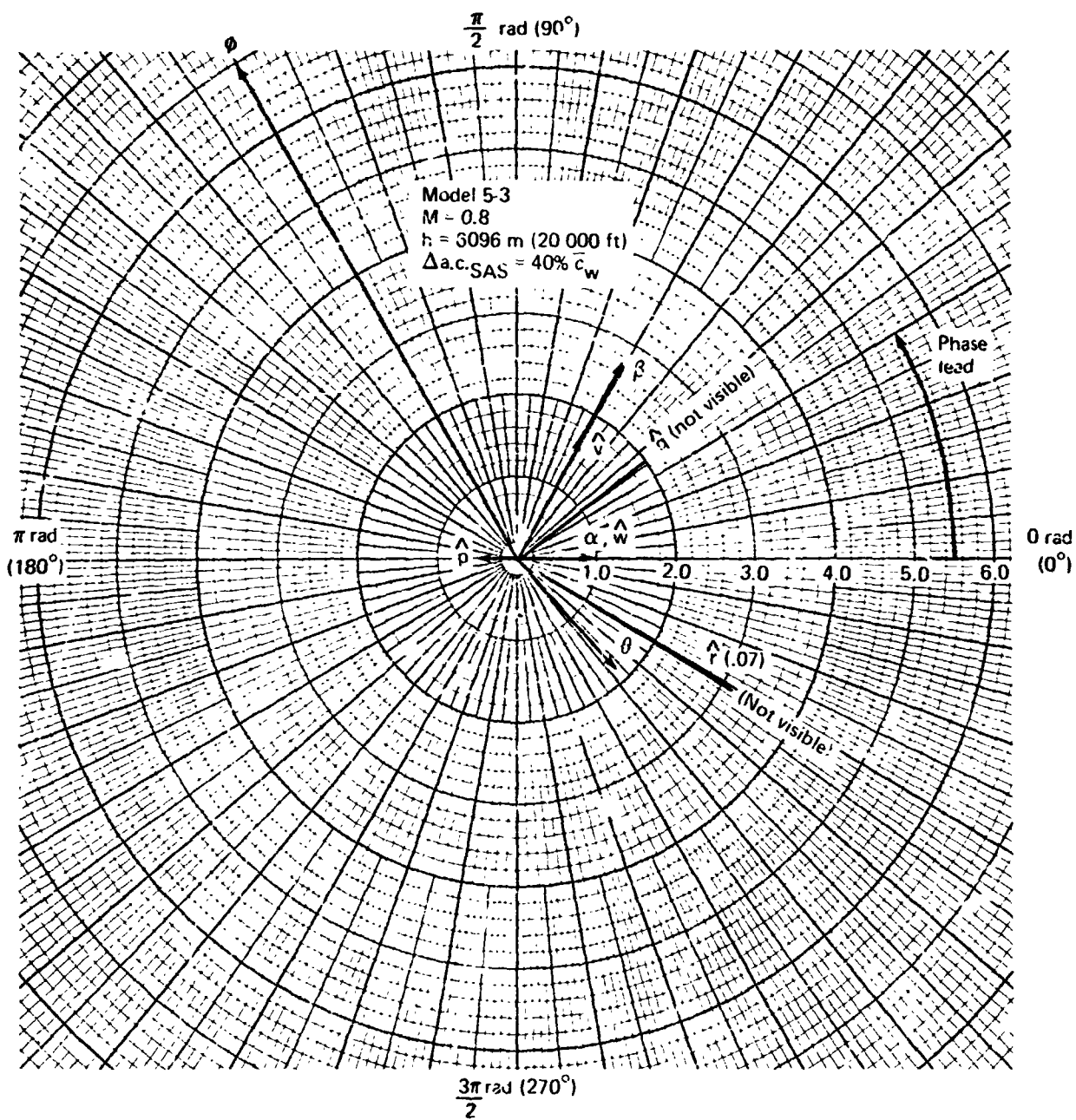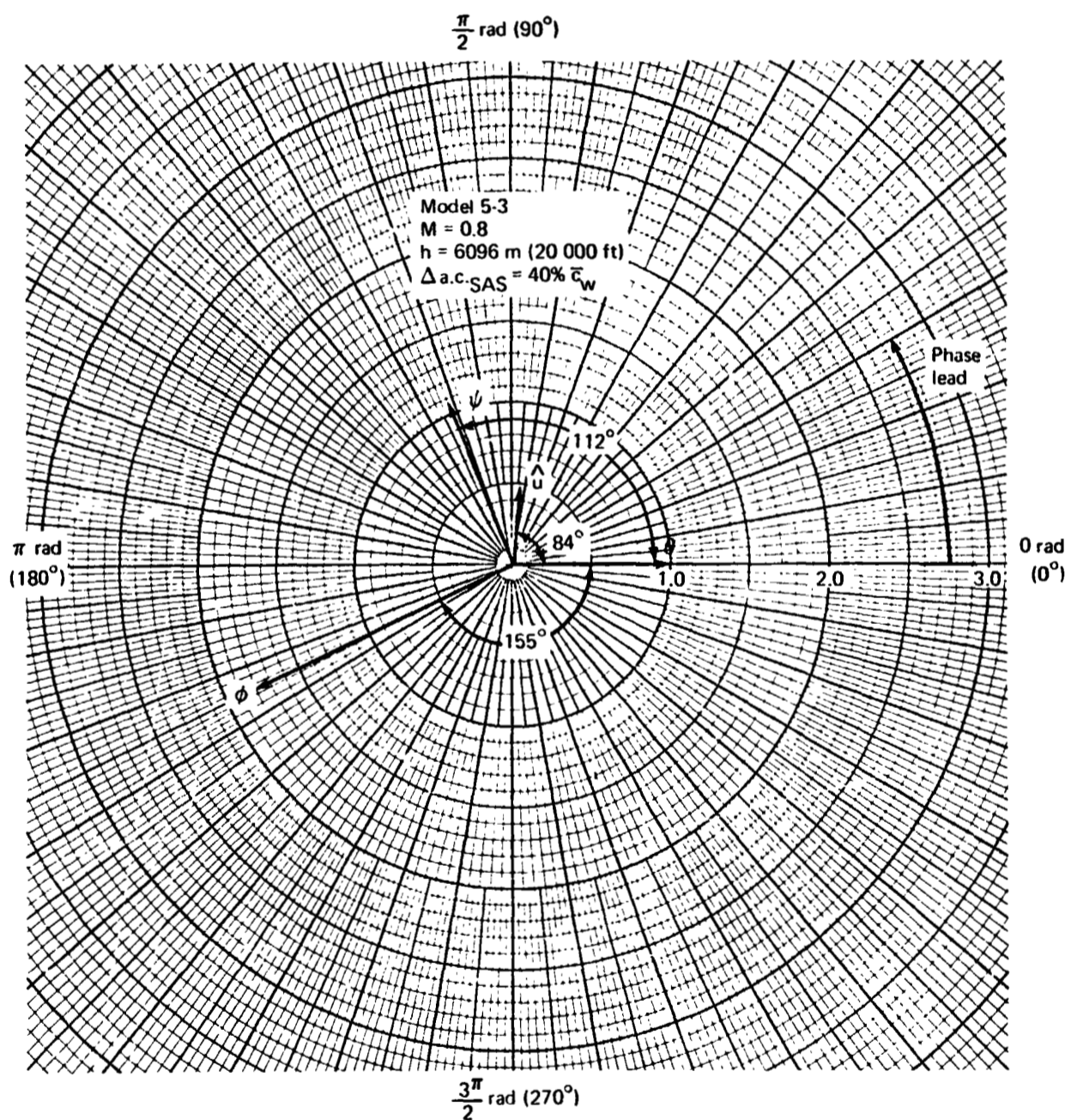
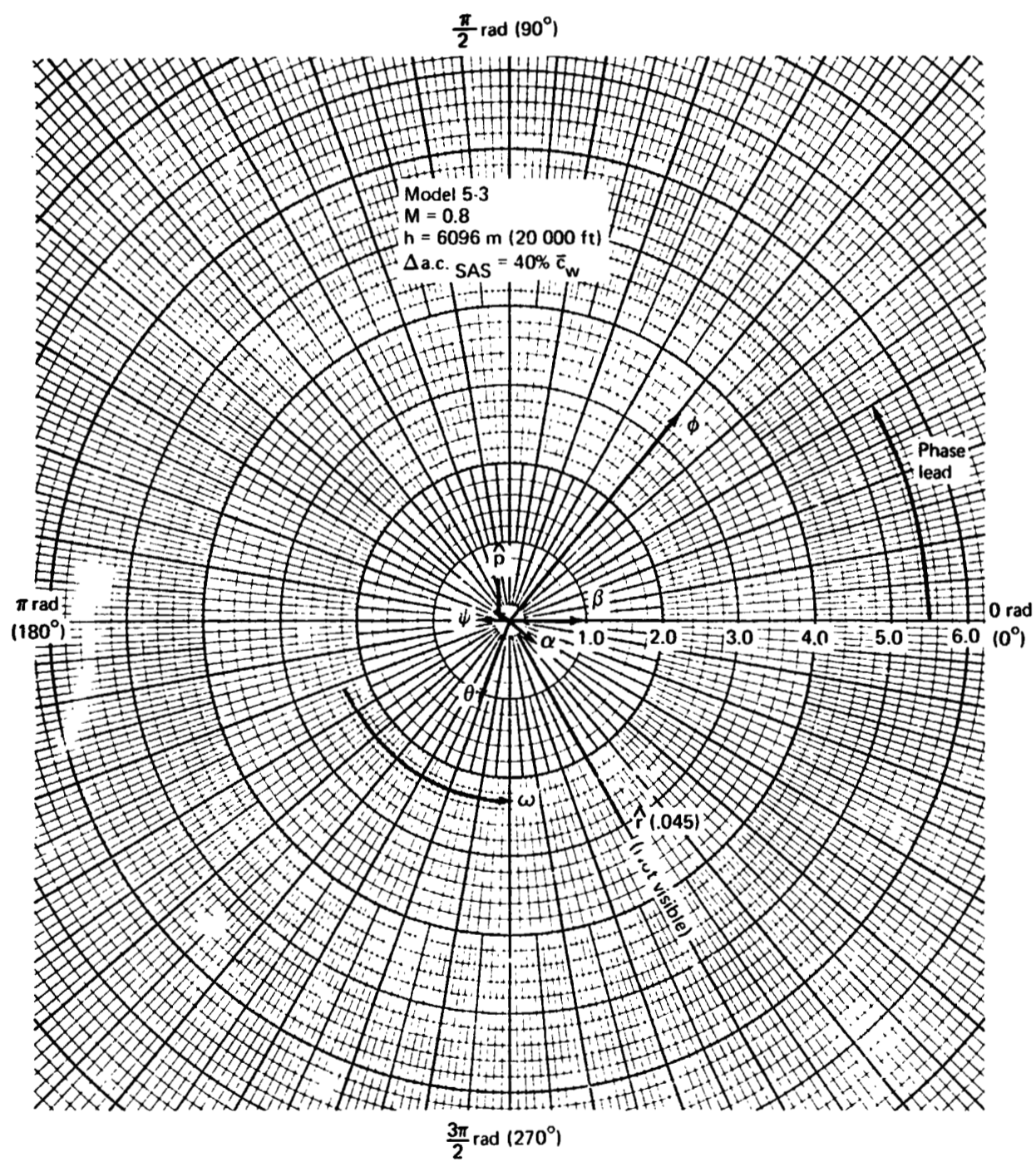FIGURE 40.—FLEXIBLE AIRPLANE, PHUGOID RESPONSE TO δ_e PULSE

FIGURE 41.—FLEXIBLE AIRPLANE, RESPONSE TO δ_r PULSE

The need for such a control system requires verification through analog or digital piloted simulation. But it is believed that satisfactory decoupling of the normal modes and control responses can be obtained by a few properly chosen feedback closures. This would permit a simplified control system that will be easier to make fail-operational, as required by the nature of the airplane.

STABILITY AND CONTROL ANALYSIS RESULTS

Wing flexibility reduced aerodynamic cross-coupling and resulted in improved airplane response. The airplane dynamic stability is dependent upon the following static stability terms and their corresponding configuration features:

- Longitudinal stability $\left(C_{m_\alpha}\right)$: cg location, horizontal tail volume coefficient

- Pitch/roll coupling $\left(C_{\ell_\alpha}\right)$: wing pivot location, cg location

- Dihedral effect and directional stability $\left(C_{\ell_\beta}, C_{n_\beta}\right)$: aft body ventral fin

The dynamic stability analyses were made with a six-degree-of-freedom program that included nonlinear dynamic coupling. The aerodynamic data used were derived from linear theory estimates. It is desirable to include nonlinear aerodynamic terms based on wind tunnel data for future analyses.

Configuration 5-3 was found to have divergent response to control surface deflections. The following configuration changes were identified as producing convergent responses:

- 30% $\bar{c}_w$ static margin increase

- 10% $\bar{c}_w$ static margin increase plus a wing pivot shift from 50% to 25% of root chord

Reducing the dihedral effect, C_{ℓ_β}, also produced convergent response; however, the required configuration changes were not investigated.

The question of whether it is important or desirable to separate the airplane motions into distinct longitudinal and lateral components can best be answered by studies with a moving base ground simulator.

CONCLUSIONS

The most significant conclusions of this study are:

- The alternate two-engine, single-fuselage, yawed-wing arrangement developed in this study has a less complex engine arrangement than the aft integrated four-engine configuration. The gross weight for the alternate configuration is approximately 2% higher than that for the integrated four-engine arrangement with equal design range and community noise levels.

- The Mach 1.2 range capability of the alternate two-engine configuration is 185 km (100 nmi) less than that of the integrated engine arrangement at the same gross weight.

- The takeoff gross weight required to achieve the Mach 1.2 design mission of 5560 km (3000 nmi) and payload of 18 140 kg (40 000 lb) depends on the cruise altitude and community noise goal. For cruise at an altitude of 11 890 m (39 000 ft) the gross weights of the alternate configuration required to achieve FAR Part 36 noise levels and 15 EPNdB below FAR Part 36 noise levels are, respectively 217 700 kg (480 000 lb) and 226 800 kg (500 000 lb). Airframe noise would most likely prohibit the airplane from achieving the noise levels below FAR Part 36 minus 10 EPNdB.

- The minimum gross weight required by the alternate configuration to achieve the mission objectives is 204 100 kg (450 000 lb). This would require cruise at an altitude of 10 670 m (35 000 ft).

- A modified structural design speed placard that required a modest weight increase for added strength capability of the wing allowed the Mach 1.2 cruise altitude to be lowered 10 360 m (34 000 ft). Cruising at the lower altitudes decreased the takeoff gross weight for the integrated-engine arrangement model 5-3 and the alternate configuration 5-4-1, 8% and 6%, respectively.

- Increasing the Mach 1.2 cruise altitude above the minimum cruise altitude required an increase in takeoff gross weight, engine size, and wing area. The increase in takeoff gross weight with cruise at higher altitudes can be minimized by reducing the structural design speeds.

- The dynamic stability characteristics of the single-fuselage yawed-wing configuration were found to be very dependent on the magnitude of the pitch/roll coupling term C_{ℓ_α} and

the static longitudinal stability. The wing flexibility reduces the pitch/roll coupling and is therefore beneficial.

● The six-degree-of-freedom rigid and flexible analyses of the single-fuselage yawed-wing configuration 5-3 indicated divergent aircraft response to control surface deflections. Configuration changes in terms of wing pivot location, center-of-gravity location, tail volume coefficient, and stability augmentation were identified to produce convergent responses.

RECOMMENDATIONS

At the conclusion of the initial contract, "High Transonic Speed Transport Aircraft Study" (ref. 1), a three-phase development program was recommended to verify and further develop the potential of the yawed-wing concept. Some of the items in that development program have been investigated in this study. Additional study items have also been identified. A modified version of this three-phase development program is recommended.

Phase I

- Conduct a study to determine the benefits of wing taper on the yawed-wing configuration.

- Perform flexible and rigid aerodynamic analyses of the yawed-wing wind tunnel models and compare with the wind tunnel test data to provide the data base necessary to substantiate the aerodynamic performance levels.

- Conduct wind tunnel program and coordinated flexible model analyses to substantiate the yawed-wing configuration stability derivatives.

- Conduct detailed climb and descent analyses of one of the yawed-wing configurations. Resize this configuration with the calculated climb and descent fuel allowances and distances.

- Conduct an engine bypass ratio study to optimize the performance of the yawed-wing configuration.

- Redesign either the basic or alternate yawed-wing configuration to improve the dynamic stability response characteristics and determine the impact on the airplane performance.

- Develop a low-transonic-speed yawed-wing configuration to compare directly with the advanced technology transport (ATT) study configurations.

- Match the engine cycle, the amount of noise suppression required, the flap system, and the takeoff and landing procedures to minimize the community noise for the synthesized basic and alternate yawed-wing configurations.

- Conduct a theoretical and experimental wing development study to fully identify the maximum practical wing thickness/chord ratio and the minimum achievable drag due to lift.

- Analyze operational characteristics of a yawed-wing commercial transport in airline operation and estimate total operating costs. Compare these costs with wide-body and ATT operating costs for similar payload/range categories.

Phase II

- Verify the performance of the best Mach 1.2 configuration developed in phase I by a coordinated theoretical-experimental program covering both the low- and high-speed flight regimes.

- Conduct a market analysis to determine potential total airline fleet requirements.

- Based on the results of the phase I stability and control study and available test data, develop a moving-base simulation of the airplane in order to evaluate flight control systems.

- Perform an aeroelastic model wind tunnel test to confirm the wing divergence and flutter characteristics.

- Develop detailed plans, including the design criteria, for a yawed-wing flight test vehicle.

Phase III

- Design and fabricate a yawed-wing flight test airplane.

Supporting Technology Development

In addition to the development work described above for the yawed-w ,g configuration, the basic advanced-technology programs recommended as part of the advanced transport technology study (ref. 8) should be pursued since they apply nearly universally to this concept. This is particularly true in the structures, flight control, and power systems areas, which require the projected technology advances to achieve the potentia identified in this study.

Boeing Commercial Airplane Company,
P.O. Box 3707,
Seattle, Washington 98124, May 15, 1974

REFERENCES

1. Kulfan, R. M., et al.: High Transponic Speed Transport Aircraft Study—Final Report. NASA CR-114658, 1973.

2. Kulfan, R. M.: High Transonic Speed Transport Aircraft Study—Summary Report. NASA CR-xxxxx (number to be assigned), 1973.

3. Etkin, Bernard: Dynamics of Flight. John Wiley and Sons, publishers, 1959.

4. Roskam, J. and Dusto, A.: A Method for Predicting Longitudinal Stability Derivatives of Rigid and Elastic Airplanes. Journal of Aircraft, vol. 6, no. 6, 1969.

5. USAF Stability and Control Datcom. Air Force Flight Dynamics Laboratory, Wright Patterson Air Force Base.

6. Gray, W. L. and Schenk, K. M.: A Method for Calculating the Subsonic Steady-State Loading on an Airplane With a Wing of Arbitrary Planform and Stiffness. NACA TN 3030.

7. Jones. R. T.: New Design Goals and a New Shape for the SST. Astronautics and Aeronautics, December 1972.

8. Final Report—Study of the Application of Advanced Technologies to Long Range Transpo.. Aircraft; Volume II, Advanced Technology Program Recommendations. NASA CR-112093, May 1972.